Summer 2021

Rock Glacier Hydrological Significance in a Warming World: A Geoecological Transect in the North Cascades, Washington

Jessica Abadie Coffey
Central Washington University, jessiecoffey96@gmail.com

ROCK GLACIER HYDROLOGICAL SIGNIFICANCE IN A WARMING WORLD: A GEOECOLOGICAL TRANSECT IN THE NORTH CASCADES, WASHINGTON

A Thesis

Presented to

The Graduate Faculty

Central Washington University

In Partial Fulfillment

of the Requirements for the Degree

Master of Science

Cultural and Environmental Resource Management

---

by

Jessica Abadie Coffey

June 2021

CENTRAL WASHINGTON UNIVERSITY

Graduate Studies

We hereby approve the thesis of

Jessica Abadie Coffey

Candidate for the degree of Master of Science

APPROVED FOR THE GRADUATE FACULTY

_____ _____
Dr. Karl Lillquist, Committee Chair

_____ _____
Dr. Jennifer Lipton

_____ _____
Dr. Susan Kaspari

_____ _____
Adam Riffle, M.S.

_____ _____
Dean of Graduate Studies

ABSTRACT

ROCK GLACIER HYDROLOGICAL SIGNIFICANCE IN A WARMING WORLD: A GEOECOLOGICAL TRANSECT IN THE NORTH CASCADES, WASHINGTON

by

Jessica Abadie Coffey

June 2021

Mountain environments are some of the most climate-sensitive areas on the planet. Due to recent warming trends, the 0°C isotherm is rising in elevation and subsequently melting glaciers, snowpack, and permafrost. However, rock glaciers are a type of permafrost that is climate-resilient; therefore, research on their distribution and water volume equivalence (WVEQ) will be increasingly valuable in a warming world.

The purpose of this research was to determine the hydrological significance of different altitude belts of alpine permafrost in Washington State's North Cascades. Additionally, this study analyzed how much rock glacier permafrost will be exposed to melting temperatures with climate change. In the North Cascades, field surveys using ground penetrating radar (GPR) were conducted on a sample of ten intact rock glaciers in an E-W geoecological transect. Based on the GPR surveys, the total WVEQ estimated for North Cascades rock glaciers in this study was 19,750,000 m^3. Climate modeling was used to project the mean annual air temperature (MAAT) for each rock glacier by the year 2100 under different greenhouse gas emissions scenarios. This

model projected a MAAT ≥ 3°C by 2100 for all 53 sites, indicating the rock glacier permafrost will be degrading. Nonetheless, rock glaciers are more climate-resilient than glaciers and snowpack, so they can potentially buffer the water scarcity this region will experience with climate change.

Geoecological analysis revealed a minor relationship between continentality and rock glacier WVEQ in the North Cascades. Furthermore, rock glacier altitude distribution did not reveal an elevation range wherein rock glaciers developed preferentially. However, the WVEQ of rock glaciers substantially increased with elevation and nearly two-thirds of the total rock glacier WVEQ was confined within a 173 m elevation bracket, occupied by only one-third of the rock glaciers. This implies that water content may be distributed differently than can be observed by only recording rock glacier distribution, which should be considered in rock glacier analyses as water resources around the world.

ACKNOWLEDGEMENTS

This research was made possible through the combined effort and support of many exceptional people. I would like to express my deepest appreciation for my thesis committee. Through developing my Master's research and in my life, their guidance has been invaluable. Thank you to my advisor and committee chair Dr. Karl Lillquist for helping me grow as a researcher and a geographer. You pushed me in my writing and in developing a successful strategy to accomplish this field intensive study. I would also like to extend my sincere gratitude to my committee member Adam Riffle who was the first to do GPR on rock glaciers in the Cascades. He showed me the ropes with GPR and his work was essential to my research. Thank you to Dr. Jennifer Lipton, another committee member, whose valuable insight helped develop this study, especially in its early stages, which provided me with a strong foundation. Additionally, thank you to my committee member Dr. Susan Kaspari, who has been inspirational to my work and my path after grad school.

Special thanks to my funding sources: the Stoltman Scholarship Award, the Kittitas Audubon Scholarship, the Graduate Student Research Support Award, the Graduate Student Summer Fellowship, and the Braden-Dodd Memorial Graduate Fellowship. These generous donors allowed me to purchase specialized gear, travel to the North Cascades four times with my team, and hire a mule convoy to transport equipment for part of our journey. Their support of this study allowed me to give the attention necessary to successfully complete this logistically and physically challenging research during a pandemic. Additionally, I would like to recognize Monica Reece-

Bruya of the CWU Geography Department who helped me by coordinating funding sources, keeping me on track with paperwork, and sharing treats from Vinman's bakery.

In addition, it was a great pleasure working with Aaron and the wranglers of Early Winters Outfitting in Mazama, WA. They were the mule team that helped us transport gear for 20 miles on our second research trip and we would not have three of the rock glacier surveys without them. On the third research trip, my team also received help from a group of gold miners who assisted us in accessing a trailhead that was located 8 miles down an 'impassable' dirt road and I am very appreciative of their help.

Many thanks to my mom, Sherry, and other family members and friends who have supported me while I have been fully invested in this work and not able to visit often. Their encouragement and unconditional love kept my spirit and motivation high. Furthermore, I am sincerely thankful to Steve, Brad, and Mars for taking great care of my dog Fitz Roy during these research trips.

Finally, my field crew was instrumental to the success of this thesis. The team included: Bailey Duvall, Alex Mathews, Jamie Trotto, Michael Fischer, Matt Hadden, Seth Urbanski, Spencer Stinnett, Nacho Ward, Darryl Coffey, Cathy Raymond, and Will Raymond. This outstanding team hauled heavy equipment across burn zones, through bee hives, and up craggy mountains with me all of summer 2020. Special thanks to Will who went on all four research trips for the full 200 miles of backcountry travel this study required. His exceptional work ethic, problem solving, and team mindset were essential to our success and I am deeply grateful to Will and his mom,

Cathy, for helping in my work. Additionally, I cannot over-exaggerate my sincere gratitude to Spencer, Nacho, and my dad, Darryl, for flying across the country to trek through the North Cascades with me and help make this research possible. Our main takeaway was always bring more rope than you think you need!

TABLE OF CONTENTS

TABLE OF CONTENTS (CONTINUED)

Chapter Page

LIST OF TABLES

LIST OF FIGURES

LIST OF FIGURES (CONTINUED)

Figure Page

LIST OF FIGURES (CONTINUED)

Figure Page

LIST OF FIGURES (CONTINUED)

Figure Page

CHAPTER I

INTRODUCTION

Problem Statement

Melting alpine glaciers, snowpack, and permafrost contribute to river discharge that supports downstream communities and ecosystems (Iribarren et al., 2018). In a warming climate, the 0°C isotherm (i.e., contour lines of equal temperature) will gradually increase in elevation. These rising temperatures will alter mountain geoecological zones (i.e., elevations of similar climate, vegetation, and landforms) (Troll, 1971). Subsequent melting of snowpack, glaciers, and permafrost will eventually stress communities and ecosystems that rely on mountain water resources. However, within the periglacial environment (i.e., areas that are subject to repeated freezing and thawing and may be underlain by permafrost), rock glaciers could be substantial, climate resilient water resources that help buffer these changes (Brenning, 2005; Rangecroft, 2015; Millar and Westfall, 2019). Therefore, research on rock glacier water capacity and distribution will be increasingly valuable for community and ecosystem health in a warming world.

Rock glaciers are bodies of colluvium or till that contain permafrost in the form of interstitial or massive ice, and exhibit movement by creep (Wahrhaftig and Cox, 1959; Giardino et al., 1987; Barsch, 1996; Haeberli et al., 2006; Jones et al., 2019a). These geomorphic phenomena facilitate downslope transport of debris (Wahrhaftig and Cox, 1959; White, 1976; Corte, 1987) and potentially host significant volumes of water (Brenning, 2005; Rangecroft, 2015; Millar and Westfall, 2019). The upper, insulating debris layer (i.e., active layer), and cooling effects associated with cold air sinking into

the debris matrix, make rock glaciers somewhat climate-resilient by protecting internal permafrost from warm surface temperatures (Haeberli et al., 2006).

A complex set of environmental factors influences rock glacier development. Catchment area (i.e., "contributing area" of Janke, 2007 or "talus shed" of Brenning 2005) controls the amount of debris available for rock glacier formation. Debris size modifies active layer depth by affecting the size of air voids. Larger debris sizes result in larger air voids which enhance the insulating effect because cool air sinks into these spaces (i.e., Balch ventilation). Therefore, the active layer can be thinner on a rock glacier composed of coarse debris than one made of fine-grained material (Barsch, 1996). Mean Annual Air Temperature (MAAT) and annual temperature range also modulate active layer depth which annually adjusts in response to these variables. With warmer temperatures, a deeper active layer is required to maintain the same insulating effect, thus the active layer thickens and the underlying permafrost partially degrades. Continentality is a measure of how much the climatic conditions typify that of the continental interior. This gradation affects regional temperature and precipitation, which modifies the altitude range occupied by rock glaciers (Johnson et al., 2007; Onaca et al., 2017). Additionally, aspect and elevation influence incoming solar radiation and MAAT, and rock glaciers will preferentially develop on shaded aspects and high elevations. Rock glacier formation depends on this complex set of environmental variables which are modified by climate change as temperature and precipitation patterns are altered and the degree of frost wedging (i.e., mechanical weathering associated with freeze-thaw processes) decreases. Such changes eventually drive permafrost degradation in active rock glaciers.

The water capacity of rock glaciers is disputed (Brenning, 2005; Arenson and Jakob, 2010); therefore, additional studies are needed to determine rock glacier water resource value (Rangecroft, 2015; Millar and Westfall, 2019). Riffle (2018) estimated a total water volume of approximately 23,000,000 m^3 for Eastern Cascade rock glaciers in Washington State; however, Cascade Range geoecological environments change dramatically from the west versus east sides of the Cascade Crest, and with distance from the Cascade Crest. This change provides the opportunity for understanding rock glacier hydrologic contributions across a range of climates. Furthermore, the literature lacks sufficient investigation into the relationship between climate change and altitude distribution of alpine permafrost as noted in Haeberli (1975). The rock glacier inventory of Lillquist and Weidenaar (2021) shows a concentration of rock glaciers in the Northeastern Cascades; therefore, this area is highly suitable to investigate the hydrologic significance of rock glaciers in distinct geoecological belts in a warming climate.

Purpose and Objectives

The purpose of this research was to determine the hydrological significance of different altitude belts of subalpine and alpine permafrost along an E-W transect within the periglacial environment of Washington State's North Cascades. Specifically, I: 1) determined the geoecological zones across the study area based on glacial equilibrium line altitude (ELA), rock glacier initiation line altitude (RILA), and timberline; 2) subdivided the periglacial belt into altitudinal zones of varying permafrost concentrations by rock glacier quantity and surface area; 3) surveyed the composition and structure of select rock glaciers from each periglacial altitude belt of the transect; 4) estimated the

water storage for each altitude belt within the transect; 5) assessed altitude belt sensitivity thresholds to a warming climate; and 6) made results accessible to water resource managers to inform policy decisions.

Significance

Rock glaciers function as ecologic refugia by providing cool, fresh water and shelter that form critical habitat for high-altitude biodiversity in a warming climate (Millar and Westfall, 2008, 2018; Nolin, 2012; Brighenti et al., 2019). This study area is hydrologically divided by the Cascade Crest. Headwaters east of the crest flow into the Methow River and those west of the crest flow into Skagit River. The communities of Mazama, Winthrop, and Twisp depend on the Methow River system for agriculture, recreation, and tourism. On the West side, the Skagit River is impounded in a series of reservoirs: Ross Lake, Diabolo Lake and Gorge Lake. These reservoirs generate power as part of the Skagit River Hydroelectric Project. Both basins provide ecosystem support for endangered sockeye salmon, chinook salmon, steelhead and bull trout which require sustained base flow within the tributaries and play key roles in ecosystem health with marine nutrients transport and as a food source for large birds of prey, bears, and orcas (Cederholm et al., 2000). These ecosystems and communities will be put under stress as climate change reduces snowpack and glaciers; hence, information on more climate-resilient water resources will become increasingly valuable (Jones et al., 2019a).

Water storage is critical to ecosystem and community health in mountain environments around the world. However, in some areas, climate-driven depletion of mountain frozen reservoirs is further accelerated by mining operations that exploit alpine

environments for precious minerals (Khadim, 2016). Furthermore, these extractive industries contaminate glacial and periglacial meltwater which threatens downstream communities and ecosystems (Christel and Torunczyk, 2017). Argentina, Chile, and Kyrgyzstan are responding by protecting glacial and periglacial landscapes to prevent accelerated resource exhaustion of mountain environments (Ley de los Glaciares, 2010; Iribarren et al., 2018). These nations recognize rock glaciers as freshwater resources that function as basin regulators during seasonal drought (Barsch, 1996; Schaffer et al., 2019) and are important to alpine hydrology, especially in areas lacking glaciers (Rangecroft, 2015; Millar and Westfall, 2019). Therefore, research on hydrologic contributions of rock glaciers and their relationship to climate change will facilitate informed decisions on periglacial water resources in mountain systems worldwide.

CHAPTER II

LITERATURE REVIEW

Alpine Permafrost

Permafrost consists of frozen rock or soil characterized by a MAAT below 0ºC for a minimum of two consecutive years (Dobiński, 2018). This subsurface phenomenon can exist as massive or interstitial ice in the matrices of unconsolidated material (Washburn, 1980). Additionally, an active layer composes the supra-permafrost zone which freezes and thaws in response to ambient thermal fluctuations, while buffering underlying permafrost from high temperatures (Cryosphere Glossary, National Snow and Ice Data Center, n.d.; Büdel, 1982). Following these criteria, permafrost may define subsurface ice that is interstitial or massive, given that the MAAT remains below freezing and summer temperatures do not penetrate to the base of the frozen material due to an active layer (Haeberli, 2000; Berthling, 2011; Dąbski 2019).

Permafrost is classified by spatial distribution, which consists of continuous (90-100% coverage), discontinuous (50-90% coverage), and sporadic zones (0-50% coverage) (Washburn, 1980). Permafrost moves downslope by creep (i.e., plastic deformation under the sustained pressure load of the entire permafrost body) (Washburn, 1980; Haeberli et al., 2006; Jones et al., 2019b). Enhanced frost action and alpine permafrost creep manifest a continuum of related features in transitionary phases; thus, consensus on terminology proves challenging (White, 1976; Wahrhaftig, 1987; Martin and Whalley, 1987; Haeberli et al., 2006). This discrepancy is further complicated by equifinality of different alpine geomorphic processes (Jones et al. 2019a).

Rock Glaciers

Rock glaciers are expressions of discontinuous alpine permafrost. The rock glacier active layer and associated thermal regimes (e.g., low thermal conductivity, convection, the chimney effect, and Balch ventilation) serve as insulation against fluctuations in ambient temperature (Haeberli et al., 2006; Onaca et al., 2017; Millar and Westfall, 2019). Therefore, rock glaciers are bodies of climate-resilient, ice storage that occupy mountain environments. Mountains exhibit amplified warming rates relative to surrounding lowlands due to several mechanisms including snow-albedo feedbacks and increased downward longwave radiation related to higher atmospheric humidity (Nogués-Bravo et al., 2006; Bradley et al., 2006; Rangwala et al., 2013; Palazzi et al., 2018). The rising 0°C isotherm will rapidly transform the alpine cryosphere as a water resource; hence, rock glaciers are critical, resilient features within a delicate environment. In the contiguous United States, 10,343 rock glaciers have been inventoried using remote sensing techniques and 7,052 were classified as active (i.e., containing ice and moving) features (Johnson et al., 2020). This finding has significant implications for the water volume stored in alpine permafrost at the continental scale, especially when considering that discontinuous permafrost is likely in the vicinity of the intact (i.e., containing ice and includes both moving and stagnant features) rock glaciers (Barsch, 1996).

Composition and Structure

Rock glaciers are often composed of large, blocky debris derived from weathering and mass wasting in the higher elevation portions of catchments. Rock glacier parent material is commonly composed of granite, gneiss, limestone, or sandstone as these rock

types tend to fracture into large, angular talus blocks (Haeberli et al., 2006). The surficial, blocky, active layer may have seasonally ice-filled interstices that exhibit freeze-thaw cycles (Barsch, 1996). Local MAAT, annual temperature range, and debris size affects active layer thickness. With a warming climate, the active layer depth increases as the feature transitions into an inactive (i.e., containing ice, but no longer moving) or relict state (i.e., no longer containing ice or moving). Beneath the active layer, the massive or interstitial ice is perennially frozen. Additionally, ice lenses may be scattered throughout the rock glacier, which likely formed from a snow bank at the rock glacier rooting zone (i.e., talus source area) that was covered by talus and assimilated into the landform (Barsch, 1996; Haeberli et al., 2006). Ice lenses will typically be thin layers due to compression and entrainment within the rock glacier (Corte, 1987; Haeberli et al., 1988), compared to massive ice which has a substantially larger body that was inherited from a previous glacier (Monnier et al., 2011).

Morphology

The three distinguishing classes of morphological expressions include tongue shaped, lobate, and complex rock glaciers (Barsch, 1996). Tongue shaped morphologies are characterized by form length exceeding form width. In contrast, lobate features are wider than they are long. The final morphological category consists of complex features which may have multiple ages, compound lobes, multiple rooting zones, or may be composed of multiple rock glaciers (Barsch, 1996). The morphology of individual rock glaciers is largely controlled by the local topography that guides the downslope creep of permafrost (Wahrhaftig and Cox, 1959; Barsch, 1996).

Genesis

A method of further categorization is assessment of genesis, as revealed by rock glacier composition and the regional glaciation history. As illustrated in Humlum (1982), rock glacier internal structure consists of either massive ice (glacier-derived) or interstitial ice (talus-derived) (*Figure* 2.1). Glacier-derived rock glaciers form when a retreating glacier accumulates such large quantities of debris that the rock is more abundant than ice. This process results in an ice mass that is insulated by an active layer of till and/or talus. Thus, glacier-derived rock glaciers exist in areas that were previously glaciated and are evidence of a warming climate (Morris, 1987; Vitek and Giardino, 1987; Jones et al., 2019a). By comparison, talus-derived rock glaciers are composed of an ice-rich, talus matrix throughout the entirety of the feature (White, 1976). Talus-derived rock glaciers represent a different origin with external equifinality (Haeberli et al., 2006). In contrast to the climatic amelioration indicated by glacier-derived rock glaciers, talus-derived rock glaciers form by climatic deterioration (Morris, 1987). As a cooler climate facilitates enhanced frost-wedging and permafrost development within talus, the accumulation of debris and interstitial ice begins advancing downslope (Washburn, 1980). These features are characteristic of the periglacial environment and may exist in glaciated or non-glaciated regions (Haeberli et al., 2006).

Some authors have argued that only talus-derived rock glaciers are permafrost, while glacier-derived rock glaciers should be excluded from this category because the internal ice is glacial in origin rather than periglacial (Barsch, 1996; Haeberli, 2006). However, regardless of the speculated origin, the current conditions of both talus-derived

and glacial-derived, intact rock glaciers are, by definition, permafrost (i.e., has subzero temperatures perennially and an active layer that insulates underlying ice) (Cryosphere Glossary, National Snow and Ice Data Center, n.d.; Haeberli, 2000; Dabski, 2019). Given that both talus-derived and glacial-derived rock glaciers satisfy these criteria, both classifications will be referred to as permafrost in this manuscript.

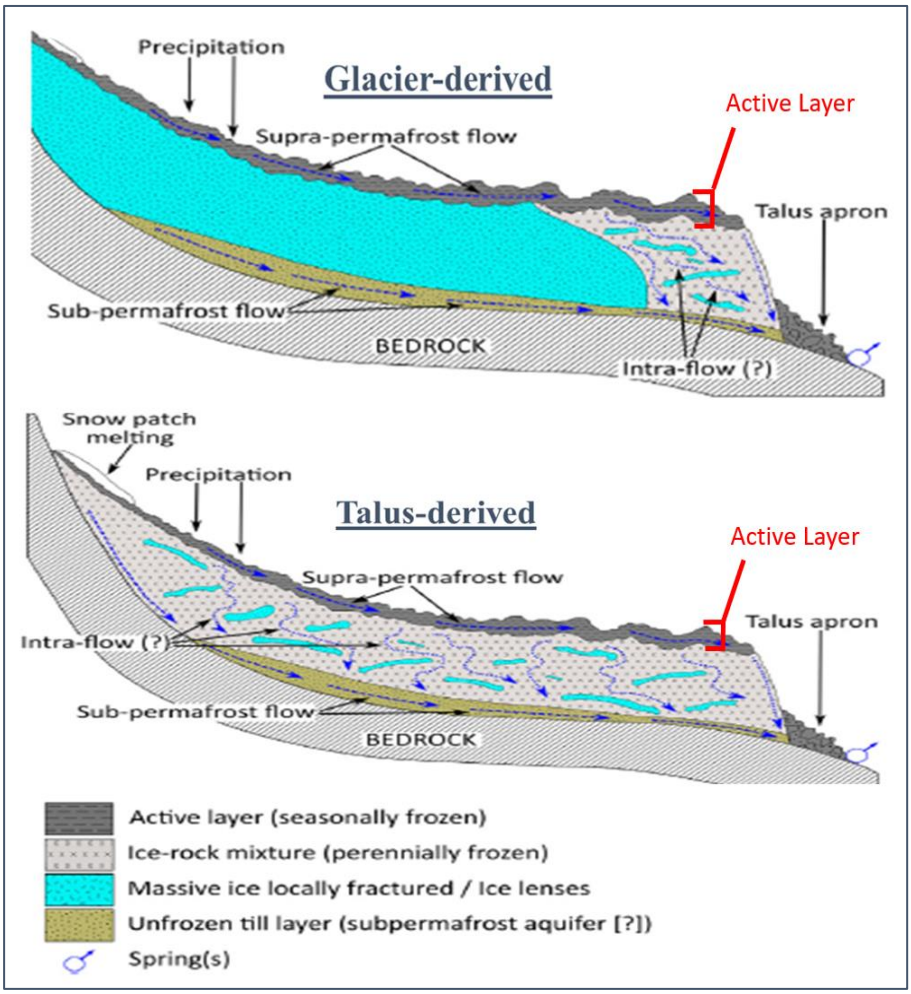

Figure 2.1. Glacier-derived and talus-derived rock glaciers. Adapted from Jones et al., (2019a).

Activity

When the climate is suitable for active rock glacier development, a rock glacier accumulates talus by frost-wedging sourced from the catchment area. Correspondingly, subzero annual temperatures preserve the internal ice mass or facilitate permafrost development from precipitation, seasonal snowpack melt, and groundwater (Büdel, 1982; Jones et al., 2019a). Beyond exhibiting movement and having an inflated appearance, active rock glaciers are distinguished by their over-steepened snouts that are constantly receiving debris supply. Additionally, active features will express compressional and extensional stress in surface microrelief of pressure ridges and furrows (White, 1976), although this microrelief may also form from talus accumulations in the catchment area (Wahrhaftig and Cox, 1959). Lack of vegetation is another indicator that the rock glacier body is mobile, although there are examples of resilient vegetation (e.g., subalpine larch) developing on active rock glaciers in the Washington Cascades (Goshorn-Maroney, 2012; Riffle, 2018).

As the climate warms, many periglacial processes cease and active rock glaciers transition into inactive states. Inactive rock glaciers maintain internal ice due to their climate-resilient capacities; however, inactive features no longer demonstrate dynamic flow. Inactive rock glaciers are recognized by partial inflation, more gentle fronts and microrelief, and partial vegetation development (Jones et al., 2019a). Collectively, active and inactive rock glaciers are termed “intact” (Millar and Westfall, 2019; Jones et al., 2019a), as they both accommodate volumes of stored ice.

The third activity classification consists of relict rock glaciers. These landforms no longer host internal ice and are completely stagnant. These characteristics give the features a deflated appearance and are often overrun with vegetation. Relict features are evidence of a past, colder environment; hence, they are useful in paleoclimatic reconstruction (Washburn, 1980; Vitek and Giardino, 1987; Morris, 1987).

By mapping different rock glacier activity levels that appear in discrete elevation ranges, different periods of rock glacier advance can be inferred (Wahrhaftig and Cox, 1959; Humlum, 1988). Due to climatic fluctuation, there may be instances when an active rock glacier overrides an inactive or relict feature thus becoming a complex feature (Barsch, 1996). Establishing a foundation for rock glacier activity classification allows scientists to decipher a complex history of climate change (Morris, 1987).

Rock Glacier Spatial Distribution

Many studies have described the environmental factors that influence rock glacier spatial distribution (Morris, 1987; Brenning, 2005; Janke, 2007; Johnson et al., 2007; Rangecroft, 2015; Onaca et al., 2017; Millar and Westfall, 2019). Factors that affect rock glacier formation include debris supply and exposure to wind or solar energy. Furthermore, aspect, altitude, latitude, and continentality influence temperature (by affecting insolation) and precipitation patterns which are important for sustaining permafrost conditions. The periglacial belt modifies in response to these environmental factors, thereby affecting rock glacier distribution.

An environment with MAAT below 0°C is conducive to rock glacier formation because subzero temperatures enhance frost wedging of talus slopes and growth of

perennial ice (Corte, 1987). Altitudinal-latitudinal factors are major controls of MAAT (Onaca et al., 2017) and permafrost benefits from subzero annual temperatures in mid-latitude mountain ranges and in polar and subpolar regions (Washburn, 1980, Johnson et al., 2007). Moreover, global patterns of modern, active rock glaciers reflect the importance of altitudinal-latitudinal factors (Jones et al., 2018; Haeberli and Weingartner, 2020). Increase in latitude depresses the 0°C isotherm thereby expanding the altitude range in which rock glaciers can develop (Janke, 2007). Furthermore, increasing altitude corresponds with decreasing temperature. Therefore, high relief walls that exist at altitudes above the 0°C isotherm are suitable for permafrost development until the glaciation threshold (i.e., lower elevation limit of glaciation) is reached. In those mountain environments that are non-glaciated due to insufficient precipitation, periglacial processes dominate the landscape (Rangecroft et al., 2015). In the Eastern Cascades of Washington, Lillquist and Weidenaar (2021) found that rock glaciers occur above 46° 30’ latitude, with increasing frequency moving northward, and rock glaciers formed above 1870 m a.s.l.

Another prominent factor of rock glacier development is slope aspect, which controls the amount of solar energy that reaches the landform. In the northern hemisphere, southerly aspects receive significantly more insolation than northerly aspects, resulting in cooler MAAT on northerly slopes (Brenning and Trombotto, 2006; Millar and Westfall, 2019). Similarly, windward versus leeward aspects determine the exposure to prevailing wind patterns. Wind exposure which could either deposit windblown snow on the rock glacier surface (i.e., insulating the rock glacier from cold,

winter temperatures that benefit permafrost development) or remove snow from the rock glacier surface (i.e., further exposing the rock glacier to cold winter temperatures conducive to permafrost development) (Vitek and Giardino, 1987; Anderson et al., 2018). Corte (1987) reported a difference of several hundred meters between the lower altitude limit of rock glaciers that developed on different aspects. In the Eastern Cascades, rock glaciers develop almost exclusively at north-facing aspects in the numerous cirques (Lillquist and Weidenaar, 2021) due to limited solar radiation.

Maritime climates are associated with high precipitation and moderated annual temperatures, which allows glaciers to exist at relatively low elevations. In contrast, rock glaciers typically develop in mountains with more continental climates, which are generally further from large moisture sources and have greater variance in annual temperatures (Rangecroft, 2015; Onaca et al., 2017). Less precipitation in continental environments means that less snow cover insulates the ground during the winter relative to marine environments (Noetzli et al., 2007; Allen et al., 2008; Charbonneau and Smith, 2018). Another relevant factor is the increased number of frost alteration days (i.e., freeze-thaw) associated with continental settings that accelerates periglacial processes such as frost wedging in high-relief mountain ridgelines (Höllermann, 1985). Globally, the lower limit of the rock glacier altitude belt generally ascends from marine settings to more continental environments (Washburn, 1980; Büdel, 1982), as shown in Alberta (Luckman and Crocket, 1978). Additionally, Höllermann (1985) mapped a circumglobal profile for the periglacial belt in midlatitude mountains for 42-43° latitude. He showed an elevation increase in the periglacial belt from the continental margins of North America

and Eurasia toward the continental interior that was closely linked to low MAAT and low winter snow cover. However, the opposite pattern (i.e., periglacial belt decreasing in elevation with continentality) has been documented in New Zealand (Allen et al., 2008), Norway (Lilleøren and Etzelmüller, 2011) and in China (Guodong and Dramis, 1992). In the Cascades, prevailing westerly winds and high-relief mountains create an orographic precipitation gradient that produces a continental, semi-arid climate on the eastern slopes, which favors rock glacier development. Overall, the 159 rock glaciers that have been inventoried in the Eastern Cascades (Lillquist and Weidenaar, 2021) show rising elevations with continentality.

Recent deglaciation can produce systems that are not adjusted to the current environment. Areas that still possess a glacial signature and experience rapid geomorphological change following deglaciation are known as paraglacial environments (Ballantyne, 2002; Harris and Murton, 2005; Slaymaker, 2011; Serrano et al., 2018; Jones et al., 2019a). Perpetual rock fall activity can be triggered from glacial unloading as well as weathering expedited by periglacial processes (Haeberli et al., 2006). As rock glaciers facilitate mass transport, a balance emerges between debris removal and input from the talus catchment area. The area of the catchment (Olyphant, 1977) and fracturing in the catchment bedrock (Haeberli et al., 2006), affect the debris accumulation available for rock glacier growth. High relief cliff faces composed of rock types that weather into coarse, blocky talus are favorable to rock glacier formation by providing enhanced Balch ventilation (White, 1979; Haeberli et al., 2006; Goshorn-Maroney, 2012). Wahrhaftig and Cox (1959) documented a rock type transition from granodiorite to a highly fissile, platy

schist in the periglacial zone in the Brooks Range of Alaska. The former area contained rock glaciers, but once the rock type changed to schist, rock glaciers did not develop. These findings are consistent with studies in the Cascade Range that have found rock glaciers to develop in volcanic-clastic rocks, quartz monzonite, and granodiorite (Crandell and Miller, 1974) and, in the North Cascades, a majority of rock glaciers are composed of intrusive igneous rocks (Lillquist and Weidenaar, 2021), which fracture into large, angular talus.

Geoecology

The concept of geoecological zonation was introduced by Troll (1971), who was inspired by the work of Alexander von Humboldt in high mountain geography and altitudinal climate belts (Ives, 2012; Wulf, 2015). Geoecology, also referred to as landscape ecology (Troll, 1971; Risser et al., 1984), investigates the interactions and spatial patterns of climate, geomorphic processes, and ecosystems that produce altitudinal heterogeneity of mountain systems (Troll, 1971; Risser et al., 1984; Wu and Hobbs, 2007; Opdam, 2009). Significant elevation change creates environments of substantial geoecological diversity across small spatial scales. Due to the close relationship of vegetation and landform spatial distribution with climate, these patterns are valuable indicators of discrete geoecological belts (Troll, 1973; Höllermann, 1985; Barsch, 1996; Garcia et al., 2017). Timberline is a useful vegetation pattern in defining the ecotone (i.e., transition between geoecological belts) between the forest and periglacial belts (Arno, 1984; Höllermann 1985; Young et al., 2017). Landforms (e.g., glaciers, moraines, permafrost features) signal processes unique to their respective geoecological belt and

have proven to be reliable proxies for reconstructing high mountain zonation (Troll, 1973; Leonard and Fountain, 2003; López-Martínez, et al., 2011; Serrano et al., 2018; Garcia et al., 2017). Rock glaciers are massive expressions of alpine permafrost that can be identified from aerial imagery or in the field, thus they have diagnostic value, particularly in semi-arid, continental climates that lack significant vegetation cover or other geoecological belt indicators (Höllermann, 1985; Barsch, 1996). Understanding mountain geoecology helps illustrate the distribution of water reserves which is critical with ubiquitous reduction in snowpack and glaciation worldwide (Pelto, 2006, 2008; Ives, 2012; O'Donnell et al., 2016; Millar and Westfall, 2019).

High mountain environments consist of three geoecological zones: nival, periglacial, and forest (*Figure 2.2*). Environmental factors modify the altitude range of each zone; therefore, significant climate gradients across mountain ranges are reflected in geoecological zone variation (Porter, 1977; Höllermann, 1985; Morris, 1987; Guodong and Dramis, 1992; Allen et al., 2008). The nival belt is the uppermost geoecological zone in mountain systems and occupied by modern glaciers, glacial features, and alpine tundra (Arno, 1984; Barsch, 1996). The nival belt depends on a sensitive balance of subzero temperatures and high precipitation to maintain a positive annual mass balance for glacial development (Morris, 1987). The boundary where mass accumulation is equivalent to mass ablation is the glacial equilibrium line altitude (ELA). This boundary marks the lower limit of the nival belt (Humlum, 1988; Barsch, 1996), and is documented most accurately in the field using longitudinal transects to calculate overall positive or negative glacial mass balance. Field based ELA records of nine North Cascades glaciers have been

systematically documented by the North Cascade Glacier Climate Project (NCGCP) and the World Glacier Monitoring Service (WGMS) starting as early as 1960. When glacier access is limited or impractical, the ELA can be identified with the kinematic inflection method using topographic maps (Hess, 1904; Leonard and Fountain, 2003; Cogley and McIntyre, 2003). There are several other methods of indirectly measuring the modern ELA including the elevation ratio of 2:1 for accumulation to ablation area (Gross et al., 1977), the regional mean elevation of glaciers (Porter, 1977), and elevation under which debris and medial moraines outcrop the glacier surface (Humlum, 1988). However, these methods are not empirically field tested to confirm their accuracy. Additionally, several studies have used remote sensing to estimate glacier mass balance based on displacement velocities and hyperspectral imaging (Berthier et al., 2006; Willis et al., 2011; Rabatel et al., 2013). However, the kinematic inflection method has consistently shown high correlation with systematic ELA measurements recorded by the WGMS (Leonard and Fountain, 2003). Thus, the kinematic inflection method can provide complementary data to field-based measurements and is an efficient tool for regional case studies (Cogley and McIntyre, 2003).

Below the nival zone is the periglacial belt. This intermediate geoecological zone is defined by frost-induced conditions with distinctive landforms (e.g., patterned ground and rock glaciers) and processes (e.g., frost wedging and frost creep) in non-glacierized, alpine tundra (Washburn, 1980; Arno, 1984; Büdel, 1982). The modern periglacial belt provides opportunity for alpine permafrost formation and its approximate altitude range can be inferred from intact rock glaciers (Höllermann, 1985; Barsch, 1996; Brenning,

2005; López-Martínez, et al., 2011; Charbonneau and Smith, 2018; Jones et al., 2018). Within the periglacial environment, Humlum (1988) assessed rock glacier altitude parameters including the rock glacier initiation line altitude (RILA), which is the elevation of a rock glacier's "rooting zone". Through regional mapping of RILA, Humlum (1988) inferred different generations (i.e., belts of the same age and genesis) of rock glaciers. Furthermore, the highest and lowest elevations of rock glacier rooting zones in the region (i.e., the range in RILA) is a useful tool in estimating the limits of the periglacial belt (Höllermann, 1985; Barsch, 1996). In a British Columbia rock glacier inventory (Charbonneau and Smith, 2018), the periglacial belt was estimated using the spatial distribution of rock glaciers compared to glaciers and timberline. In the Eastern Cascades, the uppermost RILA measurements were found to taper off at elevations exceeding 2400 m, marking the lower glacial limit (Porter, 1977; Lillquist and Weidenaar, 2021).

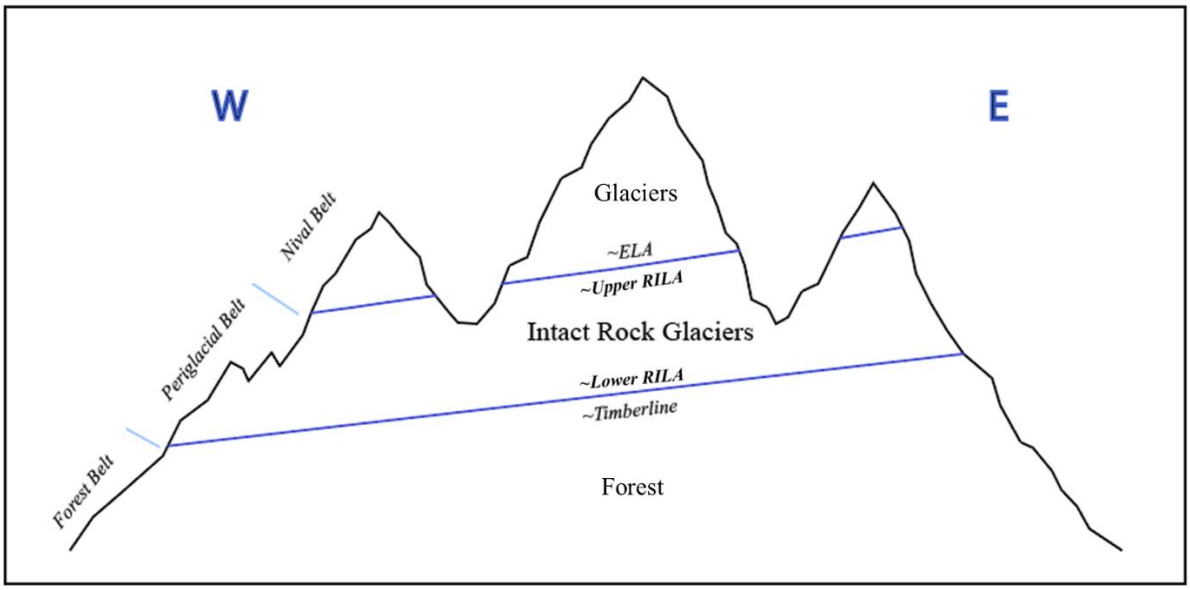

Figure 2.2. The geoecological zonation of mid-latitude, high mountain environments with westerly maritime influence. Adapted from Barsch (1996) and Humlum (1988).

The lower boundary of RILA indicates the periglacial lower limit and the upper limit of the forest belt, marked by the timberline (i.e., altitude above which harsh conditions prevent tree growth); and 0°C MAAT (Charbonneau and Smith, 2018). At this ecotone, the environment transitions from the highly morphodynamic system of alpine tundra to one stabilized by the forest belt and warming temperatures (Wardle, 1971; Arno, 1984; Höllermann, 1985). In the North Cascades, Arno (1984) found that the timberline ecotone rises eastward due to decreasing maritime influence from 1400 m at Mt. Baker in the Northwestern Cascades to 2100 m in the Northeast Cascades. This zone may have a few intact rock glaciers in its upper limits, but most rock glaciers of this belt are relict features, which indicate the periglacial environment extended to these lower elevations in a previous, colder climate (Morris, 1987). Estimates in the Eastern Cascades

map the 0°C isotherm at 2050 – 2100 m based on PRISM data, which indicated a 250-300 m rise in the past 100-150 years (Weidenaar, 2013).

Mountain Hydrologic Cycle

The cryosphere encompasses glacial and periglacial environments and is a subset of the global hydrosphere. The hydrologic cycle offers additional mechanisms of storing water in mountain environments where precipitation may be captured in glaciers, snowpack, or permafrost. The alpine cryosphere represents a delay phase within the hydrologic cycle, before the water continues transport through melting, evaporation or sublimation (Büdel, 1982). Once glaciers disappear from a mountain, water resource contribution from the nival belt is limited to direct precipitation, snowmelt, and permafrost melt (Kaser, 2006). Thus, in response to climate-driven melting of the nival belt, the entire mountain system must adapt (Pelto, 2006). Varying geoecological zones have different mechanisms of water storage; therefore, altitudinal subdivision of geoecological zones could offer a more detailed map of water resource distribution as demonstrated in Haeberli (1975).

Water Resources of the Periglacial Belt

Within the periglacial belt, snowpack and alpine permafrost are the primary means of water storage. In the glacier-poor Great Basin, rock glaciers contributed 93% of the total water present (i.e., cumulative rock glacier water equivalence of 0.89 km^3 compared to ice-field water equivalence of 0.07 km^3) (Millar and Westfall, 2019). Similar findings are documented in other non-glacierized areas (Perucca and Angillieri, 2011; Rangecroft, 2015). In the glacier-rich Himalaya, Jones et al. (2017) inventoried

>6000 rock glaciers which are estimated to contain ~21 trillion liters of frozen water. Furthermore, Barsch (1996) explained that intact rock glaciers can signal widespread continuous or discontinuous permafrost in the surrounding area, thus the permafrost water content of the Himalaya is likely much higher. For the Eastern Cascades, Riffle (2018) found the total water volume withheld in rock glaciers to be 18,646 acre-feet (AF) which constitutes a 1:46 rock glacier to glacier water volume for this region. At the global scale, Jones et al., (2018) compiled an inventory exceeding 73,000 rock glaciers with a water equivalence of 83.72 +/- 16.74 Gt and water volume ratio of 1:456 compared to glaciers.

Haeberli (1975) categorized the entire periglacial belt into 200 m vertical increments and established that 60% of alpine permafrost existed between 2600 – 2800 m in the Grialetsch area of the Swiss Alps. Heterogeneous distribution of permafrost suggests variation in water quantities across altitude. Altitudes of high permafrost concentrations equate to large water reserves that will melt away when the 0℃ isotherm rises to that elevation with climate change; therefore, these are considered climate-sensitive altitude thresholds. Relict rock glaciers exist at lower elevations and are past water reserves that have already been depleted due to the rising 0℃ isotherm (Morris, 1987; Jones et al., 2018).

Climate Change

Earth's atmosphere has warmed 1℃ since pre-industrial levels. Future warming is projected to rise 1.5℃ to >4℃ above pre-industrial levels by the end of the 21st century (IPCC, 2014). The amount of warming will depend on the success of our climate change

mitigation efforts. This warming trend will trigger numerous ecological feedback loops that compound the issue (Pecl et al., 2017). The profound effects of a warming climate will influence geoecological processes and ecosystem services, thus altering patterns of human well-being and catalyzing potential for conflict (Young and Lipton, 2006; Opdam, 2009). Therein lies the importance of water sources that may mitigate stress put on the human environment.

Climate Change with Elevation

One important climate-driven feedback in the alpine environment is Elevation-Dependent Warming (EDW). EDW refers to progressively increasing rates of warming with increased elevation or an elevation band of enhanced warming rates (Salathé et al., 2010; Pepin et al., 2015; Karmalkar and Bradley, 2017; Palazzi et al., 2018; Minder et al., 2018). This phenomenon is driven by several mechanisms and feedback loops in the mountain system. The most commonly cited factor in EDW is snow reduction and snow-albedo feedbacks, which effectively decrease the reflectivity of high mountain environments (Pepin and Lundquist, 2008; Rangwala et al., 2013; Palazzi et al., 2017; Minder et al., 2018; Palazzi et al., 2018). Additionally, increased warming leads to a higher ratio of precipitation falling as rain rather than snow, which contributes to melting of glaciers and snowpack (Pepin et al., 2015). Black carbon deposits are another important mechanism because these deposits are highly absorptive and decrease albedo of the alpine cryosphere (Kaspari et al., 2020). Furthermore, atmospheric humidity is expected to increase with climate change (Minder et al., 2018), which augments downward longwave radiation (DLR) (i.e., increased atmospheric humidity and cloud

cover reflect longwave radiation back to Earth) and amplifies warming at high altitudes (Rangwala et al., 2013; Pepin et al., 2015; Palazzi et al., 2017; Palazzi et al., 2018; Minder et al., 2018). Moreover, increased surface humidity decreases the vapor pressure gradient over glaciers and snowpack, which leads to reduced sublimation and more melting (Bradley et al., 2004). Melting requires less energy expenditure than sublimation to ablate the same amount of ice thereby further driving albedo reduction (Bradley et al., 2006).

Climate Change in the Nival Belt

The nival belt relies on perennial maintenance of snow and ice. As glaciers respond annually to winter accumulation in relation to the summer ablation (i.e., mass balance), they offer useful information on climate-system equilibria. In the Alps, Zemp et al. (2006) documented that modern glaciers only held one third of the 200 km^3 ice volume estimated in 1850. They noted that many alpine environments across the globe were experiencing a substantial decrease in glacial mass at a rate that has accelerated over the past twenty years. In the North Cascades, glaciation is expected to decrease to 42-5% of the total area observed in 1900 (Gray, 2019).This warming trend will result in widespread deglaciation over entire mountain ranges, which will affect the entire alpine system, including the water cycle.

Climate Change in the Periglacial Belt

Rock glaciers are significantly less climate-sensitive than glaciers. Glaciers exhibit ubiquitous retreat worldwide (Pelto, 2006; 2008), whereas rock glaciers are advancing in many cases (Osborn, 1975; Haeberli et al, 2006; Monnier and Kinnard,

2013; Jones, 2018), or at least have a delayed response to the warming climate before internal permafrost starts degrading (Rangecroft, 2015; Anderson et al., 2018). A debris-covered glacier to rock glacier transformation may occur as quickly as <100 years (Anderson et al., 2018). Jones et al., (2019b) used stereo photogrammetry to study the Chola Glacier in the Himalaya and concluded that it is quickly transitioning into a rock glacier due to rapid climate change, thereby prolonging this water reserve. Alternatively, Haeberli et al., (1998) argued that talus-derived rock glaciers typically form over thousands of years based on documented flow velocities. Therefore, it is possible that talus-derived rock glaciers require longer time scales to develop compared to glacier-derived rock glaciers. In any case, rock glaciers are less thermally coupled to ambient temperatures so they are less sensitive to climate fluctuations than glaciers; however, with continued warming, intact rock glaciers will eventually transition into a relict, ice-absent state (Jones et al., 2018a, 2019a). Thus, relict features are important representations of water resources already foregone to rising global temperatures.

Climate Change in the Forest Belt

Within the forest belt, the expected response to warming temperatures is upslope migration of the timberline and tree growth enhancement (Peili et al., 2020). According to Moir and Huckaby (1994) who studied timberline from Canada to New Mexico, warmer temperatures force alpine tundra retreat as this zone is displaced by timberline advance. In the Himalaya between 1982-2006, records show an increase of 1.5°C and remote sensing revealed a significant timberline shift upslope (Peili et al., 2020). Similarly, in the Andes, aerial imagery spanning 42 years was used to observe a

timberline shift of 10 m, which has severe implications for biodiversity of narrow elevation ranges in steep elevation gradients (Lutz et al., 2013). High mountain areas are warming at disproportional rates (Rangwalla and Miller, 2012; O'Donnell et al., 2016; Jones et al., 2019b) and the increasing MAAT is causing permafrost to melt, periglacial processes to decline, and timberline to advance.

Climate Change in the North Cascades

Snowmelt provides 70% of annual streamflow in semi-arid mountain ranges in the United States (Mote et al., 2007). With warming temperatures, precipitation increasingly falls as rain rather than snow which causes snowpack decline and shifts peak streamflow to earlier in the water year (Elsner, 2010; Cohen et al., 2020). In the Cascades, April 1st snow-water equivalence (SWE), which is strongly correlated to summer water supply, has declined 15-30% and mirrors the trends expected with rising greenhouse gas emissions (Mote et al., 2007; Mote et al., 2018). Temperatures are expected to increase 0.3℃ per decade in the Pacific Northwest and climate simulations project a 56-70% decrease in April 1st SWE for Washington by the end of the 21st Century (Elsner, 2010).

The most heavily glacierized area of the contiguous United States is the North Cascades and spatial analysis over a half-century indicate that 240 of the 742 glaciers are shrinking (O'Neal et al., 2015). Granshaw and Fountain (2006) reported a 7% decline in glacial area from 1958-1998, a net loss that equated to 6% of late summer streamflow. In the upper Columbia River Basin in British Columbia, glacier contribution ranged from 9-19% of annual water yield in heavily glacierized areas (Moore et al., 2020). The same

study also compared the time periods of 1985-1999 and 2000-2018, and the results strongly indicated that glacial contributions to river discharge have already passed peak water for this river and will continue declining with climate change.

The lower threshold of glaciation rises with increased continentality in the Cascades at a gradient of 10-12 m/km, which is similar to patterns found in other maritime mid-latitude mountain belts with westerly prevailing winds (Porter, 1977). This lower glaciation threshold has ascended 900 m +/-100 m since the maximum advance of the late Pleistocene Fraser Glaciation (Porter, 1977). This indicates radical change occurred in the elevation of mountain geoecological belts in this environment; therefore, significant geoecological change can be expected with continued global warming. In the North Cascades, Pelto (2008) conducted annual mass balance measurements on 9 select glaciers, which revealed an average 30-50 m loss of glacier thickness from 1984-2004. This deficit equates to 18-32% of the entire ice volume of the North Cascades. In the Eastern Cascades, Riffle (2018) found a glacier water equivalence of 1.074 km^3 (870,707 AF) compared to the rock glacier water equivalence of 0.023 km^3 (18,646 AF), which is a rock glacier to glacier ratio of 1:46. This finding demonstrates the hydrologic importance of glaciers regionally. Climate models forecast a 2.1 – 4.8°C median increase in temperature for the Pacific Northwest throughout the 21st century (Climate Impacts Group, n.d.). With warming climate, rapid deglaciation will likely produce more glacier-derived rock glaciers as ELA rises (Whalley, 1997; Anderson et al., 2018; Jones et al., 2019b); however, with continued warming, these rock glaciers will ultimately respond with ice volume loss as active layers thicken and underlying permafrost thins. Although

some rock glaciers within the North Cascades are still intact and advancing, some lower altitude rock glaciers are relict (Goshorn-Maroney, 2012; Weidenaar, 2013; Riffle, 2018; Lillquist and Weidenaar, 2021), indicating they have already succumbed to a warming climate. High mountain environments already exist in proximity to the 0°C isotherm (Washburn, 1980), hence these are highly sensitive environments and rapid climate change will significantly affect these geoecological zones.

CHAPTER III

STUDY AREA

Physiographic Setting

Located in Washington State, the study transect is nested within the North Cascades; the northern section of the N-S oriented Cascade Range extending from Mt. Garibaldi in British Columbia to Mt. Lassen in California (Haugerud and Tabor, 2009). The E-W transect is bounded longitudinally at 120.1°W - 121.3°W and latitudinally at 48.6°N - 49°N (*Figure 3.1*). This study area lies within Whatcom and Okanogan counties, and the Pasayten Wilderness of the Okanogan-Wenatchee National Forest.

This study area contains 53 rock glaciers that represent either side of the Cascade Crest and multiple altitude belts. This region has more intact rock glaciers west of the Crest than other areas in the Washington Cascades, along with an abundance of rock glaciers east of the Crest; therefore, it is the most suitable transect for this research. Ten rock glaciers were surveyed in the field, representing 17% of the total population in the study area.

Geology and Glaciation

The Cascades are an expression of polygenetic orogeny that decorate the skyline with high-altitude peaks and produce a significant W-E climatic gradient. The North Cascades are geologically complex, consisting of sedimentary, metamorphic, and intrusive igneous rocks. Crustal thickening and metamorphism caused many sedimentary layers to recrystallize into schist, phyllite, and orthogneiss. Furthermore, periods of folding and strike-slip faulting have structurally influenced this area (Haugerud and

Tabor, 1999). The region has been deeply incised, creating the impressive relief of the North Cascades. These mountains commonly exhibit 1,200-1,800 m of relatively uninterrupted elevation gain. The highest summits in the region (but outside of the study area) are Glacier Peak (3,213 m) and Mt. Baker (3,286 m).

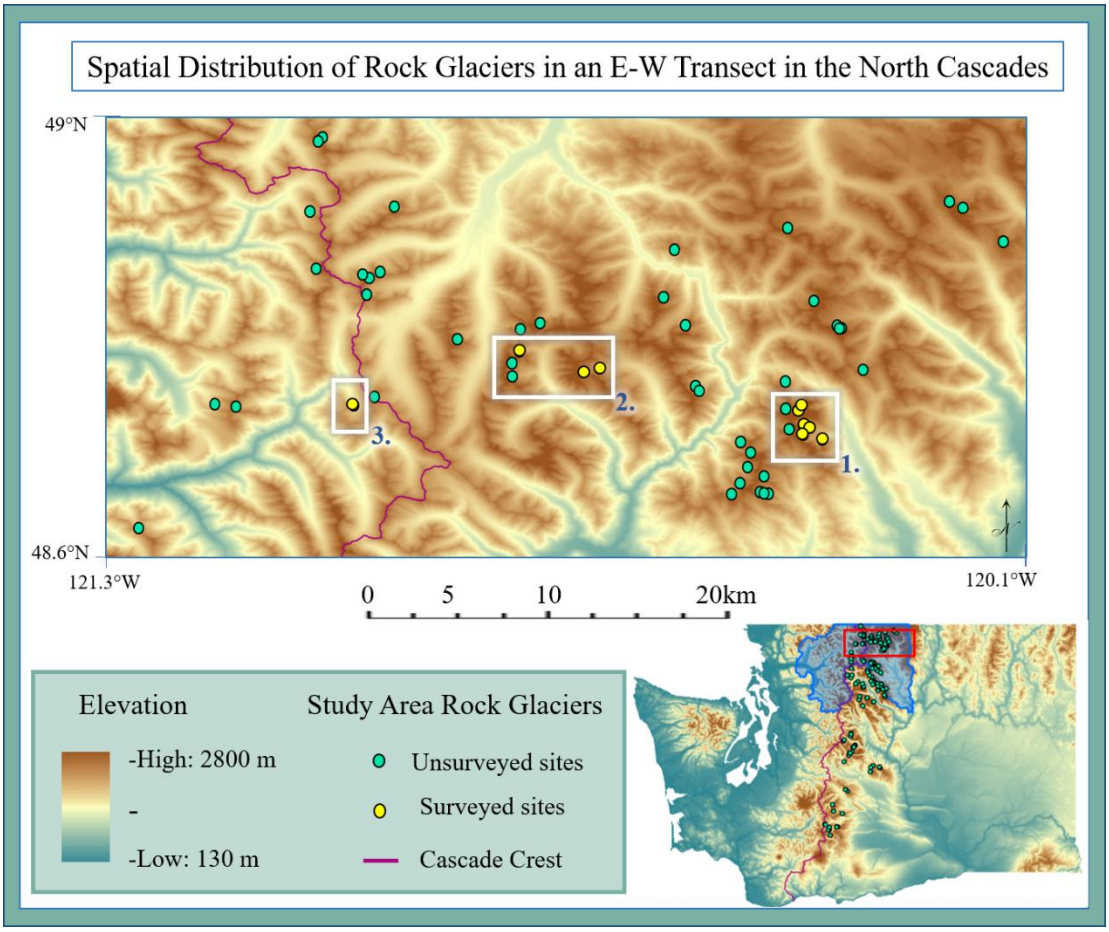

Figure 3.1. Spatial distribution of rock glaciers and their elevations in the North Cascades study area. The white boxes indicate the sites that were visited in the field: 1. Eightmile Creek, 2. Lost River, 3. Canyon Creek. Headwaters in this transect drain into the Skagit River (west) (site 3) and Methow River (east) (sites 1 and 2) watersheds shown in the inset map. Elevation data courtesy of the USGS.

During the late Pleistocene, the Cordilleran Ice Sheet covered much of this region and reached a maximum extent around 16.3 ka, after which it started back wasting to the

north (Riedel et al., 2007; Riedel, 2017). Examples of the profound glacial modification of this environment include reorganized drainages, moraine deposits, kame terraces, and prominent scouring on the landscape (Haugerud and Tabor, 2009; Riedel, 2017). Repeated alpine glaciation is revealed through over-steepened cirques, underfit streams, and extensive, interconnected valleys (Riedel et al, 2007). This history of intense glaciation produced the high-profile peaks and valleys that dominate North Cascade topography (Haugerud and Tabor, 2009).

Climate

During the Miocene, the Cascades reached sufficient elevation to create very different climates across only 1-2° change in longitude. West of the Cascades Crest at Mt. Baker (site A., *Figures 3.2, 3.3*) is a maritime climate and annual temperatures range from 5 to 24℃. Moving eastward across the mountain crest, the climate is progressively more continental, and temperatures annually range from -3 to 28℃ at Salmon Meadows (site C., *Figures 3.2, 3.3*) (WRCC). Likewise, the mountains produce a significant orographic precipitation gradient that exceeds 250 cm annually on the maritime western slopes and decreases to ~75 cm on the eastern, more continental, slopes (*Figure 3.3*) (WRCC). Enhanced precipitation on the west flank of the Cascades produces the wettest climate in the contiguous United States (Dipietro, 2018). Furthermore, the snow water equivalent (SWE) changes dramatically in this environment with an average April 1st SWE of 1480 mm at MF Nooksack (site D1) and 246 mm at Salmon Meadows (site D3) (Chart D., *Figure 3.3*) (NRCS). Prevailing winds of this mid-latitude mountain belt are westerly throughout the year (Mote et al., 2007; Cohen et al., 2020). During the winter,

the study area is within the trajectory of the Pacific storm track, whereas in the summertime, high pressure systems produce a dry climate in the Pacific Northwest (Mote, 2003; Pelto, 2006; Abatzoglou et al., 2014).

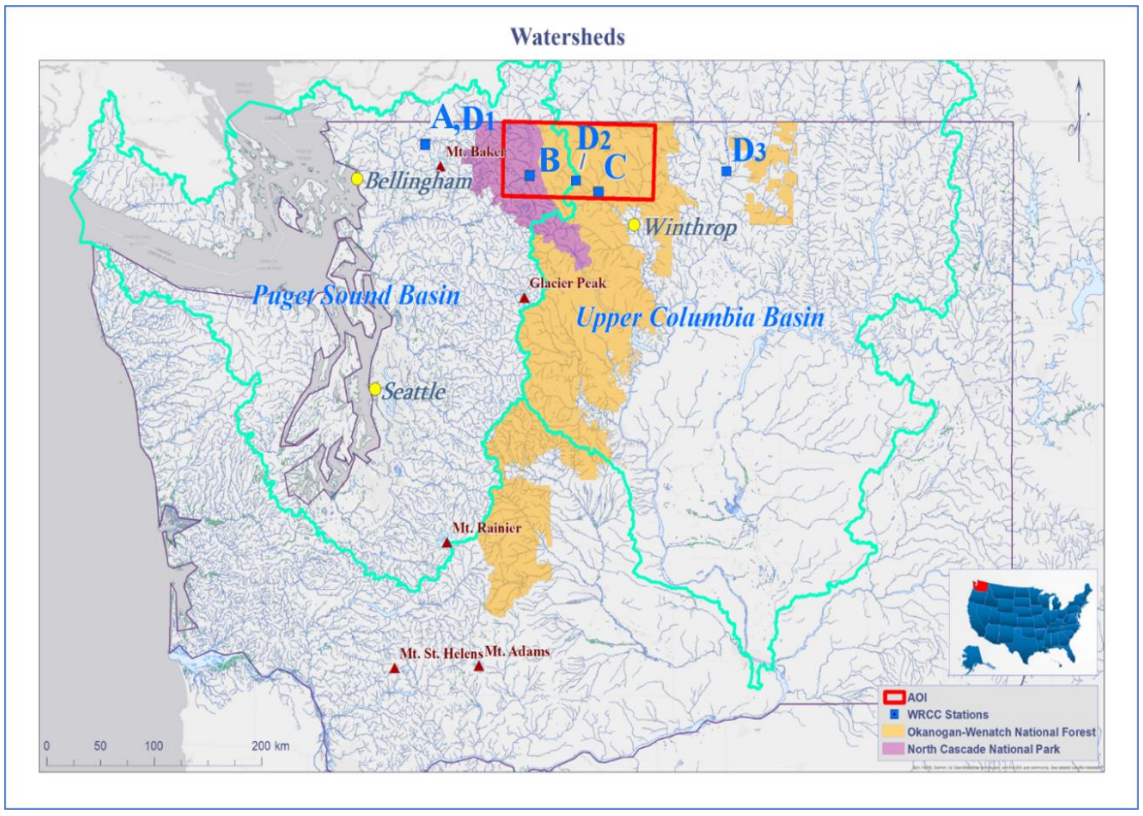

Figure 3.2. Study area in relationship to regional watersheds, cities, and prominent mountains. Sites A) Glacier Ranger Station, B) Ross Dam Station, and C) Mazama Station indicate temperature and precipitation monitoring stations by the National Resources Conservation Service (NRCS). Sites D1) MF Nooksack, D2) Harts Pass, and D3) Salmon Meadows indicate SWE monitoring sites by the Western Regional Climate Center (WRCC). The spatial hydrology data is courtesy of the National Hydrology Dataset (NHD) and the Federal Geographic Data Committee.

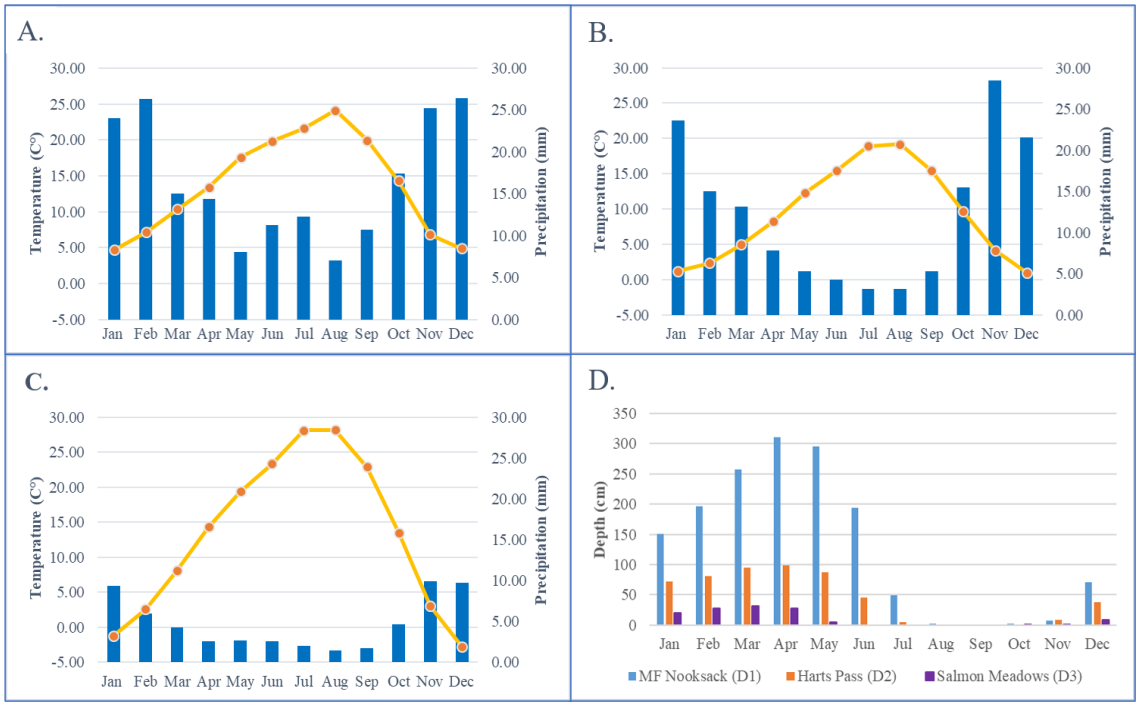

Figure 3.3. Climographs representing the orographic climatic gradient in proximity to the study area. These include: A) Glacier Ranger Station, the B) Ross Dam Station, and C) Mazama Station. Additional data on average snow depth is provided from SNOTEL sites that spatially correspond as close as possible with the temperature and precipitation sites. The SNOTEL sites include: D1) MF Nooksack, D2) Harts Pass, and D3) Salmon Meadows. Courtesy of Western Regional Climate Center (WRCC) and the Natural Resources Conservation Service (NRCS).

Hydrology

North Cascade drainages were structurally influenced by northwest-southeast strike slip faulting (Haugerud and Tabor, 2009), and subsequent Pleistocene glaciation reorganized stream patterns. The Skagit tributaries display dendritic and rectangular drainage patterns, whereas, in the Methow headwaters, divide migration produced a reversed dendritic drainage and fish hook tributaries (Riedel et al., 2007). Interlacing this complex network are long U-shaped valleys that are connected through V-shaped canyons (Riedel, 2017).

The North Cascades have over 700 glaciers and is the most glaciated region in the Pacific Northwest. Water stored in glaciers or rock glaciers within the study area is released seasonally and flows into the Skagit tributaries and into the Puget Sound or into the Methow, an upper Columbia River tributary. Water sources collected in these high-altitude systems, eventually support downstream ecosystem services, hydroelectric power, domestic use, and irrigation (Iribarren et al., 2018).

Timberline and Vegetation

The lower elevation limit of intact rock glaciers aligns approximately with timberline. At this ecotone, trees are under extreme stress and may only partially develop into dwarf-like forms (i.e., krummholz). This gradual decline in tree development is the ecotone transition into treeless alpine tundra. Multiple variables drive the change from forest to krummholz to tundra with increasing elevation, but the primary factor appears to be insufficient summer temperatures (Arno, 1984; Sakio and Masuzawa, 2020). Timberline around the world exists in similar climates and is associated with 10°C mean air temperatures during the growing season (Wardle, 1971; Kupfer, 1996; Cheng et al., 2020). In the North Cascades, the timberline elevation is 1400 m at Mt. Baker. Approximately 100 km to the east, the same ecotone rises to 2100 m in the more continental environment (Arno, 1966, Fagre et al., 2003). This incline in timberline is related to distance from the maritime influence of heavy snow and cloudy summers (Arno, 1984).

The timberline trees vary depending on location relative to the Cascade Crest. West of the crest, the timberline vegetation is dominated by mountain hemlock (*Tsuga*

mertensiana), subalpine fir (*Abies lasiocarpa*), and the occasional Alaska cedar (*Callitropsis nootkatensis*). In the east, subalpine fir still composes the timberline, accompanied by Engelmann spruce (*Picea engelmannii*), whitebark pine (*Pinus albicaulis*), and subalpine larch (*Larix lyallii*) (Arno, 1966, 1984; Mack et al., 1979).

Study Sites

Eightmile Creek

On the USFS road 5130, the Billy Goat and Copper Glance trailheads were used to access 6 rock glacier sites along the North and East faces of Isabella Ridge (*Figure 3.4*) during July 10-15 and August 24-28, 2020. This ridgeline consists of glacially eroded, andesite peaks crowned by Big Craggy Peak at 2,580 m (Stoffel and McGroder, 1990). Headwaters at this site flow to the valley floor at 1,320 m into Eightmile Creek which is a tributary of the Methow River. This site is approximately 29 km east of the Cascade Crest and the general latitude is 48.7 - 48.8 N°. The climate of this area is sub-humid with 1538 mm mean annual precipitation (MAP) and 1.1°C mean annual temperature (MAT) (PRISM Climate Group, n.d.). The Diamond Creek Fire burned much of the vegetation in this area in 2017. The remaining vegetation is often confined to higher elevations and includes many Englemann spruce and subalpine larch. Several alpine lakes occupy cirques below this ridgeline including No Dice Lake and Copper Glance Lake. These are tarns that formed from melting ice and snow that filled the depressions left behind by alpine glaciers. Isabella Ridge was partially inundated by the Cordilleran Ice Sheet, which reached 2000-2200 m elevation at this site, so peaks above this elevation remained exposed (Riedel, 2017).

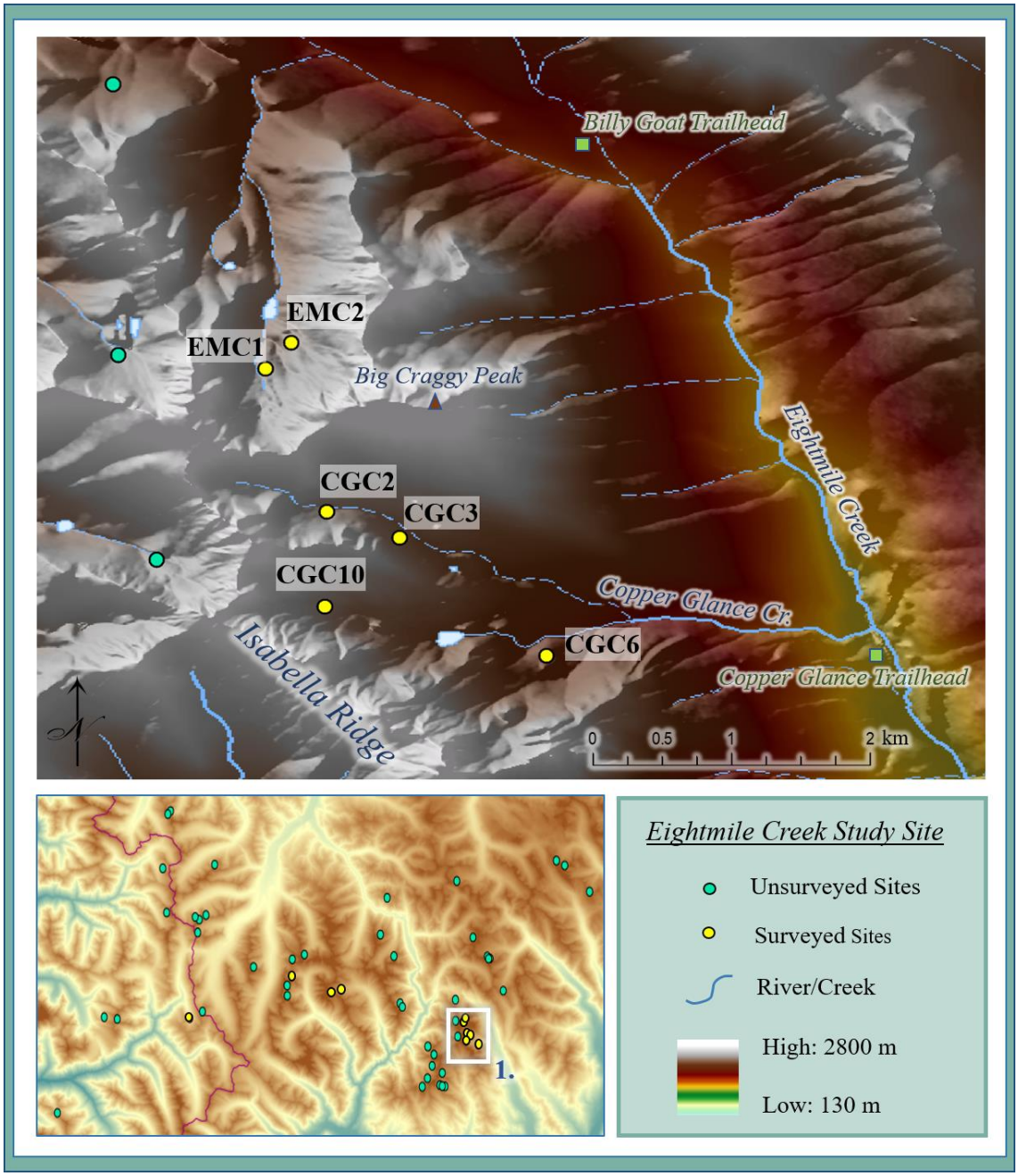

Figure 3.4. Eightmile Creek Study Site. Note the six rock glaciers that were surveyed in this area. EMC1 and EMC2 represent the Eightmile Creek 1 and Eightmile Creek 2 rock glaciers. CGC2, CGC3, CGC6, and CGC10 indicate the Copper Glance Creek 2, Copper Glance Creek 3, Copper Glance Creek 6 and Copper Glance Creek 10 rock glaciers.

Lost River

East of the Middle Fork Pasayten River, numerous rock glaciers occupy the northern slopes of several high-relief peaks accessible from the Slate Peak trailhead near Harts Pass. Our team followed the Middle Fork Pasayten Trail then Eureka Creek Trail toward Shell Pass before deviating from the trail to access these remote backcountry sites. We surveyed three sites that exist in the shaded catchments below Monument Peak (2,618 m) and Mount Rolo (2,467 m) (*Figure 3.5*) between July 23 – August 2, 2020. Monument Peak consists of granite and Mount Rolo is composed of shales, sandstones, and conglomerates (Stoffel and McGroder, 1990). Elevations of this study site ranged from 2,665 m (Mount Lago) to 900 m (Lost River). The Cordilleran Ice Sheet occupied this area, but many nunataks above 2,200 m protruded through the top of the ice sheet (Riedel, 2017). The topography retains the signature of the Pleistocene ice sheet and alpine glaciation expressed in long U-shaped valleys and the abundance of steep cirques. The western boundary of this study site was marked by the Cascade Crest and it spanned 16 km to the east with an approximate latitude of 48.7 – 48.8°N. The climate is sub-humid with a MAP of 1524 mm and a MAT of -0.8°C. Numerous alpine lakes are scattered across the cirques in this area and tributaries drain into the Methow River Watershed. The vegetation observed included Englemann spruce, subalpine larch, and whitebark pine.

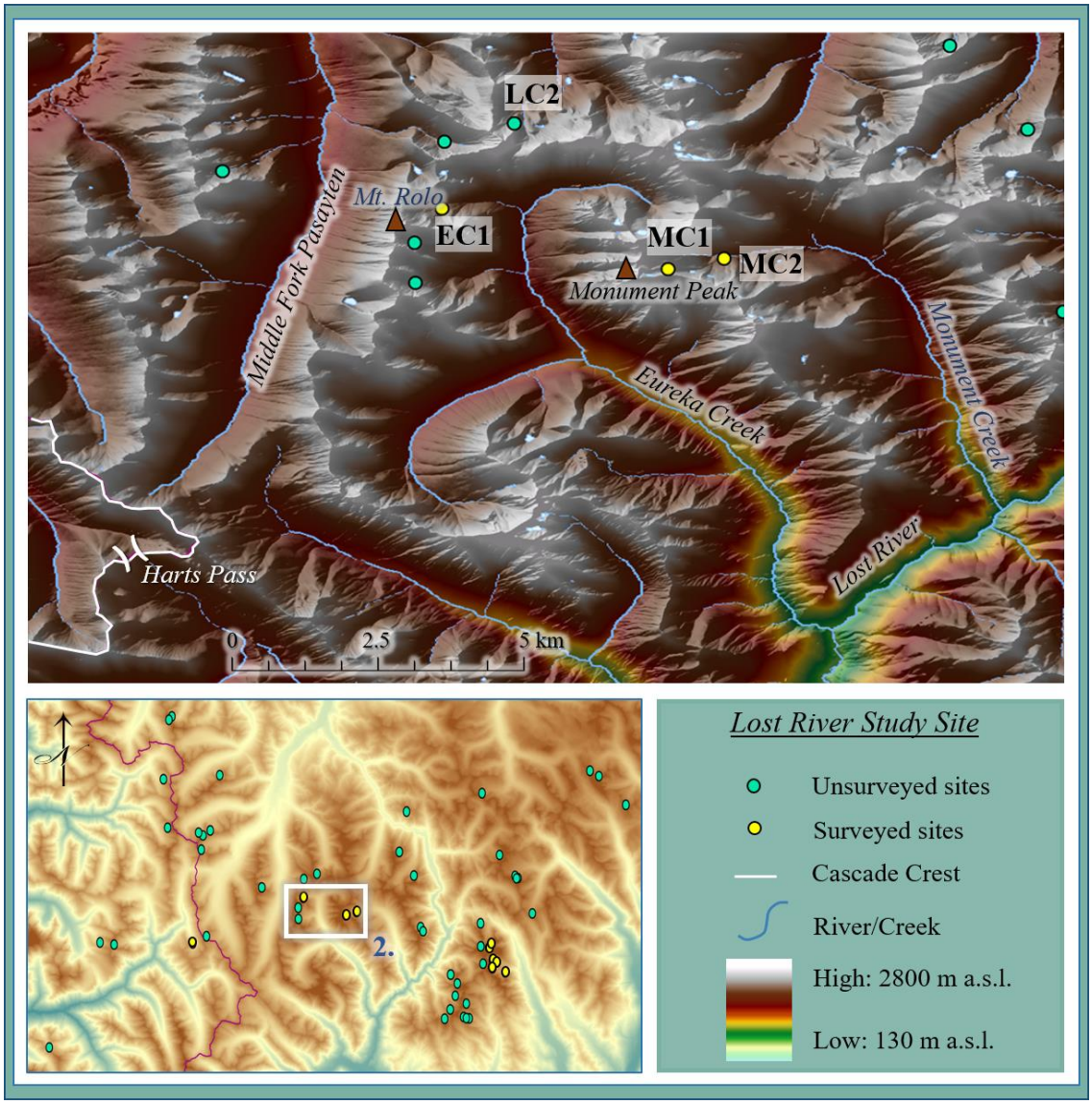

Figure 3.5. Lost River Study Site. Note the three rock glaciers that were surveyed plus the eight other rock glaciers that were not surveyed in this area. MC1 and MC2 indicate the Monument Creek 1 and Monument Creek 2 rock glaciers. EC1 marks the Eureka Creek 1 rock glacier. LC2 shows the Lease Creek 2 rock glacier which proved inaccessible for surveying.

Canyon Creek

This site is located in a north-facing cirque on the west side of the Cascade Crest. The bedrock consists of marine sedimentary rock deposits including shale, conglomerate, and sandstone (Stoffel and McGroder, 1990). Elevation of this study site ranged from 2221 m (Tamarack Peak) to 1000 m (Canyon Creek). The approximate latitude of this area is 48.7 – 48.8°N. Our team visited this site August 19-23, 2020 by using the Pacific Crest Trail starting at Harts Pass then taking mining roads, and finally traveling off trail. The highest point of this catchment is Tamarack Peak (2221 m), thus the Cordilleran Ice Sheet, which reached 2000-2200 m elevation in this area (Riedel, 2017), likely covered most of this site. This area has a maritime climate with a MAP of 1480 mm and a MAP of 1.8°C. The vegetation was abundant and consisted of subalpine firs and mountain hemlocks, as well as thick underbrush. Water from this catchment contributes to the Skagit River watershed.

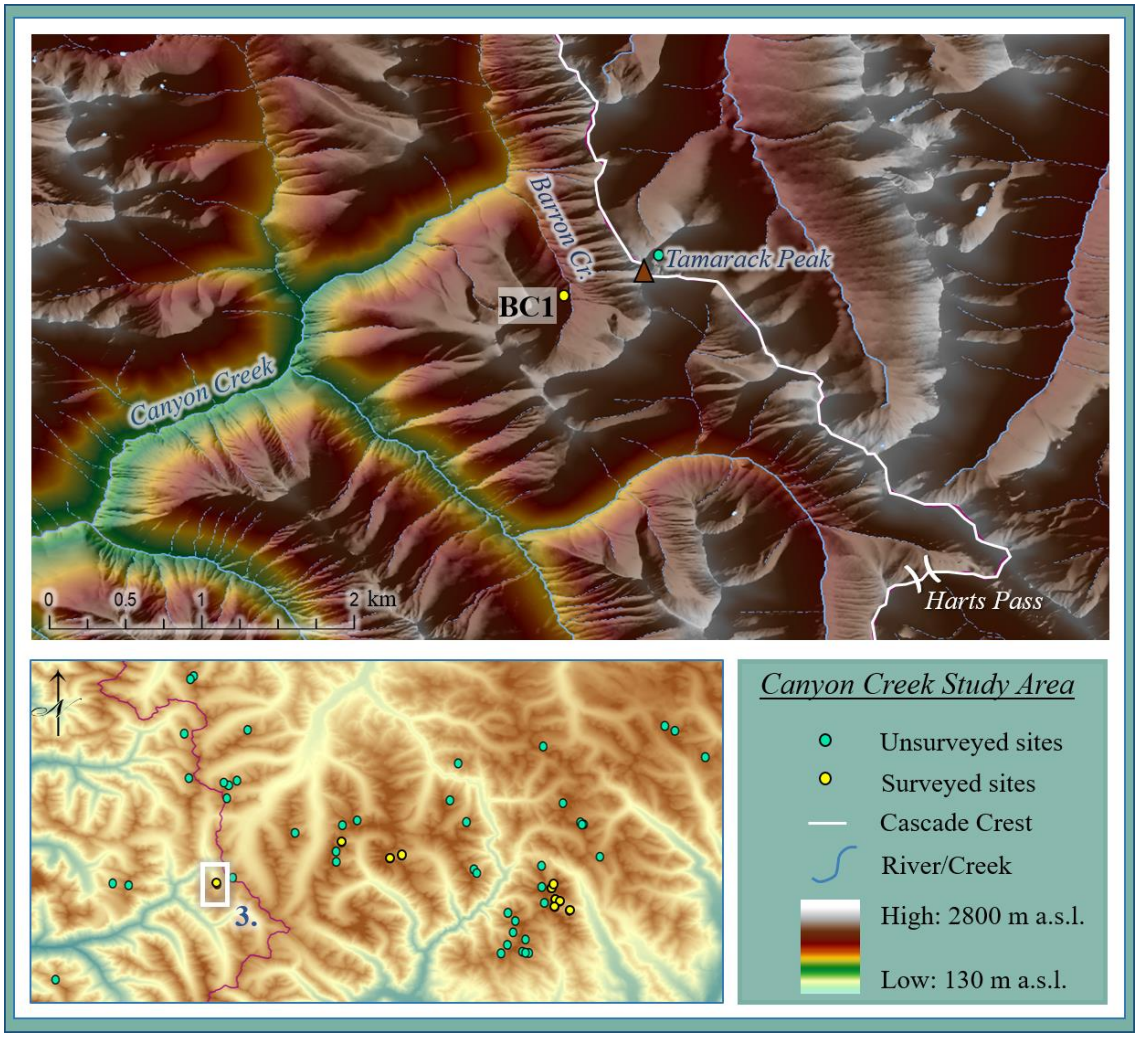

Figure 3.6. Canyon Creek Study Area. Note the west side rock glacier that was surveyed and the east side rock glacier that was not surveyed. BC1 indicates the Barron Creek 1 rock glacier.

CHAPTER IV

METHODS

Geoecological Zonation

An E-W transect in the northern Washington Cascades was selected for its relatively high concentration of rock glaciers that exist on both sides of the divide. The abundance of rock glaciers in this region offers the best prospect for understanding geoecological belt change across the Cascade crest. Furthermore, this area provides ample opportunity to study how water resources are distributed in different climatic environments trans-crest.

Equilibrium Line Altitude

Equilibrium Line Altitude data were provided by the North Cascades Glacier Climate Project (NCGCP) and the World Glacier Monitoring Service (WGMS) for glaciers in North Cascades National Park. Additional data on ELA progression along the transect outside of North Cascades National Park was calculated using contour inflection (the kinematic ELA). Also incorporated into this dataset are measurements on the South Cascade Glacier. Mass balance measurements are well documented at this site since 1960 (WGMS), and kinematic ELA measurements, recorded by Leonard and Fountain (2003), were within a few meters of that documented by the WGMS. This resolution is more than sufficient for the purpose of regional geoecological mapping (Cogley and McIntyre, 2003).

The kinematic ELA was derived from topographic maps and 1 m Digital Elevation Models by analyzing the altitude at which a glacier transitions from concave to

convex curvature (Leonard and Fountain, 2003). The combined mass balance ELA and kinematic ELA measurements provided a robust dataset for the regional nival belt and the upper limits of the periglacial belt.

Rock Glacier Initiation Line Altitude

I identified rock glaciers in the Western Cascades using aerial imagery following the criteria outlined in Lillquist and Weidenaar (2021). RILA was recorded at the highest elevation with observable inflation, furrows, or pressure ridges for each of the Western Cascades rock glaciers. These data were compiled with the Eastern Cascades rock glacier inventory to produce a dataset with the rooting zone elevations of each rock glacier. The RILA of all (n = 53) intact Cascades rock glaciers within the study area (48.6° to 49°N latitude) were used to map the elevation range of the periglacial belt (Humlum, 1988; Barsch, 1996).

Timberline

Timberline was mapped using aerial imagery on Google Earth by dividing the study area longitudinally into 10 km increments. At each segment, three timberline elevations were recorded at latitudes 48.6°, 48.8° and 49°, then averaged together to estimate the timberline elevation for that longitude. When surveying timberline, only sites revealing a gradual decline in tree development were selected as true representations of timberline. Abrupt limits of vegetation were avoided because they could be caused by external factors such as mass wasting, avalanches, or wind; thus, these tree limits may not accurately capture true timberline. Timberline elevations were based on the observable upper limit of fully developed trees, before they start transitioning into krummholz

(Wardle, 1971; Arno, 1984). These criteria were prioritized over consistency of aspect or landform while recording the change in timberline elevation across the transect. Averaging together sites of the same longitude compensated for this limitation at a sufficient resolution for regional geoecological mapping. Moreover, these methods produced a timberline trend that is consistent with the findings of Arno (1984) who documented a 700 m rise from west to east across the Cascade Crest at a similar latitude.

Measurements were halted slightly short of the east longitudinal boundary of the study area due to the semi-arid climate that does not permit full tree cover, thus timberline could not be recorded. This limitation shows the importance of rock glaciers as indicators of the periglacial-forest ecotone in areas lacking significant vegetation cover (Höllermann, 1985; Barsch, 1996). Compiling these data revealed change in this ecotone across the Cascade Crest (Charbonneau and Smith, 2018) and reinforced measurements on the regional lower limit of the periglacial belt.

Alpine Permafrost Distribution

The intact rock glaciers were classified by natural breaks in their elevation distribution using ESRI ArcMap. This classification revealed altitude variation in rock glacier concentrations and potential "goldilocks" belts of significant alpine permafrost as documented in Haeberli (1975). Next, representative sample rock glaciers were selected from each altitude classification based on spatial distribution and backcountry access. The rock glaciers in this area are spread out across the many high peaks of the North Cascades (*Figure 3.1*); however, the spatial distribution of several rock glaciers aligns nearly perfectly in a latitudinal band at 48.7°N. The aim was to survey rock glaciers in

this vicinity to isolate longitude (i.e., marine versus continental climate) as a variable in the water volume present in rock glaciers. From the rock glaciers in this latitudinal band, survey sites were selected by accessibility. Each site still required 2-4 days of backcountry travel to visit, but the other rock glaciers at this latitude were even more remote. All rock glaciers in this study area exist at northerly aspects so this parameter was consistent throughout the analysis.

Field Data Collection

In the summer of 2020, geophysical surveys of ten rock glaciers were conducted to determine the composition and structure of each feature. Ultimately, these data were used to map rock glacier water volumes across altitude and longitude within the study area. This provided information on geoecological change through the E-W transect. A series of multi-day backpacking trips, which required 30 days in the field, 200 miles of backcountry travel, and a mule convoy, enabled the study of ten rock glaciers in the Pasayten Wilderness. A map, compass, and handheld GPS were the primary means of backcountry route planning and navigation.

Internal Structure and Composition

Ground penetrating radar (GPR) is an indirect surveying method used for subsurface mapping and is often employed in the fields of anthropology and geology. Along with electrical resistivity, gravimetry, and seismic techniques, GPR has been utilized to acquire information about the internal structure of rock glaciers (Monnier et al., 2008). Degenhardt (2009) argued that GPR is an exceptionally effective mapping tool for permafrost due to the significant contrast in the electromagnetic properties of ice,

water, rock, and sediment. Additionally, GPR is particularly suitable for rock glaciers because these features have low electrical conductivity which equates to less radar wave attenuation (Annan, 2003; Monnier et al., 2008). Furthermore, some studies have drilled boreholes and conducted GPR at the same site (Maurer and Hauk, 2007; Monnier and Kinnard, 2013). These dual methodologies effectively ground-truthed the geophysical data and confirmed GPR to be an accurate rock glacier survey method as indicated by direct observations from the boreholes.

The portable pulse EKKO-Pro (Sensors & Software Inc.) GPR was provided by the Central Washington University (CWU) departments of Anthropology and Geological Sciences. The unit consists of a transmitter *(Figure 4.1)* that sends radar waves through the ground which reflect off subterranean contact layers of different materials. The radar wave propagates at different velocities depending on the density of the medium through which it is traveling. When there is a change in velocity, this indicates a change in material and the signal is reflected back towards the surface to be collected by the receiver. The return signal contains information on the impedance contrast between the object detected and the neighboring host material, as well as the shape of the detectable phenomenon (Annan, 2003). Once the receiver collects the data, the system evaluates differential radar velocities to reveal varying subterranean material. Information on internal structure is depicted as hyperbola that indicate radar reflection depths and velocities which can provide valuable insight to the internal structure and composition of rock glaciers (Monnier et al., 2008; Degenhardt 2009; Monnier and Kinnard, 2013).

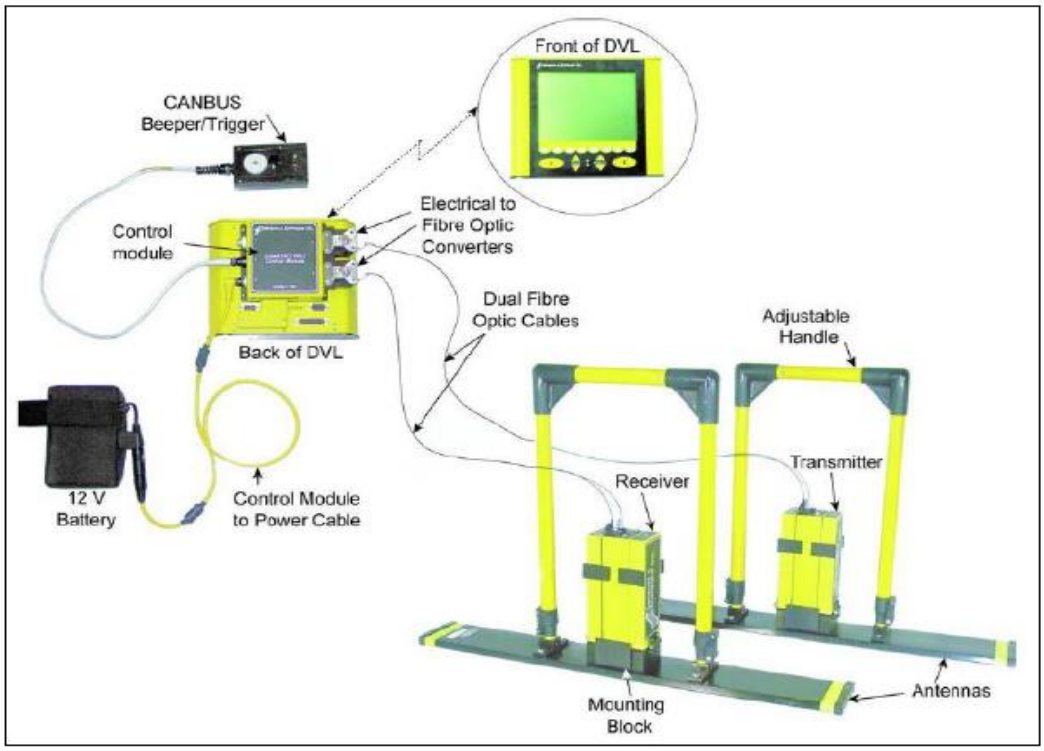

Figure 4.1. The pulse EKKO Pro System used in this research. Adapted from Sensors & Software Inc. (2012).

Depth penetration is important when utilizing geophysical methods for volumetrics. Depending on the subject being detected, the appropriate GPR antenna must be employed for the most valuable data collection. GPR has a frequency range capacity of 1-1000 MHz. High frequencies offer high-resolution data, but at the cost of depth penetration. Drilling on rock glaciers has proven that these features can exceed 70 m in thickness (Haeberli et al., 2006), thus depth range is prioritized. In general, rock glacier studies use lower frequency antenna (25-500 MHz) to reach the necessary depth for obtaining meaningful data, while sacrificing some image clarity (Annan, 2003). For this study, 50 MHz antennas were used in the field.

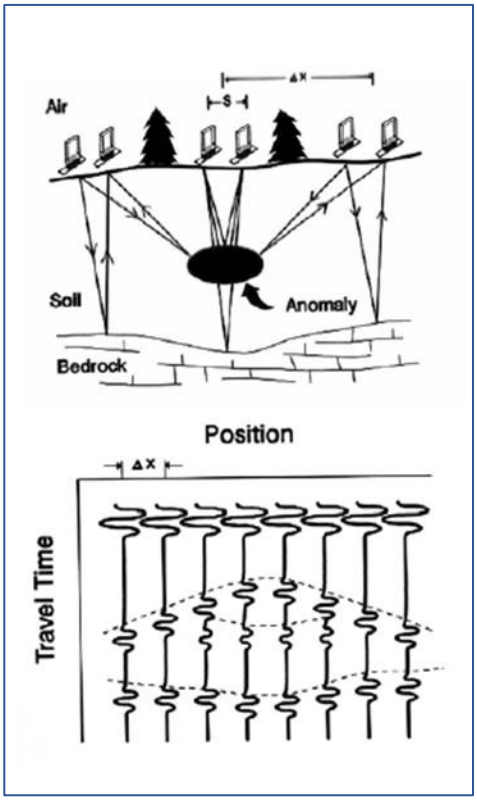

Figure 4.2. The GPR unit is moved along a survey line to acquire reflection data at regular intervals and output a profile of subterranean composition and structure. Adapted from Annan (2003).

The GPR surveys were conducted using linear transects (*Figure 4.2)* across the rock glacier surface *(Figure 4.3).* All longitudinal surveys started from the snout of the rock glacier, moving along the centerline toward the rooting zone. Transverse transects were planned out perpendicular to the flow of the rock glacier. Several transverse and longitudinal cross-sections were obtained for each feature until there was sufficient data to accurately depict the interior of the rock glacier. Each transect was first planned with a 100 m measuring tape that followed a set azimuth. After the measuring tape was laid out,

the transmitter, the DVL (Digital Video Logger), and the receiver were each operated by a team member and moved in concert along the measuring tape, stopping at 0.5 m increments to send and receive radar pulses for the entirety of each transect. GPR data were electronically saved in a database on the DVL and laser range finder data were manually recorded (see below). This method provided stratigraphic profiles that were used to estimate water volume.

Common Mid-Point (CMP) surveys were also collected at each site for accurate time-depth conversions. The process for a CMP survey is similar to the other GPR surveys we conducted. However, the team started in the center of the 100 m measure tape and the DVL operator remained stationary, while the transmitter and receiver operators moved in opposite directions away from the center point at 0.5 m increments. With CMP data, signals of the correct velocity add up constructively and the amplitude is high. Conversely, signals of the wrong velocity add up destructively and produce low amplitude signals. This process yields hyperbolas that are a weighted sum of the two-way travel time (TWTT) through different materials to find the average signal velocity for each rock glacier and accurately calibrate the GPR survey data (Annan, 2003).

Figure 4.3. The PulseEKKO PRO GPR survey at the Eightmile Creek 1 rock glacier. This image shows the transmitter (left), the DVL (center), and the receiver (right) during a transverse survey across the unstable terrain typical of rock glacier surfaces. Photo captured by Bailey Duvall, 7/13/2020.

Topography

Along with stratigraphy and composition data, high-resolution topographic data of the rock glacier surface was also surveyed. Topographic field data was collected using a CWU Geography TruPulse 360 Laser Range finder. This device uses a laser to calculate and digitally record distance, inclination, and azimuth which was collected during every survey at 10 m increments or when there was a significant change in topography. These data were compiled into Microsoft Excel spreadsheets for further analysis. A handheld Garmin GISmap 62s GPS unit was used to obtain spatially accurate data for each survey.

Data Processing and Analysis

Data processing and analysis was conducted using EKKO_Project Pro in the CWU Geography Department GIS Laboratory. The primary goal of obtaining geophysical data of rock glaciers was to determine the average active layer depth, average rock glacier depth, rock glacier composition, and rock glacier structures. In Ekko_Project Pro, depth measurements of the active layer and rock glacier base were recorded every 25 m for the entire transect of each feature. Depth measurements of the active layer were subtracted from the depth measurements of the rock glacier base and these values were averaged to determine the mean permafrost thickness of each feature.

In order to determine accurate depths for different stratigraphic layers, an average velocity for the subsurface was obtained through Semblance Analysis. In this method, CMP data were uploaded and the most distinct signal at the greatest depth was used to measure velocity in m/ns (*Figure 4.4*). The CMP data were also analyzed in a second method using a velocity calibration routine to fit a curve to the hyperbolic response in the data. *Figure 4.4* shows how the velocity extracted from the lowermost hyperbola (0.143 m/ns) matches that derived from the semblance analysis. Therefore, these mutually exclusive techniques function as a tool for verifying one another.

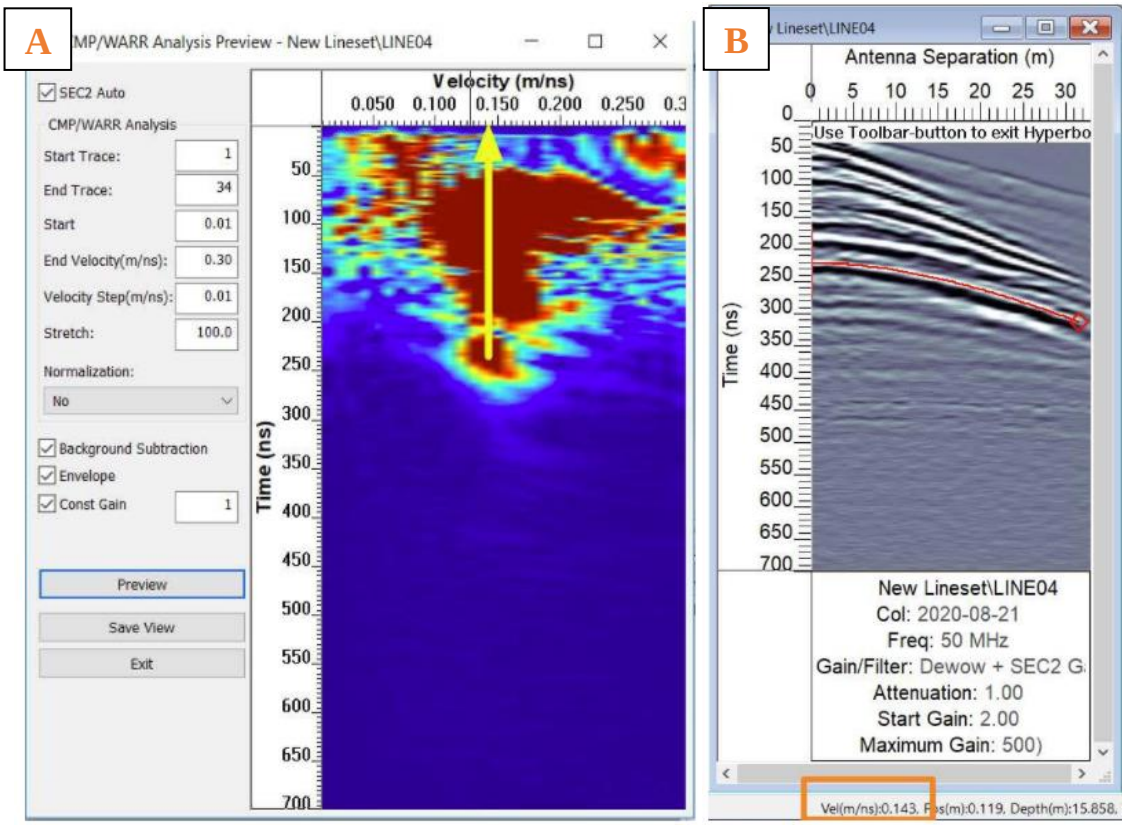

Figure 4.4. An example of the Semblance Analysis and the CMP hyperbola fitting for extracting average velocities.

Both the Semblance Analysis and hyperbola fitting methods use known propagation velocities of a given material (*Table 1*) to do a time-depth conversion and provide precise depths (Monnier et al., 2008). Average velocity and accurate depths are key to interpreting active layer thickness and rock glacier thickness, which are essential to calculating rock glacier water equivalence. Information on the internal environment of the rock glacier can provide insight to the activity and genesis of the feature as well as its role as a hydrologic storage in mountain regions (Haeberli et al., 2006; Riffle, 2018).

Table 1. Radar velocities of known material.

Water	0.033 m/ns^{-1}
Saturated Material	0.060-0.10 m/ns^{-1}
Rock	0.10-0.150 m/ns^{-1}
Ice	0.160 m/ns^{-1}
Air	0.300 m/ns^{-1}

Adapted from Annan (2003).

Once average velocities were obtained for each survey, the data were processed using DEWOW which effectively filters out the low frequency noise, while the high frequency signal remains. The 2D FFT Stolt migration operator functions as a spatial deconvolution which collapses the hyperbolic signals into point features which reflect subsurface stratigraphy more precisely. If there were any bad traces in the dataset (i.e., as the result of frayed fiber optic cables, instability of the transmitter or receiver while collecting the trace, or encountering a pocket of liquid water during the field survey), the Spatial Median Filter was applied to remove single high amplitude artifacts. Next, the Spreading & Exponential Calibrated Compensation tool (SEC2 Auto) was used to increase signal strength at depth to compensate for the exponential signal attenuation due to conductivity of subsurface material. Finally, the data were topographically corrected using the field data collected with the laser range-finder to produce realistic longitudinal and transverse profiles of the stratigraphy of each surveyed feature.

Ice-Water Equivalence

Individual water equivalence volumes were calculated for each rock glacier. This required surface area measurements of each feature acquired from the Google Earth-

based Eastern Cascades rock glacier inventory (Lillquist and Weidenaar, 2021) supplemented with my own Google Earth measurements for Western Cascades rock glaciers. The surface area of each rock glacier was multiplied by the average permafrost depth of each site to find average permafrost volume.

The literature varies on the estimated water volume a rock glacier can hold (Brenning, 2005; Millar and Westfall, 2008; Azócar and Brenning, 2010; Riffle, 2018; Jones et al., 2017, 2018, 2019a; Millar and Westfall, 2019). To overcome this discrepancy, I averaged the water volume estimated from different literature sources based on activity and genesis, as both strongly influence water capacity of the feature (Table 2). The permafrost volume of each feature was converted to the water volume equivalent (WVEQ) using the glacial ice density of 0.917 g/cm^3 (Paterson, 1994). The formula used to calculate the estimated WVEQ for each surveyed rock glacier is illustrated in *Equation 1*.

Table 2. Recommended ice estimation per rock glacier adjusted to the activity and genesis attributes of that rock glacier.

	Active 50% **(Jones et al., 2017)**	*Inactive* 40% **(Jones et al., 2017)**
Glacier-derived 75% **(Millar and Westfall, 2019; Jones et al., 2019a)**	(75% +50%)/2= **62.5% : active, glacier-derived**	(75% + 40%)/2= **57.5% : inactive, glacier-derived**
Talus-derived 50% **(Jones et al., 2017; Azócar and Brenning, 2010)**	**50% : active, talus-derived**	(50% + 40%)/2= **45% : inactive, talus-derived**

$$(\text{PFD}) \times (\text{SA}) \times (\%\ \text{Ice}) \times (\text{Ice Density}) = \text{RG WVEQ} \qquad (1)$$

Where *PFD* is permafrost depth; *SA* is rock glacier surface area; *% Ice* is the estimated ice percentage based on activity and genesis (Table 2); *Ice Density* is the glacial ice density of 0.917 g/cm^3 (Paterson, 1994); and *RG WVEQ* is rock glacier water volume equivalent.

Riffle (2018) estimated the WVEQ of the Eastern Cascades rock glaciers by using the empirical formula of Brenning (2005) then deducting 64% (i.e., the average error when applying Brenning's formula to the rock glaciers Riffle surveyed with GPR). However, the error ranged from 7-145% when applying Brenning's empirical formula to the eight rock glaciers that Riffle surveyed; therefore, this estimation method yielded rather large error bars. To reconstruct a method that may offer more accurate results, the WVEQs of surveyed rock glaciers in this study were extrapolated to represent the total volume of water withheld in rock glaciers of the same elevation bracket (*Equations 2 and 3*).

$$(\text{RG}_1\text{WVEQ}) + (\text{RG}_2\text{WVEQ}) + (\text{RG}_3\text{WVEQ}) + \ldots = \text{EB Surveyed WVEQ} \qquad (2)$$

Then:

$$[(\text{EB Surveyed WVEQ}) * (\text{EB Total SA})] / (\text{EB Surveyed SA}) = X \qquad (3)$$

Where *EB* is elevation bracket; *Surveyed* is the rock glaciers that were GPR surveyed in this study; *Total* is the entire population of surveyed and unsurveyed rock glaciers in an elevation bracket; and *X* is the total water volume equivalence in an

elevation bracket. This method is effective in this study area because several of the environmental variables that influence rock glacier development are controlled. Aspect is a controlled variable since intact rock glaciers are naturally limited to north-facing cirques and ridgelines in the North Cascades. The geologic composition of the surveyed sites includes two sites of granite, five sites of andesite, and two sites of shale, conglomerate and sandstone. Even with the variance in geologic composition, the importance lies in the grain size of this fractured material (Charbonneau and Smith, 2018; Jones et al., 2019b). All sites consisted of large, angular talus, thus the variable of geology is controlled, within reason. Given that these variables are controlled, it is assumed that all rock glaciers within a similar altitude range will have a similar water capacity when scaled for surface area.

Climate Forecasting Simulation

The periglacial belt in this study area was already subdivided by normal breaks in rock glacier distribution across elevation in Arcmap. Water equivalence estimations for these rock glaciers were used to determine subdivided elevation brackets of high water content. To assess water content sensitivity, the ClimateNA simulation was used which interpolated the MAAT for each site based on 800 x 800 m PRISM data for 2019 (Wang et al. 2016, PRISM Climate Group, n.d.). This simulation was also used to project the estimated MAAT of each rock glacier in the study area by the end of the 21st Century. To project MAAT, I ran two trials of this simulation for the year 2100. These trials were based on different Representative Concentration Pathway (RCP) scenarios, which range from RCP 2.6 to RCP 8.5 and are numbered based on a range of possible radiative

forcing values (i.e., the difference between incoming solar irradiance and energy radiated back into space) in the year 2100 (IPCC, 2014). These RCP scenarios were established based on the second generation of the Canadian Earth System Model which combines the coupled atmosphere-ocean circulation model and the terrestrial carbon cycle based on the Canadian Terrestrial Ecosystem Model to incorporate land-atmosphere carbon exchange. The GHG concentrations and solar energy are based on the Coupled Model Intercomparison Project, Phase 5 (CMIP5) (Chylek et al., 2011). I ran the first simulation under an RCP 2.6 scenario in which strict climate change mitigation policies are implemented and greenhouse gases (GHGs) peak mid-century, but then are reduced over time. The second trial was based on RCP 8.5 which is the scenario in which only minimal effort is put toward climate change mitigation and GHG emissions continuously increase through time. RCP 8.5 consists of 5 ensembles (i.e., group of five slightly different models of atmospheric-oceanic interactions) which were combined and averaged to output the most likely temperatures for an RCP 8.5 scenario. This process output the projected temperature range at each study site to estimate how much water storage would be subject to melting temperatures through the century.

These calculations were intended to predict the elevation range of the rising 0°C isotherm throughout this century and reveal the amount of alpine permafrost exposed to melting temperatures. Altitude belts of high permafrost concentrations that would be exposed to warm temperatures should be deemed as highly sensitive elevations. This analysis determined altitude thresholds of greater climatic sensitivity within the mountain landscape.

Water Management Implications

The final results of this thesis will be publicly available through the Central Washington University thesis repository and Dr. Karl Lillquist's CWU website. Water volume quantification results will assist water managers in making informed decisions that incorporate climate change into planning methods. Furthermore, technical information on rock glacier water content across altitude will contribute to the geoscientific knowledge base on rock glaciers and geoecological belt evolution.

CHAPTER V

RESULTS AND DISCUSSION

Geoecological Zonation

The results of geoecological mapping of ELA, RILA, and timberline are shown in (*Figure 5.1*). Regional mapping of these ecotones revealed that each geoecological belt rises in elevation with increased continentality. Some overlap between RILA and timberline is evident in *Figure 5.1*. However, this is expected as timberline delineates the upper boundary of the forest belt which may partially encroach upon the periglacial belt, especially with continued climate change (Moir and Huckaby, 1994; Lutz et al., 2013; Peili et al., 2020).

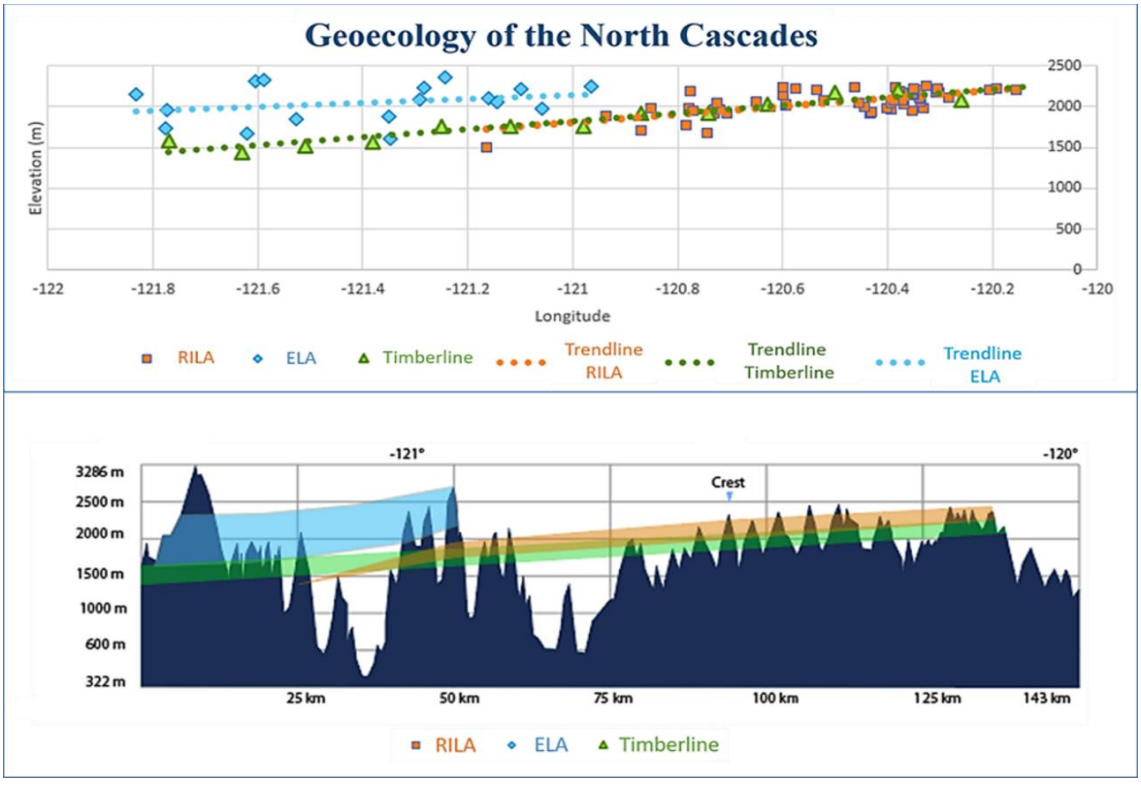

Figure 5.1. ELA, RILA, and timberline mapping at 48.8°N latitude. This mapping revealed geoecological change in the nival, periglacial, and forest belts across the maritime and continental climates of the North Cascades.

Permafrost Distribution in the Periglacial Belt

Within the periglacial belt, rock glaciers were subdivided by natural breaks in RILA to find potential clustering of rock glaciers across altitude (i.e., "goldilocks" belts) (Table 3). The six rock glaciers to the west of the Cascade Crest were not subdivided by RILA because the population was not large enough to produce meaningful data. East of the Cascade Crest, the 47 rock glaciers were subdivided by RILA; however, this did not yield any belts of preferential rock glacier development.

Table 3. Summary table of the subdivision of the periglacial belt by RILA and the associated characteristics of each elevation bracket.

Elevation Bracket (m)	***Number of Rock Glaciers***	***Number of Field Surveyed Rock Glaciers***	***Activity***	***Morphology***	***Genesis***	***Aspect Range***
East Cascades						
2353-2180	14	2	Active/ Inactive	Tongue/ Lobate/ Complex	Talus/ Glacier	341-78° (97°)
2172-2091	9	2	Active/ Inactive	Tongue/ Lobate	Talus/ Glacier	343-76° (93°)
2067-1974	14	4	Inactive	Tongue/ Lobate	Talus	351-73° (82°)
1962-1779	10	1	Inactive	Tongue/ Lobate	Talus	347-51° (64°)
West Cascades						
1981-1670	6	1	Active/ Inactive	Tongue/ Lobate	Talus	330-11° (41°)

Subdividing the rock glaciers in the study area into elevation brackets revealed a gradient of increased activity at higher elevations. Of the 9 rock glaciers in the 2091-2172 m belt, only one of them is classified as active, whereas 6 of the 14 rock glaciers in the 2180-2353 m are active, reflecting the enhanced suitability for permafrost development at

higher elevations. All rock glaciers below these elevation brackets are inactive or relict (relicts were not included in this study because they do not contain permafrost), with the exception of one active rock glacier west of the Cascade Crest (Cascade Creek 1). Tongue and lobate morphologies appear in all elevation brackets and one complex feature exists in the highest elevation bracket (Monument Creek 1). Talus-derived and glacier-derived rock glaciers appear in the upper two elevation brackets, but the lower elevations are limited to only talus-derived rock glaciers, likely indicating a previous lower elevation limit of glaciation. Additionally, all the rock glaciers had a NW-NE aspect; however, the range of rock glacier aspect progressively widened with elevation, suggesting a more suitable MAAT for permafrost development. Furthermore, the rock glaciers west of the Cascade Crest had the narrowest range in aspect, suggesting a marine environment was less suitable for permafrost development.

The results from analyzing rock glacier spatial distribution across altitude informed the decision on which of the 53 rock glaciers to survey. The selected rock glaciers represented both sides of the Cascade Crest and every elevation bracket that was delineated in Table 3. Table 4 summarizes the information about each surveyed rock glacier that was observable without geophysical instruments.

Table 4. Surveyed rock glaciers and their external characteristics.

RILA (m)	Rock Glacier	Watershed	Geology	Morphology	Genesis	Activity	Aspect (°)	Length (m)	Width (m)
East Cascades									
2353	Monument 1	Methow	G	Tongue	Glacier	Active	78	858	341
2191	Eightmile 1	Methow	A	Tongue	Glacier	Active	0	849	93
2102	Eightmile 2	Methow	A	Tongue	Glacier	Active	335	414	200
2091	Copper Glance 10	Methow	A	Lobate	Talus	Inactive	49	87	88
2066	Monument 2	Methow	G	Tongue	Talus	Inactive	18	457	288
2051	Copper Glance 2	Methow	A	Lobate	Talus	Inactive	50	98	139
2004	Eureka 1	Methow	SS, Sh, C	Lobate	Talus	Inactive	47	112	264
1981	Copper Glance 3	Methow	A	Lobate	Talus	Inactive	54	93	111
1779	Copper Glance 6	Methow	A	Tongue	Talus	Inactive	51	357	116
West Cascades									
1670	Barron 1	Skagit	SS, Sh, C	Tongue	Talus	Inactive	64	180	177

In the Geology column, the following abbreviations are used: granite (G), andesite (A), sandstone (SS), shale (Sh), conglomerate (C). This table is organized by discrete elevation brackets based on rock glacier initiation line altitude (RILA).

Rock Glacier Composition and Structure

The GPR results on the structure and composition of ten North Cascades rock glaciers are compiled in Table 5. This method proved effective at detecting evidence of permafrost and provided valuable information on the origin and activity of each rock glacier. GPR detection of the active layer base and rock glacier base enabled water volume equivalence (WVEQ) estimations for each feature.

Table 5. Surveyed rock glaciers and their internal attributes detected with ground penetrating radar.

Rock Glacier	GPR Velocity (m/ns^{-1})	$\bar{x}$ Active Layer Thickness (m)	$\bar{x}$ Bedrock Depth (m)	$\bar{x}$ Permafrost Thickness (m)	WVEQ (m^3)	Evidence of Compressional Stress	Evidence of Extensional Stress	Evidence of Shear Stress	Other Structures & Composition
East Cascades									
Monument 1	0.13	2	25.1	23.1	2,708,499				Massive Ice, Liquid water
Eightmile 1	0.142	3.9	31.1	27.2	1,314,789	X			Massive Ice
Eightmile 2	0.153	4.6	27.5	21.4	675,765			X	Massive Ice
Copper Glance 10	0.14	2.3	15.8	13.4	73,907				Debris-Rich Layers
Monument 2	0.15	2.9	17.1	14.2	618,168	X			Debris-Rich Layers, Ice-Rich Layers
Copper Glance 2	0.137	2.1	16.9	14.7	61,460			X	Debris-Rich Layers, Ice-Rich Layers
Eureka 1	0.145	2	10.6	8.5	103,626			X	Debris-Rich Layers
Copper Glance 3	0.141	1.6	11.9	10.3	27,287				Debris-Rich Layers, Liquid Water
Copper Glance 6	0.136	2	14.1	12.2	345,360				Debris-Rich Layers
West Cascades									
Barron 1	0.144	2.4	13.5	11.1	124,981		X	X	Debris-Rich Layers, Ice-Rich Layers

This table is organized by discrete elevation brackets based on rock glacier initiation line altitude (RILA).

Eightmile Creek Study Site

Eightmile Creek 1 Rock Glacier

Eightmile Creek 1 (EM1) is an active, talus-derived, tongue-shaped rock glacier (Lillquist and Weidenaar, 2021) (*Figure 5.2*). EM1 is located in a north-facing compound cirque shadowed by Big Craggy Peak. The aspect of this rock glacier is 0° and it is 849 m in length and 93 m in width. The RILA of this feature is 2,194 m and it is chiefly composed of weathered andesite with the exception of a line of relatively fine-grained, welded tuff running longitudinally on its east side. The entrainment of this tuff can be traced to the craggy ridgeline above the rooting zone where there is a vertical lenticular

layer of the same material within the predominantly andesitic cirque headwall. This tuff is a visual confirmation of the movement and debris transport occurring at this active site.

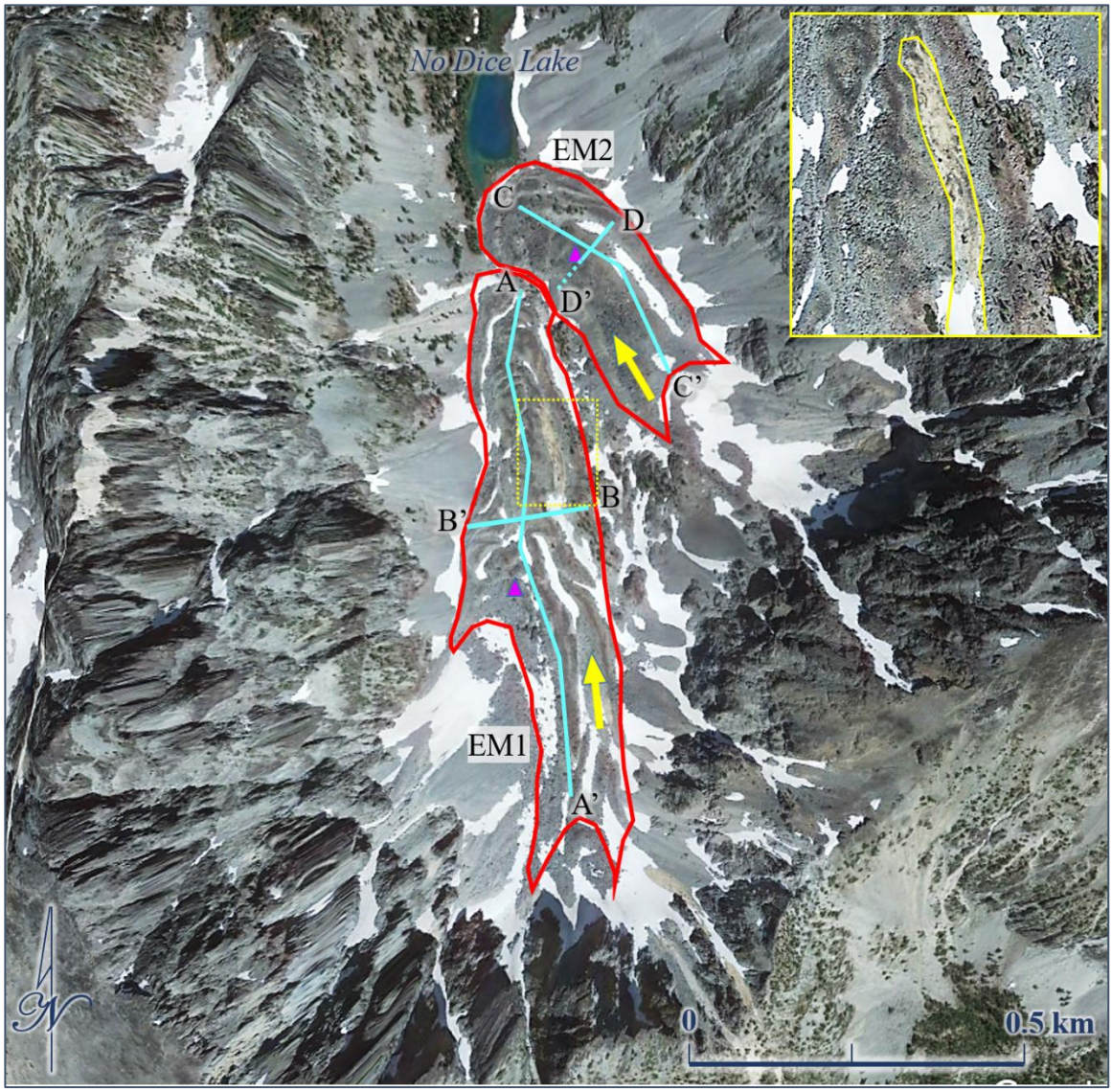

Figure 5.2. Planimetric view of the survey transects for Eightmile Creek 1(EM1) (left) and Eightmile Creek 2 (EM2) (right). The purple triangles mark the approximate locations of the CMP collection. The yellow arrows indicate flow direction. The inset map illustrates the change in rock type from andesite to the light colored, fine-grained tuff. The dotted line on EM2 indicates partial data loss of the transverse transect. Google Earth imagery from 7/14/2017.

At the time of our field visit, EM1 was entirely clear of vegetation and had patches of snow occupying linear depressions that each ran longitudinally on its surface for 100-200 m. This rock glacier is in the Methow River Watershed and ice melt from this site flows directly into No Dice Lake which feeds Eightmile Creek. The pressure ridges were exceptionally steep and the survey transect had to be adjusted several times for crew and equipment safety.

The survey revealed a distinct near reflector that was interpreted as the base of the active layer with an average depth of 3.9 m that thickened toward the snout (*Figure 5.3).* EM velocities of the active layer were >0.18 m/ns^{-1} which is expected due to air-filled voids in the debris (Monnier and Kinnard, 2013; Dr. Sébastien Monnier, e-mail from author, October 13, 2020). This well-defined near reflector at the active layer base is evidence of the permafrost contact layer because it verifies a transition to a stratigraphic layer of different composition (Monnier and Kinnard, 2015). *Figure 5.4* shows an area with a distinct rock type change from large, blocky andesite to fine-grained tuff where there is a localized increase in active layer depth. This finding is consistent with observations by Barsch (1996) and Haeberli et al., (2006) who deduced a greater active layer thickness is necessary to compensate for the diminished effect of Balch cooling due to fine grain size. Unfortunately, the GPR did not provide clear information below the active layer for the 27.5 m of tuff in the transverse transect. This may be the result of increased conductivity due to the material type and smaller grain size, which increases GPR signal attenuation.

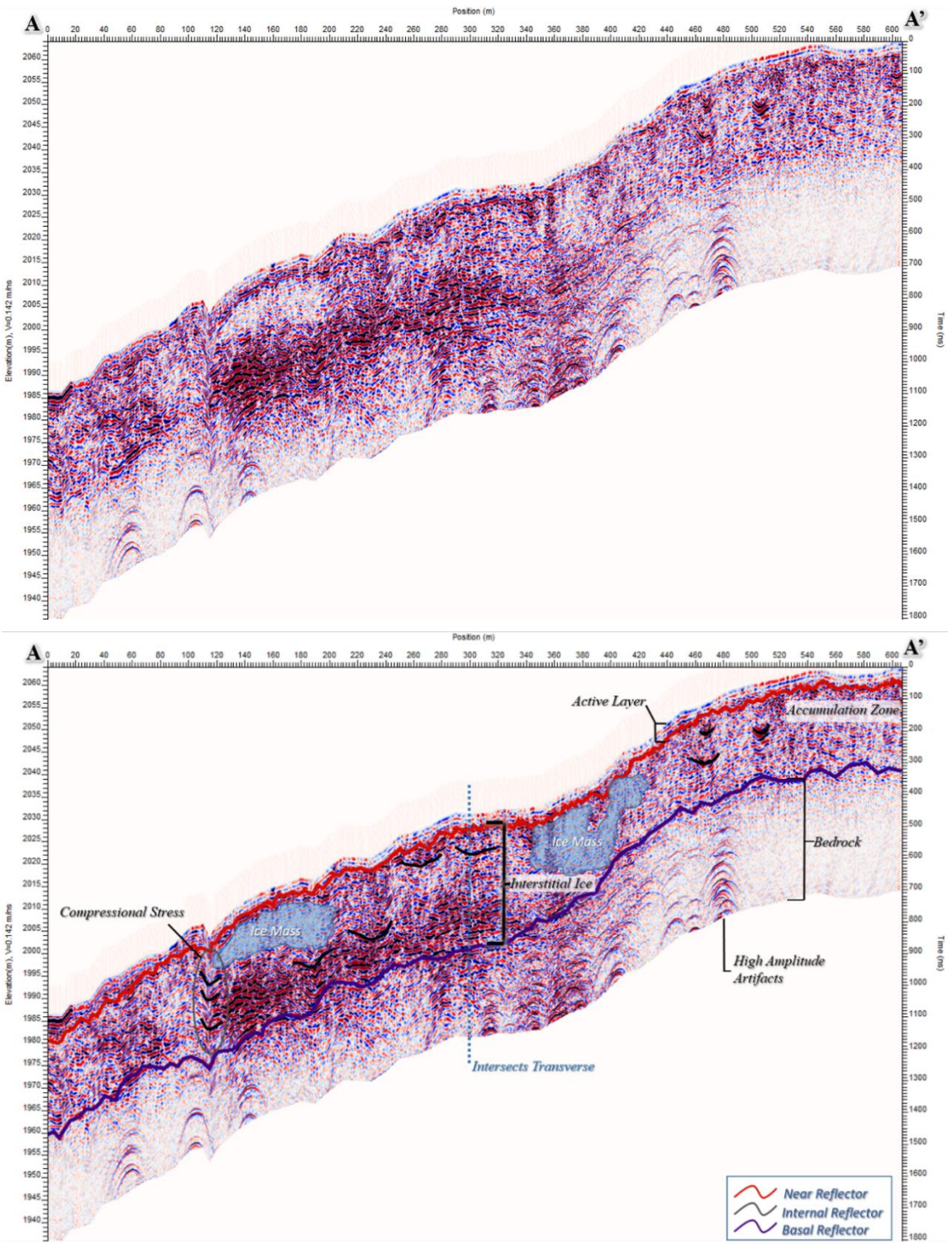

Figure 5.3. Migrated and topographically corrected longitudinal GPR profile of Eightmile Creek 1 without interpretations (upper diagram) and with interpretations (lower diagram).

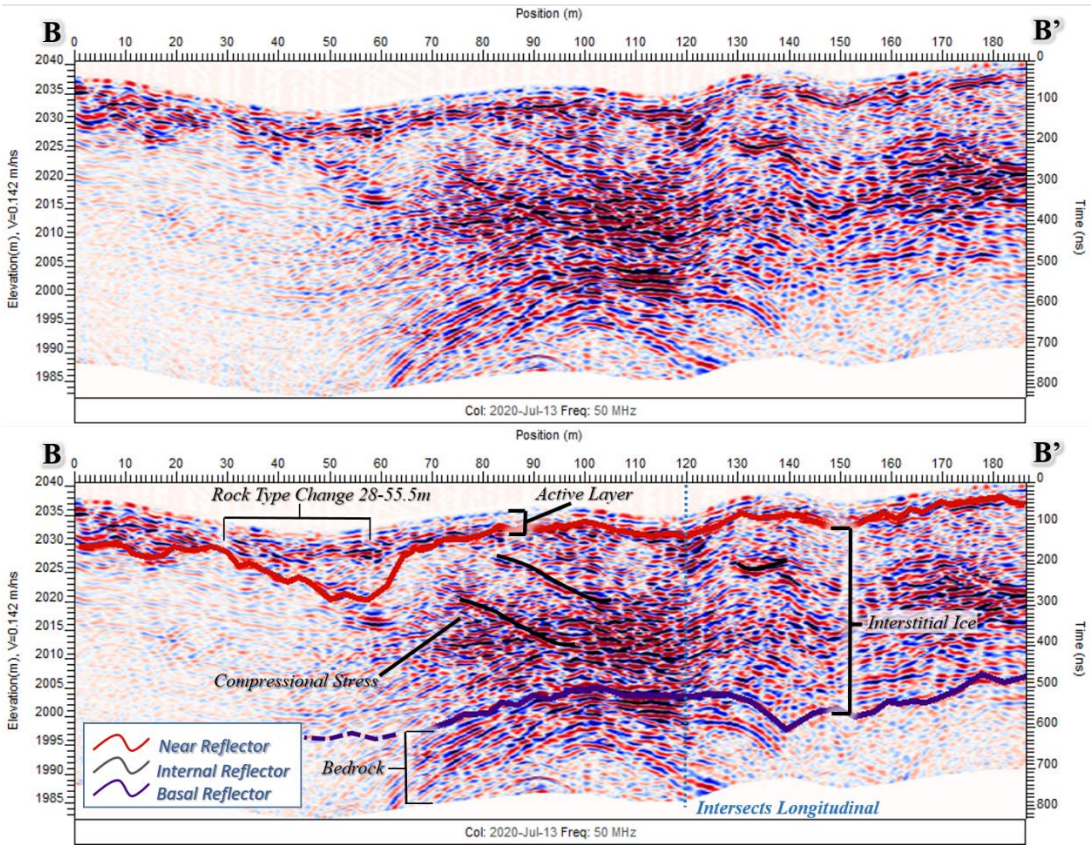

Figure 5.4. Migrated and topographically corrected transverse GPR profile of Eightmile Creek 1 without interpretations (upper diagram) and with interpretations (lower diagram). The dotted purple line indicates where the bedrock was no longer detectable due to signal attenuation.

The average electromagnetic (EM) velocity of the entire rock glacier is 0.142 m/ns^{-1} as derived from the Semblance Analysis and the Velocity Calibration routine using hyperbolic responses. This feature has a nearly continuous basal reflector which suggests contact with the bedrock at an average depth of 31.1 m (*Figure 5.3*). Several internal reflectors correspond with overlying pressure ridges and signify compressional stress caused by a decrease in the bedrock slope angle. In the transverse profile (*Figure 5.4*), the synclinal structure is reminiscent of the transverse foliation in an alpine glacier, formed by debris sedimentation that is modified by strain under plastic deformation (Hooke and

Hudleston, 1978; Fukui et al., 2008). At least two regions lack numerous diffracting points which indicates a homogenous material and suggests massive ice bodies (Kunz and Kneisel, 2020) (*Figure 5.3*). This is supported by local velocities between 0.12 – 0.16 m/ns^{-1}, which indicates permafrost-saturated material or massive ice (Monnier and Kinnard, 2013; Kunz and Kneisel, 2020; Dr. Emanuele Forte, e-mail from author, October 11, 2020). While Lillquist and Weidenaar (2021) classified EM1 as a talus-derived rock glacier, high EM velocities in areas of few diffracting signals suggest a glacial origin. This internal ice mantles a layer of numerous diffracting signals between 140 – 340 m (*Figure 5.3*) with relatively low velocities <0.08 m/ns^{-1}, which indicates a transition to a saturated debris layer (Annan, 2003; Monnier and Kinnard, 2015). This stratigraphy is comparable to borehole studies (Haeberli et al., 1988) that have reported exceptionally high ice content in the upper stratum of rock glacier permafrost which graded into reduced ice content with depth. Heterogeneity in composition across the three-dimensional body of the rock glacier is responsible for differential deformation velocities and a shear horizon may develop where the majority of movement occurs (Haeberli et al., 1998; Arenson et al., 2002; Ladanyi, 2003).

Several high amplitude artifacts show up as columns of stacked hyperbola in these data (*Figure 5.3*). These artifacts signal pockets of liquid water, which are known to create such imperfections in the dataset (Monnier and Kinnard, 2015). Encountering liquid water in rock glaciers is expected during the summer when there is likely meltwater from the active layer and snowpack.

Eightmile Creek 2 Rock Glacier

Eightmile Creek 2 (EM2) is an active, talus-derived rock glacier that shares a compound glacial cirque with EM1 (*Figure 5.1*). This feature has a tongue-shaped morphology and flows north (335°) from an andesitic sidewall (Lillquist and Weidenaar, 2021). The RILA is 2,102 m and the feature extends 414 m downslope and is 200 m wide. Several subalpine larch grew on the northeast flank of the rock glacier toward the snout. Additionally, snow patches filled longitudinal furrows in the surface topography that exceeded 100 m. Snow and ice melt from this catchment forms No Dice Lake which flows into Eightmile Creek and then to the Methow River. This rock glacier has pronounced pressure ridges, a steep snout, and highly unstable surface debris, which supports its classification as an active feature. This evidence is bolstered by the deformation velocities ranging from 4.5-7 cm/yr recorded by Goshorn-Maroney (2012) with a Terrestrial Laser Scanner.

The GPR data revealed a continuous near reflector that suggested an average active layer depth of 4.6 m. This depth corresponds with findings by Goshorn-Maroney, (2012) who recorded a -1.0 +/- 1.0°C MAAT at 3.1-5.8 m below the surface of this rock glacier from three data logger stations, indicating the active layer depth. A distinct basal reflector was observed with an average depth of 27.5 m, which was identified as the bedrock contact. The longitudinal profile (*Figure 5.5*), revealed a series of parallel layers that dip upslope. In the literature, such stratigraphy has been interpreted as shear stress planes, where overlying material is moving as one unit on a plane that is parallel (or tangential) to the plane of the underlying material (Arenson et al., 2002; Mauer and

Hauk, 2007; Fukui et al., 2008; Kunz and Kneisel, 2020). This may occur when the deepest material in the feature has a relatively slow velocity compared to the overlying material. Since these reflectors appear throughout the profile at similar depths, this zone could be the shear horizon where the majority of the deformation occurs (Haeberli et al., 1998; Arenson et al., 2002; Ladanyi, 2003).

The average EM velocity of this rock glacier is 0.153 m/ns^{-1}. At least two areas have a low concentration of diffracting signals, which indicates a homogeneous composition. These homogenous areas contained EM velocity values 0.11-0.16 m/ns^{-1}, which is evidence of massive ice. The thickest point of the homogenous area was 20 m and its shape was not lenticular as one would expect if its source were the entrainment of snow (i.e., ice lens), further bolstering the evidence for glacial ice. These ice masses are likely surrounded by interstitial ice and are interspersed with saturated debris-rich layers (i.e., layers that are primarily composed of debris rather than ice), as indicated from EM velocity measurements of 0.08 m/ns^{-1} (Annan, 2003). Since retreating glaciers may transition into debris-covered glaciers and then rock glaciers, the abundance of interstitial ice and debris-rich layers may signify buried talus from a debris-covered glacier. EM2 was originally categorized as a talus-derived rock glacier (Lillquist and Weidenaar, 2021); however, a glacier origin is indicated by these data.

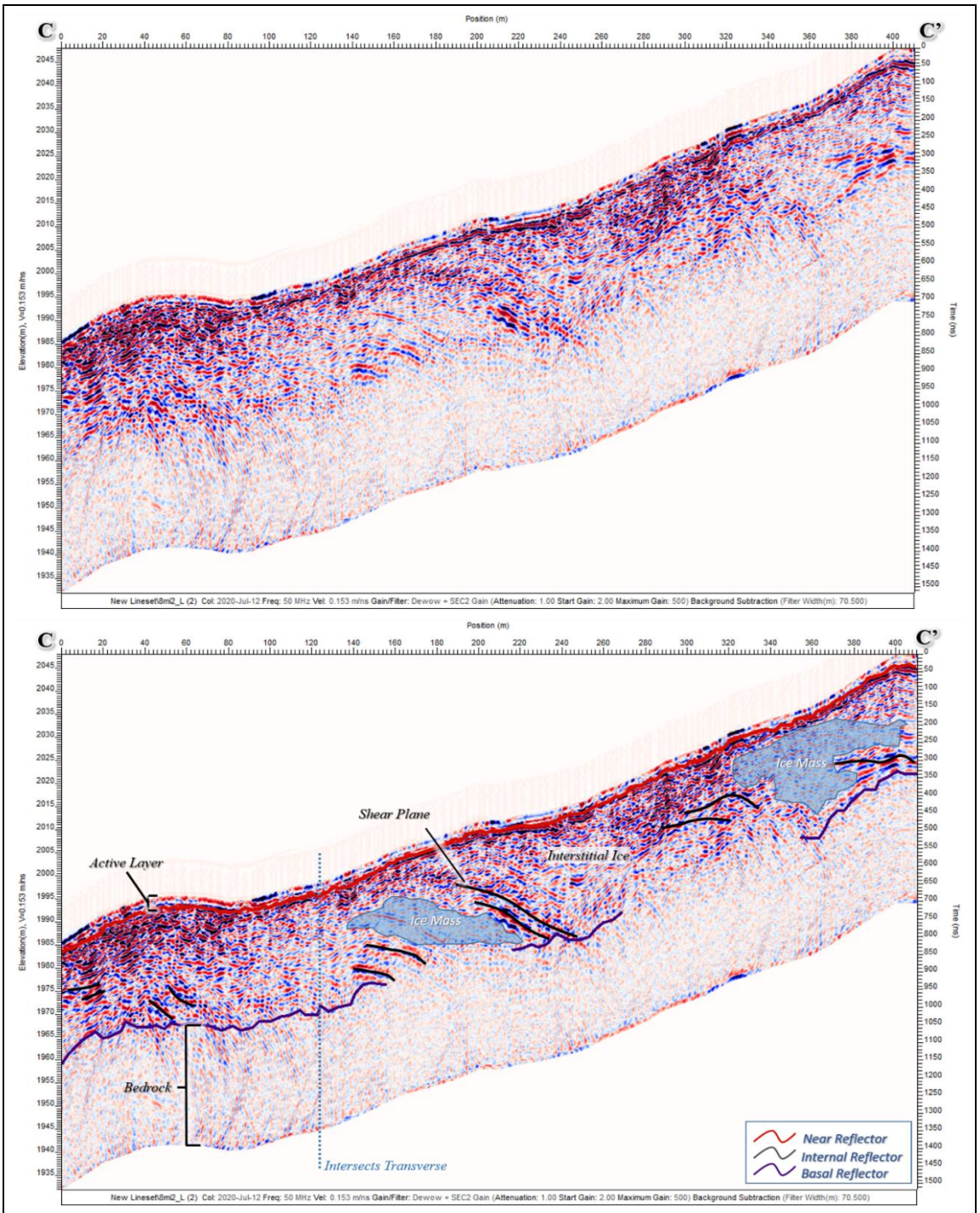

Figure 5.5. Migrated and topographically corrected longitudinal GPR profile of Eightmile Creek 2 without interpretations (upper diagram) and with interpretations (lower diagram). The gaps in the purple line show where the bedrock contact was no longer detectable due to signal attenuation.

During the survey of the 200 m transverse profile of EM2, the batteries of the DVL failed so some data were lost (*Figures 5.2, 5.6*). However, 70 m of the data in this transect were recovered and used in this analysis. The first 15 m of the transverse data show a high concentration of diffracting points which suggests heterogenous material (*Figure 5.6*). This section is adjacent to several subalpine larch trees and is likely debris-rich and relatively stagnant, which aligns with the findings of Goshorn-Maroney (2012). After the debris-rich section, the rock glacier transitions to a composition of ice-saturated debris for the remainder of the profile.

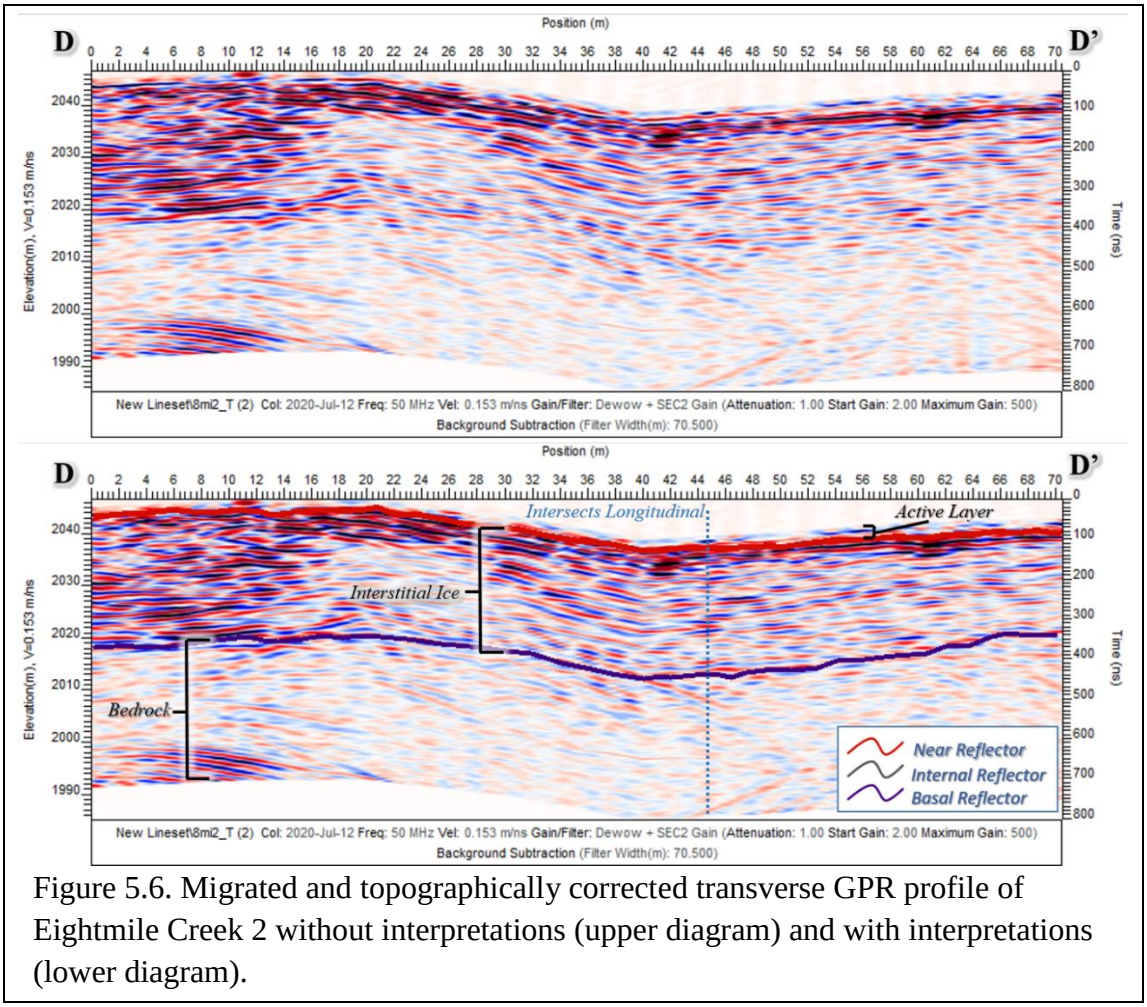

Figure 5.6. Migrated and topographically corrected transverse GPR profile of Eightmile Creek 2 without interpretations (upper diagram) and with interpretations (lower diagram).

Copper Glance Creek 10 Rock Glacier

Copper Glance Creek 10 (CG10) is an inactive, talus-derived rock glacier (Lillquist and Weidenaar, 2021). This lobate feature has a 2,091 m RILA, with a length of 87 m and a width of 88 m *(Figures 3.4, 5.7*). CG10 extends northeast (49°) from its headwall on the NW-SE trending Isabella Ridge that provides the fractured andesite that composes this feature. The pressure ridges were relatively subtle, and several subalpine larch grew on its surface near the snout. No snow was observed on the surface at the time of this survey, but numerous, small outlet streams were emerging from the snout. Down slope from this feature were two small alpine ponds and Copper Glance Lake. This site is in the Methow River Watershed and water from this source flows into Copper Glance Creek which feeds into Eightmile Creek.

Based on the longitudinal (*Figure 5.8*) and transverse (*Figure 5.9*) GPR profiles, the average active layer depth is 2.3 m and the average bedrock depth of 15.8 m, as indicated by continuous near and basal reflectors. The average EM velocity at this site is 0.14 m/ns^{-1}. Several internal reflectors were interpreted as debris-rich layers, rather than expressions of stress because this feature has not experienced significant movement, evident from its small size and low number of pressure ridges. Several regions in the GPR profiles have a relatively low density of diffracting points and EM velocities of 0.11-0.14 m/ns^{-1}, which is evidence of ice-rich zones (best observed in *Figure 5.9*). However, the majority of the data reveal a heterogeneous mixture of debris and interstitial ice, which is consistent with an inactive, talus-derived classification, as documented by Lillquist and Weidenaar (2021).

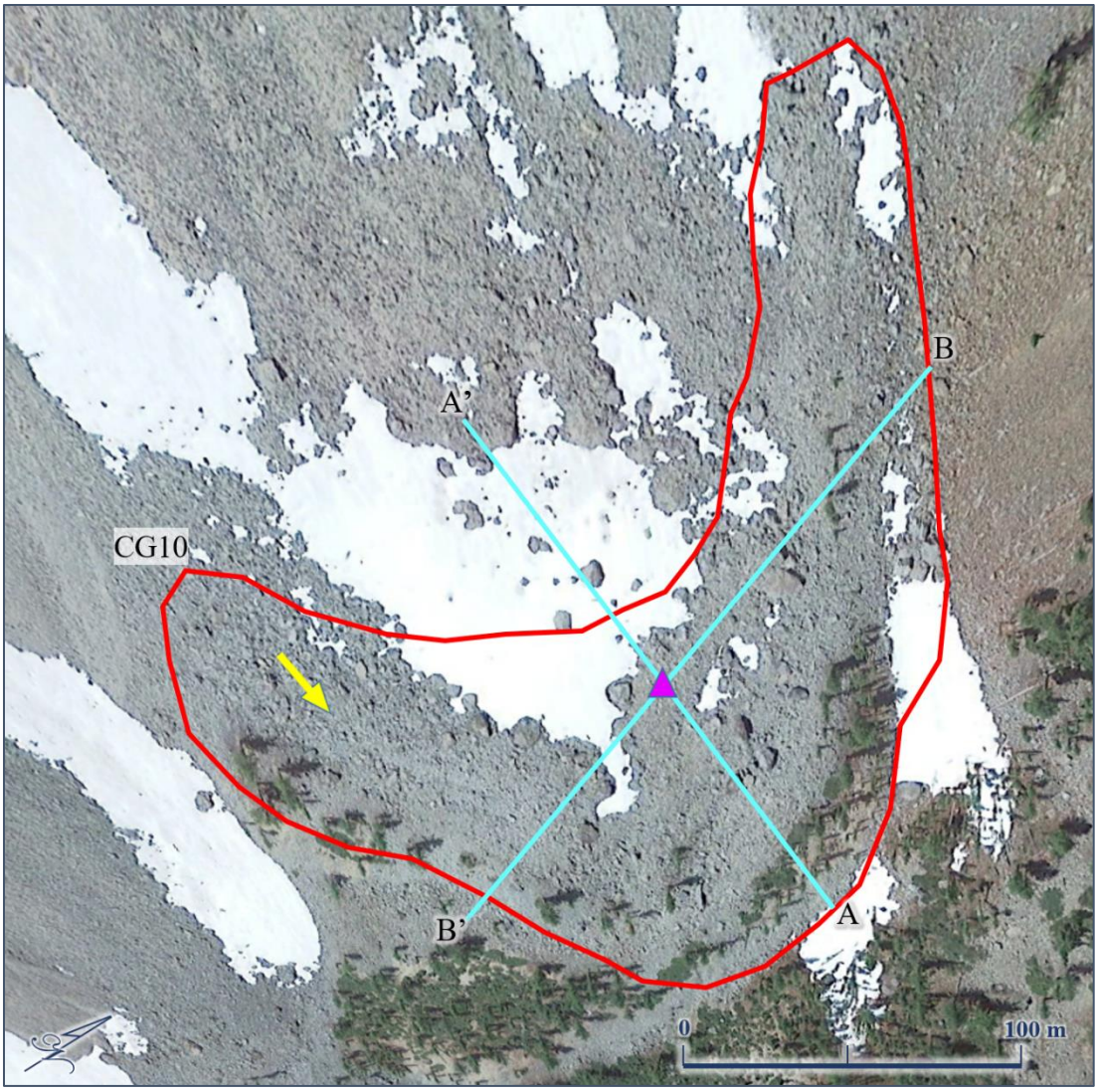

Figure 5.7. Planimetric view of the survey plan for the Copper Glance Creek 10 rock glacier. The purple marker indicates the approximate location of the CMP. The yellow arrow indicates flow direction. Google Earth imagery from 7/14/2017.

CG10 is located in the proximity of two active rock glaciers: EM1 (2191 m RILA) and EM2 (2102 m RILA) (Table 4, *Figure 5.2*). The difference in RILA between CG10 (2091 m RILA) and EM22 is only 11 m, yet CG10 is significantly less active than EM2. Likely, this is the result of more insolation at CG10, which has a 49° aspect on an

exposed ridgeline, compared to EM1 and EM2 which occupy a north-facing, shaded catchment.

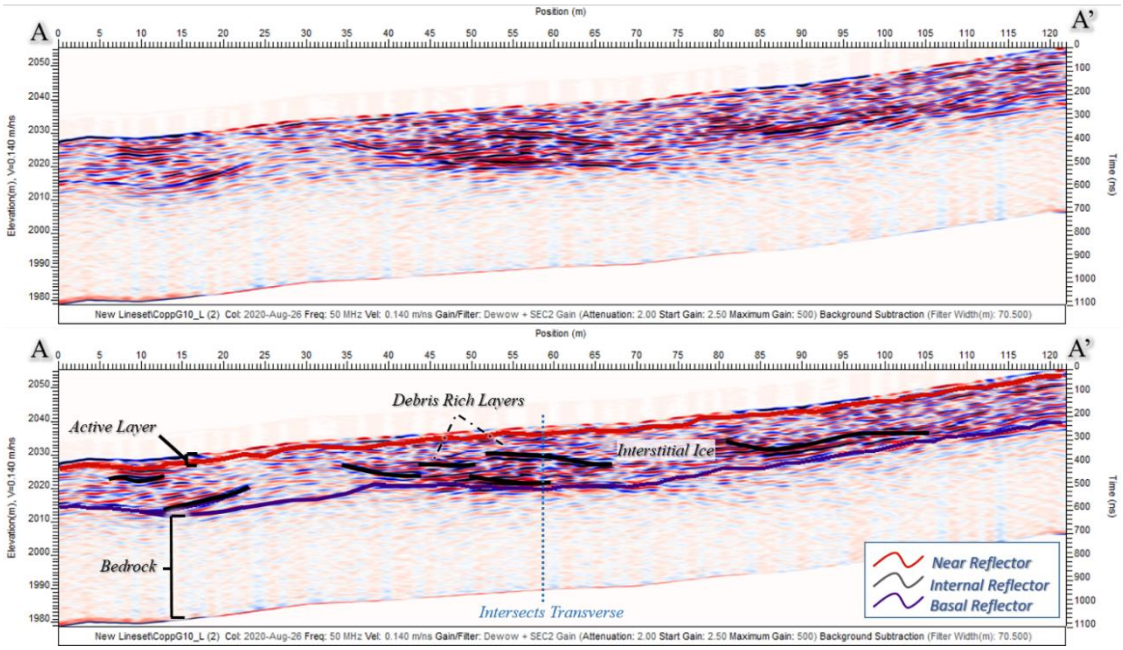

Figure 5.8. Migrated and topographically corrected longitudinal GPR profile of the Copper Glance Creek 10 rock glacier without interpretations (upper diagram) and with interpretations (lower diagram).

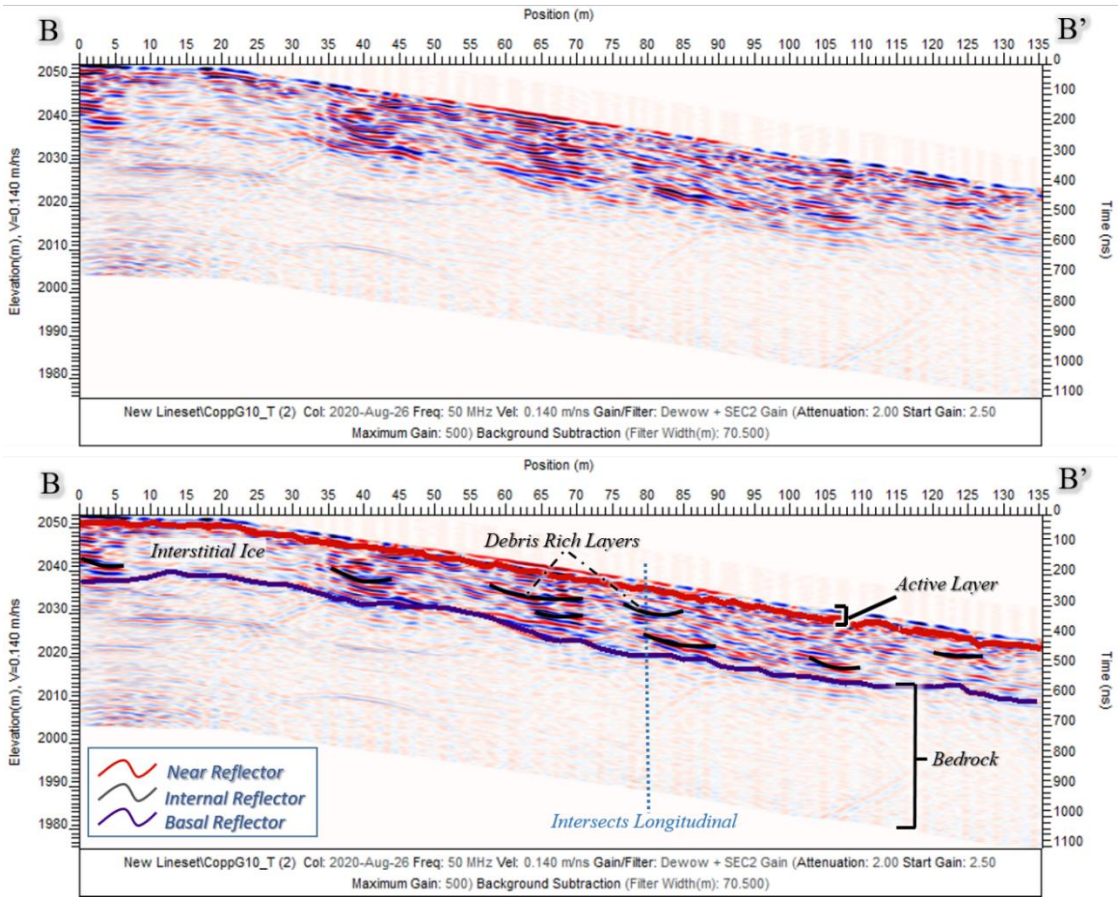

Figure 5.9. Migrated and topographically corrected transverse GPR profile of the Copper Glance Creek 10 rock glacier without interpretations (upper diagram) and with interpretations (lower diagram).

Copper Glance Creek 6 Rock Glacier

Copper Glance Creek 6 (CG6) is a talus-derived, tongue-shaped rock glacier with a RILA of 1,779 m (*Figures 3.4, 5.10*). CG6 is an inactive feature and extends from its headwall at a northeast aspect of 51° (Lillquist and Weidenaar, 2021). This rock glacier is 357 m in length and 116 m in width and composed of weathered andesite from Isabella Ridge. CG6 had the most vegetation of all the surveyed features, with subalpine larch trees covering much of its surface. Nonetheless, the pressure ridges were well-defined, indicating permafrost creep. This feature is in the Methow River Watershed and internal

water storage drained from several outlet streams at the snout of the rock glacier into Copper Glance Creek which feeds into Eightmile Creek. No snow patches were observed on this rock glacier during our field visit.

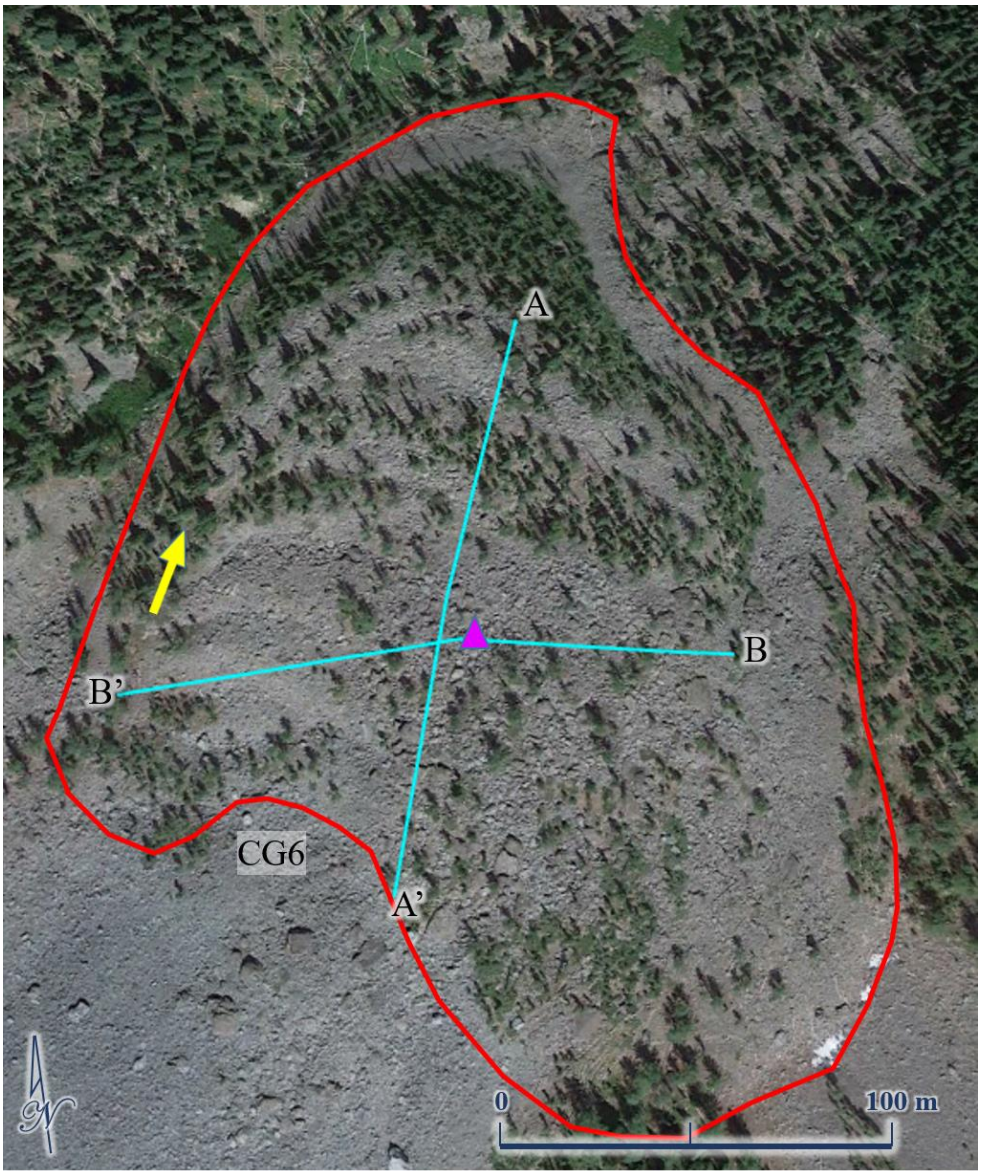

Figure 5.10. Planimetric view of the survey plan for the Copper Glance Creek 6 rock glacier. The purple marker indicates the approximate location of the CMP. The yellow arrow indicates flow direction. Google Earth imagery from 7/14/2017.

In the GPR data, the average EM velocity was 0.136 m/ns^{-1}. Additionally, the profile revealed a continuous near reflector with an average depth of 2 m, indicating the base of the active layer. Furthermore, a continuous basal reflector with an average depth of 14.1 m was interpreted as the bedrock contact. The high density of diffracting signals, coupled with EM velocities ranging from 0.08-0.12 m/ns^{-1}, for much of the permafrost layer, is indicative of a debris matrix with interstitial ice, as expected in a talus-derived feature (*Figures 5.11, 5.12*). Moreover, numerous internal reflectors were interpreted as debris-rich layers due to their orientation and apparent decoupling from the bedrock topography when viewed in the direction of flow (*Figure 5.11*). A zone of few diffracting signals indicated homogeneity of material between 30 – 65 m in the longitudinal transect (*Figure 5.11*) and 20 – 70 m in the transverse transect (*Figure 5.12*), which suggest an ice-rich zone. However, the limited number of diffracting signals in this zone prevented accurate EM velocity measurements; therefore, the composition of this zone cannot be verified through this method. Nonetheless, the average propagation velocities and diffracting signal densities in the GPR profile are sufficient to support an inactive, talus-derived classification for CG6, as documented by Lillquist and Weidenaar (2021).

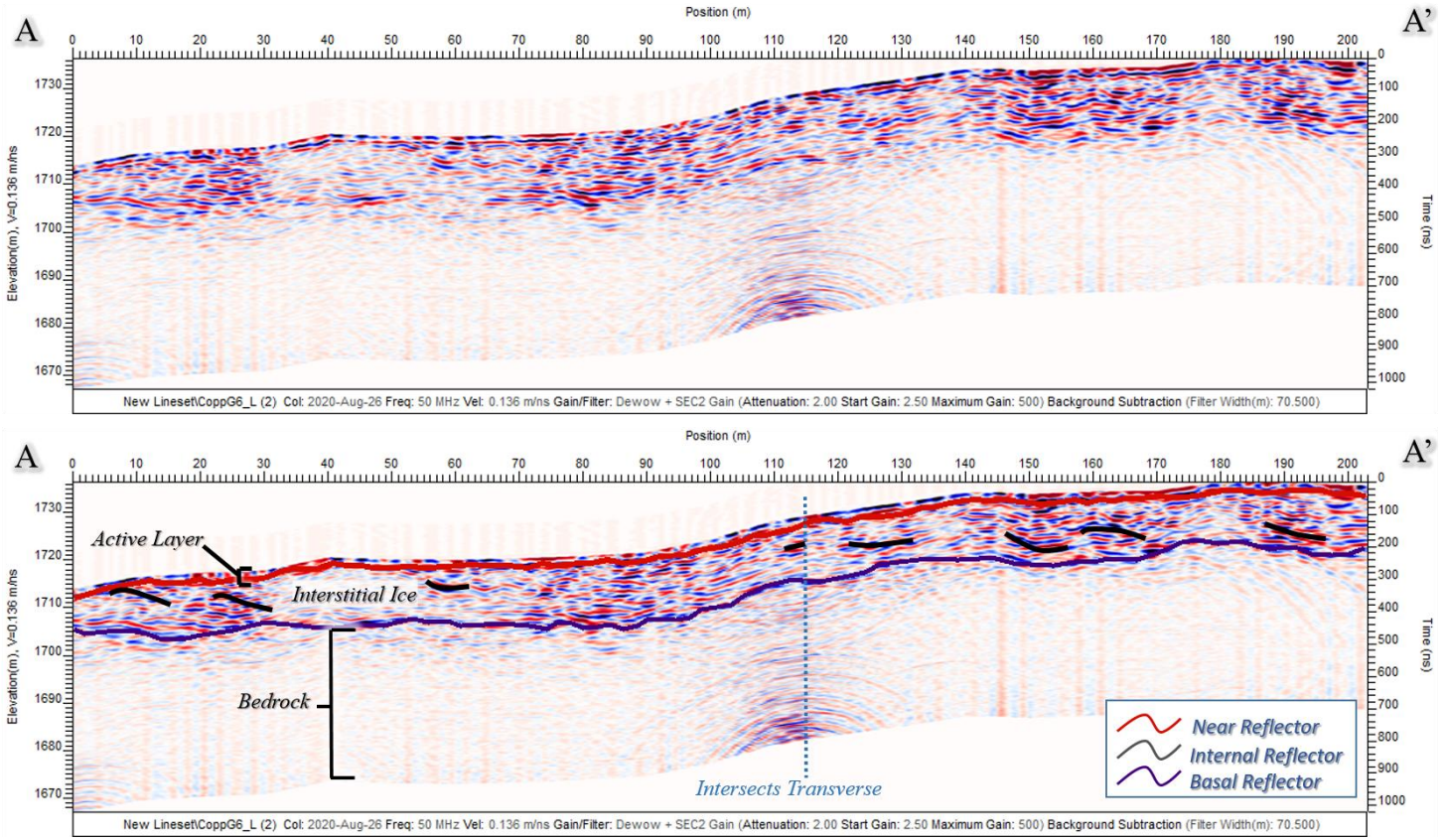

Figure 5.11. Migrated and topographically corrected longitudinal GPR profile of Copper Glance Creek 6 rock glacier without interpretations (upper diagram) and with interpretations (lower diagram).

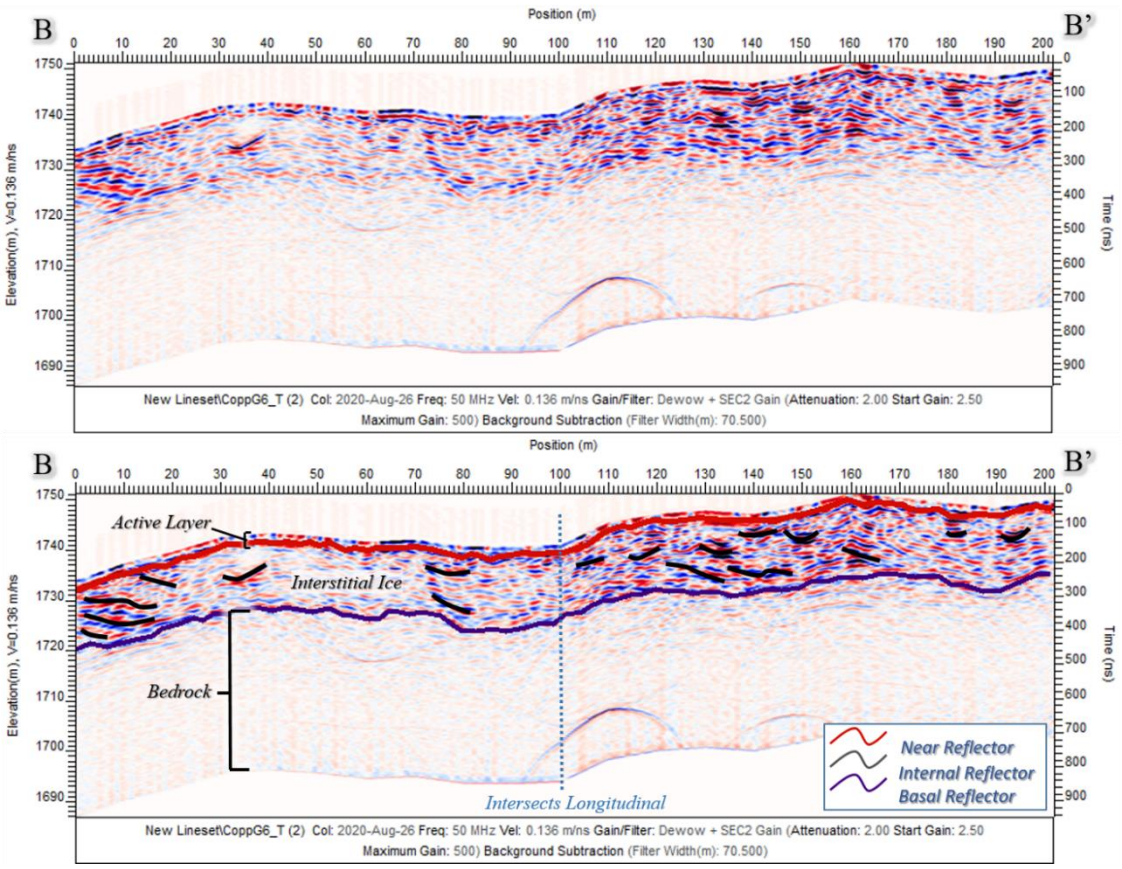

Figure 5.12. Migrated and topographically corrected transverse GPR profile of Copper Glance Creek 6 rock glacier without interpretations (upper diagram) and with interpretations (lower diagram).

Although this feature shares a ridgeline with CG10 (RILA: 2091 m), CG6 (RILA: 1779 m) is 312 m lower in RILA, which likely has a significant effect on MAAT. The aspects are similar for both rock glaciers (49° at CG10 and 51° at CG6), therefore aspect has little influence on specific differences between these features. The two sites have a substantial size difference, as CG6 (68,601m^2) is over five times the size of CG10 (13,366 m^2). Since the relatively low elevation of CG6 renders it less suitable for permafrost development than CG10, the primary factor contributing to the large size of CG6 is likely its catchment area, which is substantially larger than the source area for

CG10. It is also plausible that CG6 is significantly older than CG10 (i.e., more time to develop into a large permafrost feature).

Copper Glance Creek 3 Rock Glacier

Copper Glance Creek 3 (CG3) is an inactive, lobate, talus-derived, rock glacier. CG3 is composed of andesite and it flows northeast at an aspect of 54° from a sidewall that extends from Isabella Ridge (Lillquist and Weidenaar, 2021) (*Figures 3.4, 5.13*). The pressure ridges were poorly defined, and a few subalpine larches were growing at the low angled snout. The RILA of CG3 is 1,981 m and it has a length of 93 m and a width of 111 m. No snow patches were observed on its surface, but a few small streams were exiting the snout of CG3 and eventually flowing into Copper Glance Creek which feeds Eightmile Creek, a tributary of the Methow watershed.

The gentle snout of CG3 allowed the survey team to capture data for the entire front of this feature. This normally is not possible due to the steep and unstable conditions typical of rock glacier snouts, making them too dangerous for the team to traverse with sensitive equipment. The transect started just below the talus snout, adjacent to a stream that was partially fed by this rock glacier. Because we started on alluvial deposits, we could confirm that the signal ~15 m below the surface at 0 m in the longitudinal survey (*Figure 5.14*) represented alluvium and was separate from the rock glacier. Additionally, we observed streams exiting the feature, which suggested that the strong horizontal internal reflector shown in *Figure 5.14* was likely a saturated layer. Another similar internal reflector at 0-35 m in *Figure 5.15* was interpreted as intra-flow where water entered the flank of the rock glacier on the uphill slope and exploited the

bedrock contact as a permeable pathway. This interpretation was supported by numerous high amplitude artifacts, which had to be filtered from the GPR profile in data processing and are associated with the presence of liquid water.

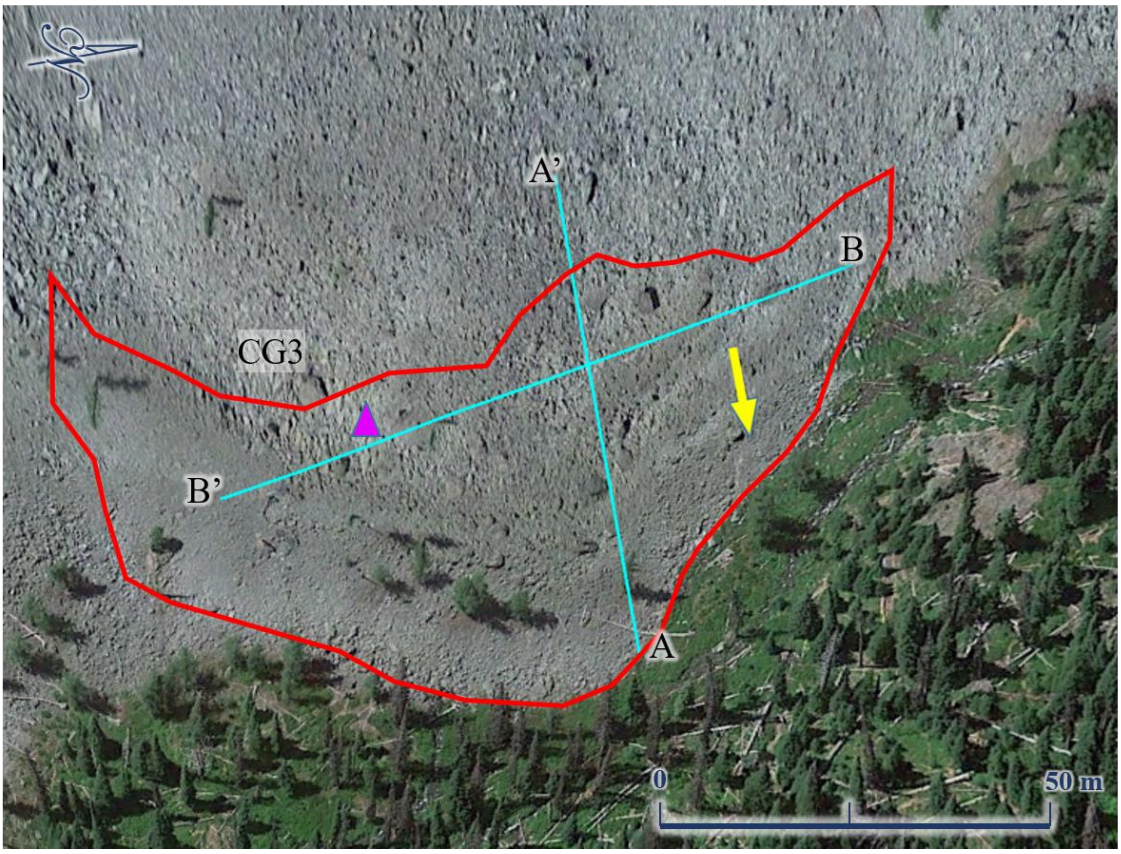

Figure 5.13. Planimetric view of the survey plan for the Copper Glance Creek 3 rock glacier. The purple marker indicates the approximate location of the CMP. The yellow arrow indicates direction of flow. Google Earth imagery from 7/14/2017.

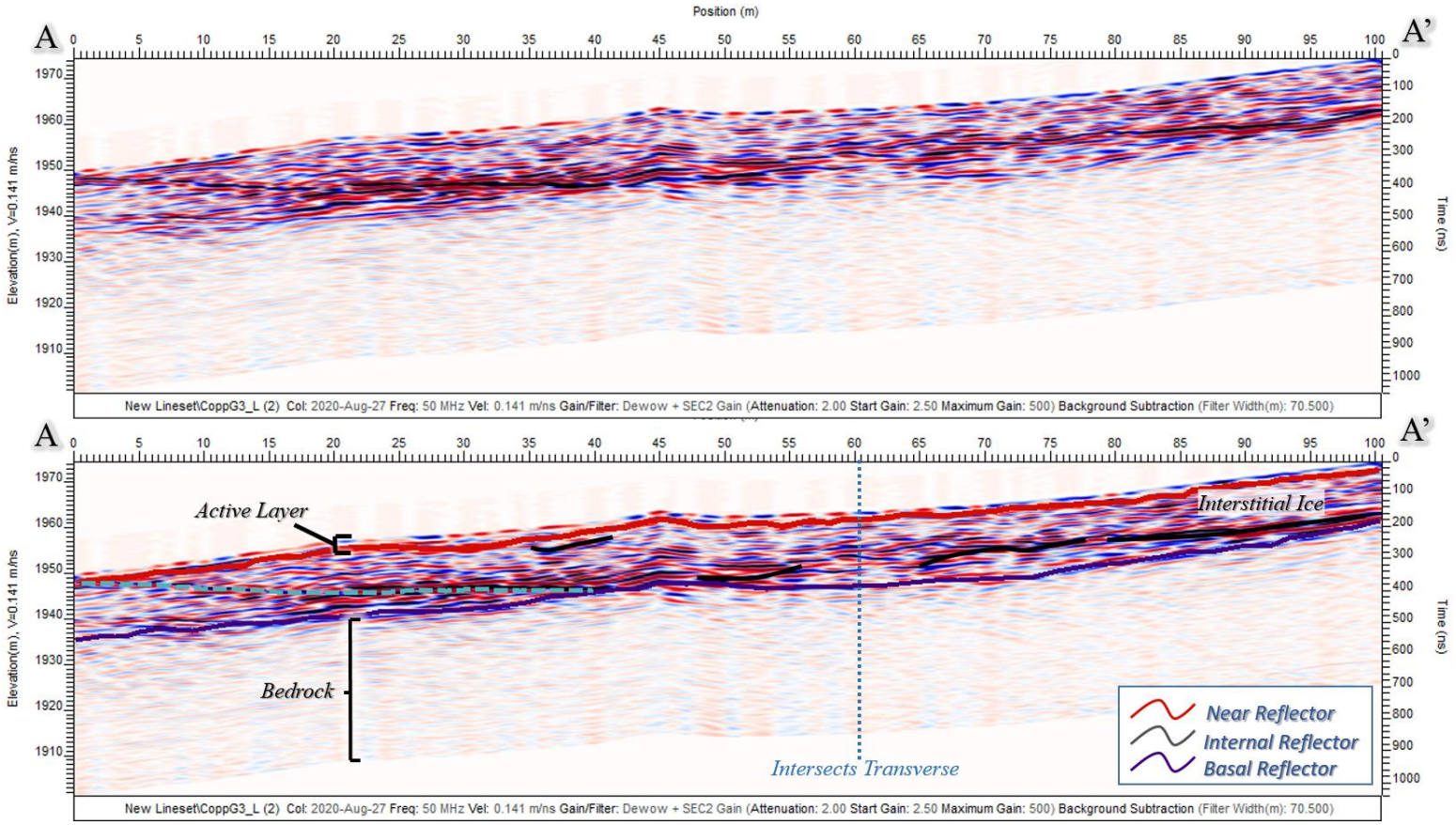

Figure 5.14. Migrated and topographically corrected longitudinal GPR profile of Copper Glance Creek 3 without interpretations (upper diagram) and with interpretations (lower diagram). The blue dashed line indicates water that is exiting the snout of the rock glacier.

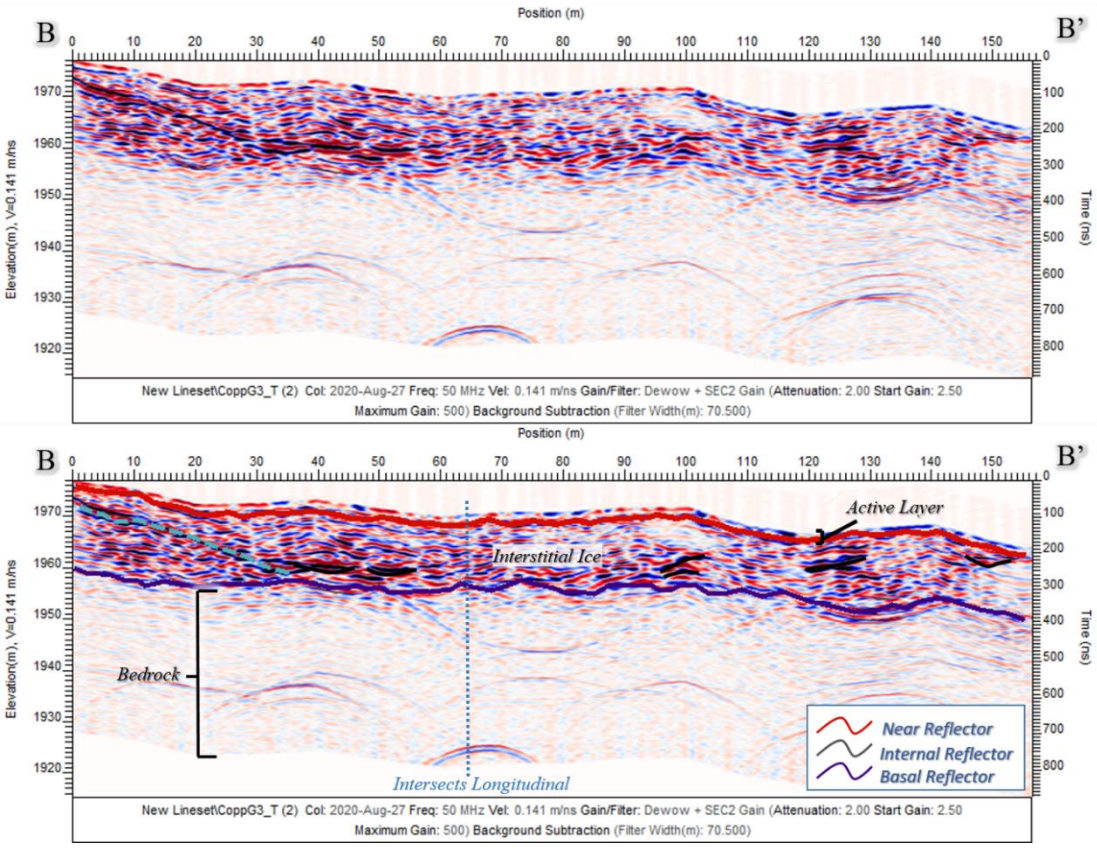

Figure 5.15. Migrated and topographically corrected transverse GPR profile of Copper Glance Creek 3 without interpretations (upper diagram) and with interpretations (lower diagram). The blue dashed line indicates intra-flow within the permafrost layer.

The GPR profile displayed a continuous near reflector, with an average depth of 1.6 m and high EM velocities (0.15 – 0.18 m/ns^{-1}), that was interpreted as the base of the active layer. Additionally, a continuous basal reflector with an average depth of 11.9 m indicated the average bedrock depth. The average EM velocity for this feature was 0.14 m/ns^{-1} and majority of the GPR profile had a high density of diffracting points indicating a heterogeneous mixture of debris and interstitial ice, typical of a talus-derived feature. Several internal reflectors were detected that did not correspond with the surface or bedrock topography; therefore, these internal reflectors were interpreted as debris-rich

layers. Homogenous zones were observed in the transverse transect (*Figure 5.15*) that had relatively high EM velocities of 0.14-0.15 m/ns^{-1}, which suggest ice-rich zones.

Despite the surface observations that imply this feature is relict (i.e., subtle pressure ridges, gentle snout, surface vegetation, and weathered debris), these data indicate the presence of permafrost and therefore support the original classification that by Lillquist and Weidenaar (2021) that CG3 is inactive. The RILA of CG3 (1,981 m) is between that of CG6 (1779 m) and CG10 (2091 m), which are both inactive features with similar environmental characteristics (e.g., aspect, geology, and insolation) and therefore support the likelihood of permafrost at CG3.

Copper Glance Creek 2 Rock Glacier

Copper Glance Creek 2 (CG2) is an inactive, lobate, talus-derived rock glacier with pronounced pressure ridges near the rooting zone that become progressively more subtle toward the snout (Lillquist and Weidenaar, 2021) (*Figures 3.4, 5.16*). This andesitic feature has a length of 98 m and a width of 139 m. CG2 flows northeast at a 50° aspect from a sidewall extending from Isabella Ridge, which it shares with CG3. No snow patches were observed on the rock glacier surface, and numerous subalpine larch were growing near the snout. Water was flowing from this feature into a small alpine pond, although this pond was nearly dry during our visit. CG2 is in the Methow River Watershed, and water leaving the snout eventually flows into Copper Glance Creek which feeds Eightmile Creek.

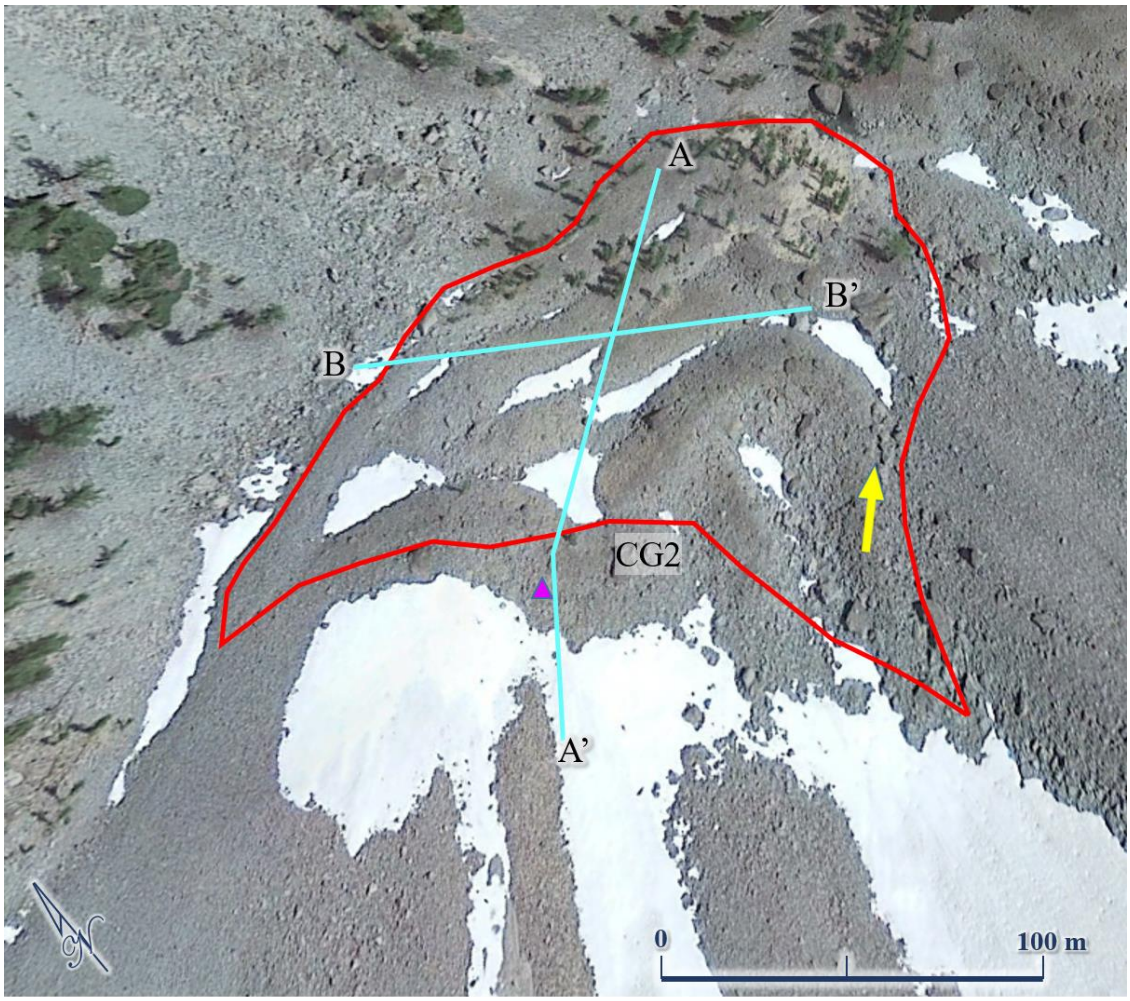

Figure 5.16. Planimatric view of the survey plan for the Copper Glance Creek 2 rock glacier. The purple marker indicates the approximate location of the CMP. The yellow arrow indicates the flow direction. Google Earth imagery from 7/14/2017.

The CG2 GPR profiles contain a distinct near reflector with an average depth of 2.1 m that was interpreted as the active layer base (*Figures 5.17, 5.18)*. Additionally, a basal reflector with an average depth of 16.9 m was indicative of the bedrock contact. The average EM velocity recorded at this site was 0.13 m/ns^{-1}. Several up-glacier dipping internal reflectors in concordance with pressure ridges and the bedrock topography revealed the shear stress plane. These shear stress reflectors may indicate the shear

horizon where the majority of down slope movement occurs (Haeberli et al., 1998; Arenson et al., 2002; Ladanyi, 2003). This feature is composed of ice-cemented talus and at least three areas of relatively homogenous material with low diffracting signal densities and EM velocities of 0.13 m/ns^{-1} were detected, which indicate ice-rich layers. The average EM velocity, the density of diffracting signals, the expression of shear stress planes, and the presence of both pronounced and subtle pressure ridges indicate a talus-derived, inactive rock glacier, which is consistent with Lillquist and Weidenaar (2021).

An interesting asymmetrical distribution of ice-content is apparent in *Figure 5.18* where the rock glacier appears to have a higher debris content on the northern half (0 – 60 m) and a higher ice content on the southern half (60 – 120 m). This permafrost distribution mirrors that of the asymmetrical morphology of the feature that extends further down slope on the southern half compared to the northern half (*Figure 5.16*). This observation suggests that the relatively high ice content of the southern half may have allowed this section of the feature to progress down slope at a faster rate than the debris-rich northern half.

In comparison to the other rock glaciers that feed into Copper Glance Creek (i.e., CG10, CG6, and CG3), CG2 has the most pronounced pressure ridges, shows the greatest amount of internal stress caused by displacement, and appears to be the most ice-rich feature for its size based on EM velocities and the density of diffracting signals. However, CG2 is not the highest elevation feature (the RILA of CG10 exceeds that of CG2 by 40 m) and CG10, CG6, CG3 and CG2 all have similar aspects ranging from 49-54°. It is likely that the large catchment of CG2 delivers an abundant supply of debris and

ice to this feature, which is highly conducive to permafrost development. The catchment of CG2 is larger than that of CG3 and CG10. CG6 has the largest catchment, but the RILA of CG2 is 275 m higher than that of CG6 which likely compensates for the slightly smaller catchment size of CG2.

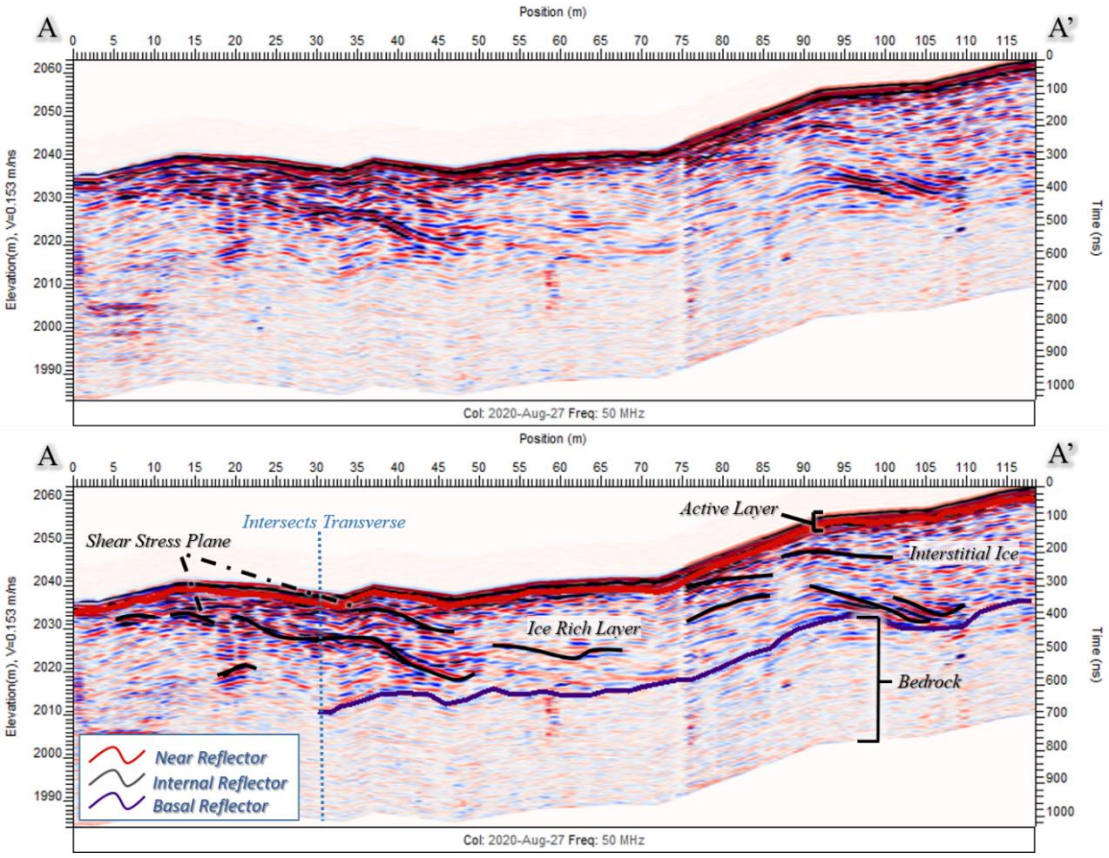

Figure 5.17. Migrated and topographically corrected longitudinal GPR profile of Copper Glance Creek 2 without interpretations (upper diagram) and with interpretations (lower diagram). The purple line ends where the bedrock contact was no longer detectable due to signal attenuation.

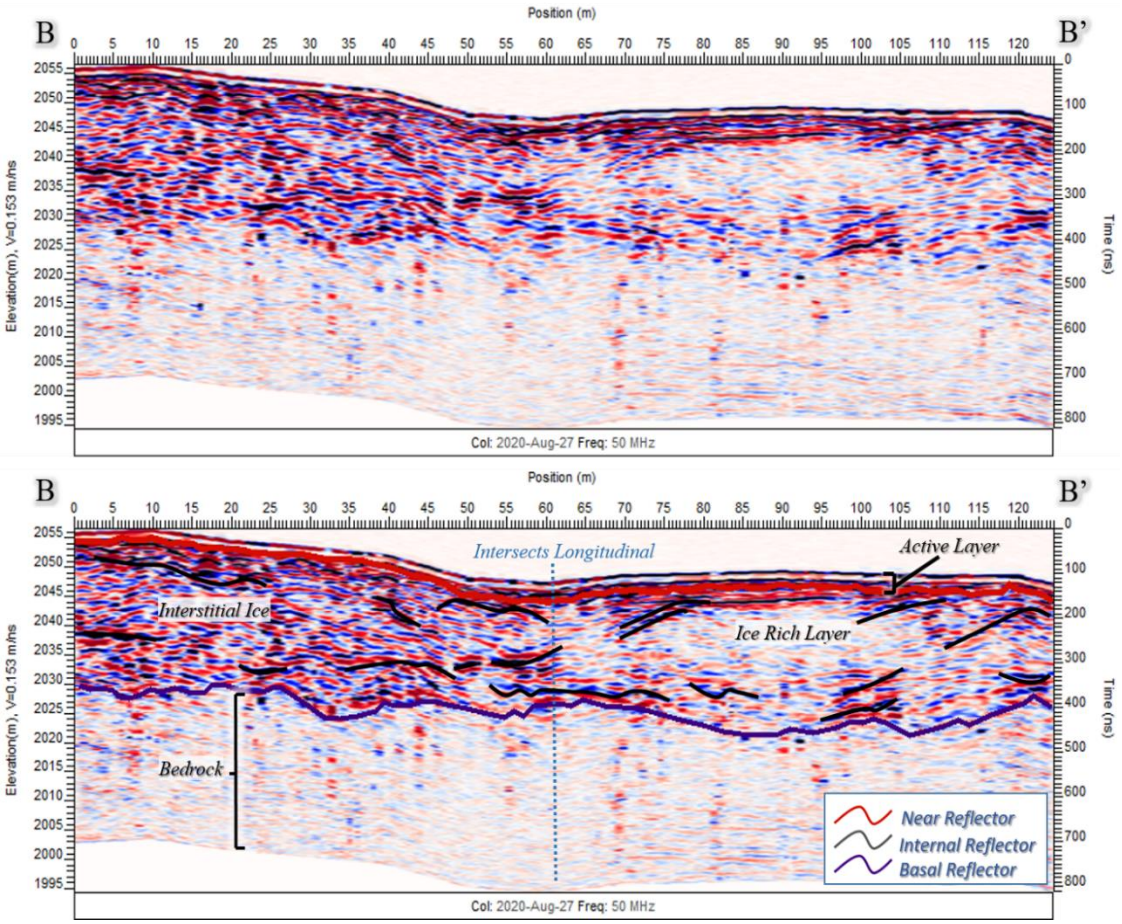

Figure 5.18. Migrated and topographically corrected transverse GPR profile of Copper Glance Creek 2 without interpretations (upper diagram) and with interpretations (lower diagram).

Lost River Study Site

Monument Creek 1 Rock Glacier

Monument Creek 1 (MC1) is an active rock glacier with the highest RILA (2,353 m) of any feature surveyed in this research (Lillquist and Weidenaar, 2021). It is likely a composite feature consisting of several generations of glacier-derived rock glaciers. MC1 is complex in form (*Figure 5.19)* with multiple levels of tongue-shaped morphologies. Starting from a high relief headwall below Monument Peak, MC1 flows toward the east

(78° aspect) along a sidewall that provides protection from solar radiation. This rock glacier has a length of 858 m and a width of 341 m. The parent material of MC1 is granite which breaks into large, blocky debris and helps insulate underlying permafrost (*Figure 5.20*) (Wahrhaftig and Cox, 1959; Onaca et al., 2017). The rock glacier surface had pronounced pressure ridges throughout the feature, indicative of its activity. The vegetation was limited to a few subalpine larch trees on the outermost rim of the lower level, which indicates the upper level is likely more mobile. The upper level also had an exceptionally steep snout, which implies the resupply of debris by permafrost creep (Wahrhaftig and Cox, 1959). The only snow patches at this site were on the upper level in the large surface depression and on the southern flank. While traversing the rock glacier there were several places where rushing water could be heard beneath the talus. At the snout, the discharge from numerous outlet streams displayed a clear diurnal flux over the two-day survey. This was first observed at high discharge around 7pm on July 27, 2020. The following day, the discharge had significantly decreased when observed around 1pm. This observation reflects the lag between peak solar radiation and peak discharge due to the time necessary for energy absorption to increase the temperature of the rock glacier surface and enhance active layer melting. Snow and ice melt in this catchment support several subalpine meadows surrounded by talus slopes where we observed grouse, pika, and marmot. This water source feeds several waterfalls that coalesce downvalley in a stream called Monument Creek that is also fed by the Monument Creek 2 rock glacier. Monument Creek is a tributary of the Lost River and ultimately feeds into the Methow River.

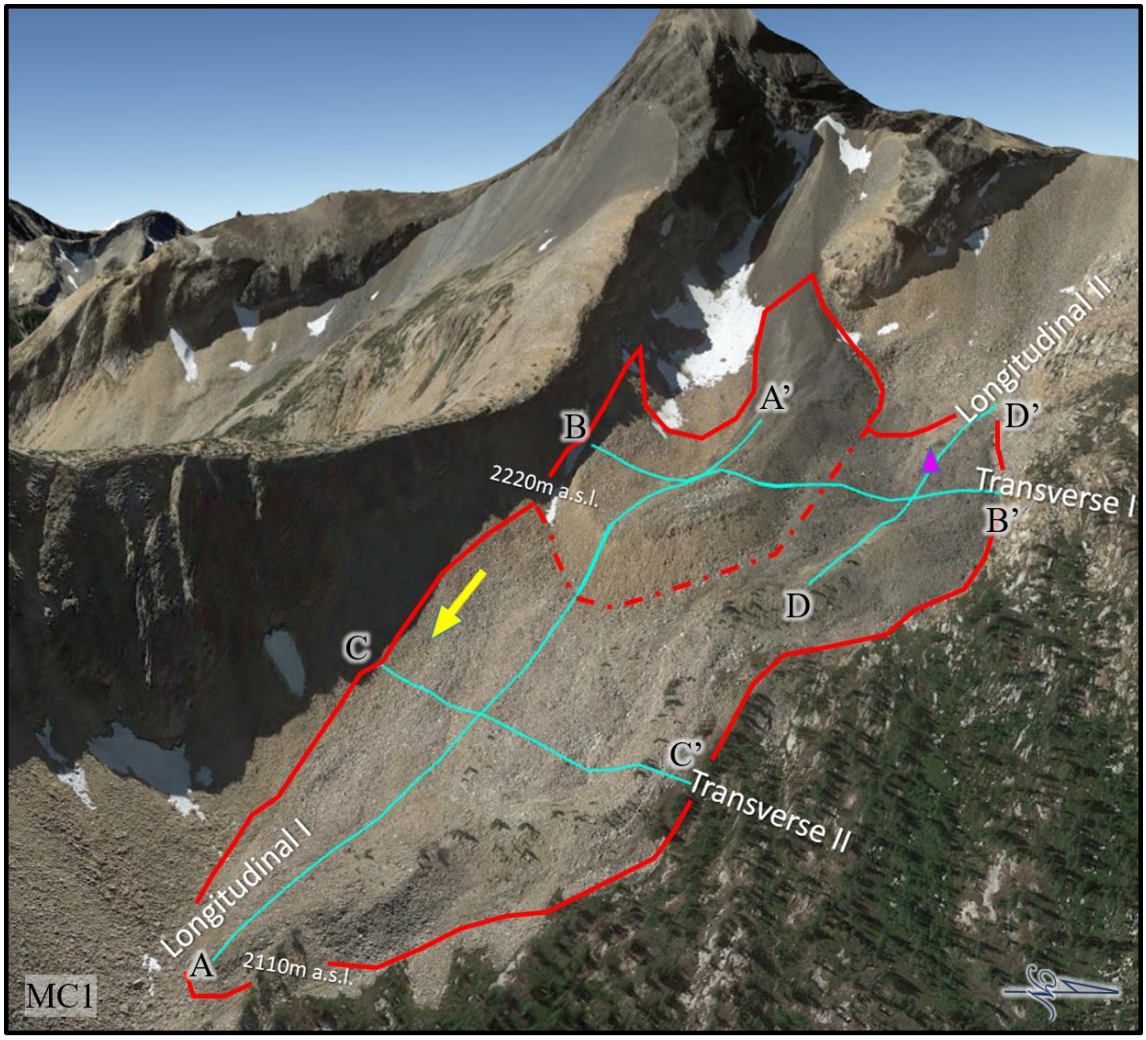

Figure 5.19. Oblique view of the survey plan for the Monument Creek 1 rock glacier. The purple marker indicates the location of the CMP. The yellow arrow indicates flow direction. The dotted red boundary indicates the upslope border of the rock glacier as mapped by Lillquist and Weidenaar, 2021, which has been updated to the solid boundary based on the ice content found with GPR in the current work. Google Earth imagery from 8/19/2016.

Figure 5.20. Upper level of the Monument Creek 1 Rock Glacier. Field crew: (left to right) Alex Mathews, Nacho Ward, Jessica Coffey, and Will Raymond. Photo captured by Spencer Stinnett, 7/27/2020.

Due to the complex morphology of MC1, two longitudinal and two transverse transects were surveyed to thoroughly investigate its internal structure and composition (*Figures 3.5, 5.21 – 5.24*). A continuous near reflector was detected with an average depth of 2 m, which was interpreted as the base of the active layer. Additionally, a basal reflector with an average depth of 25.1 m indicated the bedrock contact. One finding that was consistent in all four transects was a continuous downglacier dipping reflector. This reflector increases in depth with proximity to the snout and flanks until reaching the bedrock contact layer where the reflector runs parallel to the base of the feature. Shear stress cannot be an explanation of this reflector because a shear plane would dip in the opposite direction (i.e., upglacier) (Kunz and Kneisel, 2020). Furthermore, aerial imagery captured during periods of snow cover on this rock glacier contain numerous runnels that

indicate that hydrological pathways run beneath the relatively inflated snout and flanks of the lower level (2,145 m on *Figure 5.19*). This reflector was interpreted as intra-flow derived from melting of the active layer or permafrost in the rock glacier, as documented by (Arenson et al., 2002; Degenhardt, 2009; Monnier and Kinnard, 2013; Monnier and Kinnard, 2015, Jones et al., 2019a). This water flows downslope through the rock glacier until encountering a debris-rich layer, inferred as the boundary between different generations of rock glacier (seen best at 80 – 150 m in *Figure 5.21*), that is used as a permeable pathway for meltwater from the upper levels. The meltwater conduit continues until encountering the bedrock then flows along the base of the rock glacier, eventually exiting at the snout. Reflectors that indicate extension, compression, or shear stress were not detected in this dataset. This could indicate that this feature moves downslope by sliding more so than by creep, which may be facilitated by the high liquid water content and steep bedrock angle of this rock glacier. In the literature, this sliding effect is known as basal shear and is caused by liquid water at the bedrock contact, due to pressure melt, which provides a low-resistance surface for sliding (Giardino and Vick, 1987; Riffle, 2018). This phenomenon has been documented as basal shear in the literature and is associated with liquid water at the bedrock contact due to pressure melt that functions as a low resistance surface for the entire feature to slide. Another possibility is that most of the hummocky surface topography and periphery inflation of the upper and lower levels of this feature were inherited from a previous glacier (i.e., the moraines would not contain expressions of extension, compression or shear stress), and this feature has not

moved downslope a sufficient distance to produce large stress indicators detectable by the GPR.

Differential concentrations of diffracting signals in the GPR data reveal zones that are relatively homogenous. When these observations are coupled with EM velocity measurements 0.11-0.16 m/ns^{-1}, there is compelling evidence that this feature has a high ice content (Monnier and Kinnard 2013; Kunz and Kneisel, 2020). Because the survey plan has several intersections, there is opportunity to cross-reference the hyperbolic response velocities and signal density of different transects to increase the overall confidence level of the data. At least three major ice masses were detected in this feature, two of which appear in more than one GPR profile (*Figure 5.25*). Supporting evidence for these ice masses includes EM velocities between 0.11-0.14 m/ns^{-1} in areas that have a homogeneous composition and are relatively sharp bounded (Kunz and Kneisel, 2020). This evidence suggests an ice mass in the upper level of the feature, which was not mapped as part of this composite rock glacier (Lillquist and Weidenaar, 2021), and indicates that both levels are a single rock glacier, likely unified by several generations of advance. Although Monument Creek 1 was inventoried as a tongue-shaped rock glacier (Lillquist and Weidenaar, 2021), a complex classification better defines this composite rock glacier, as revealed by the GPR.

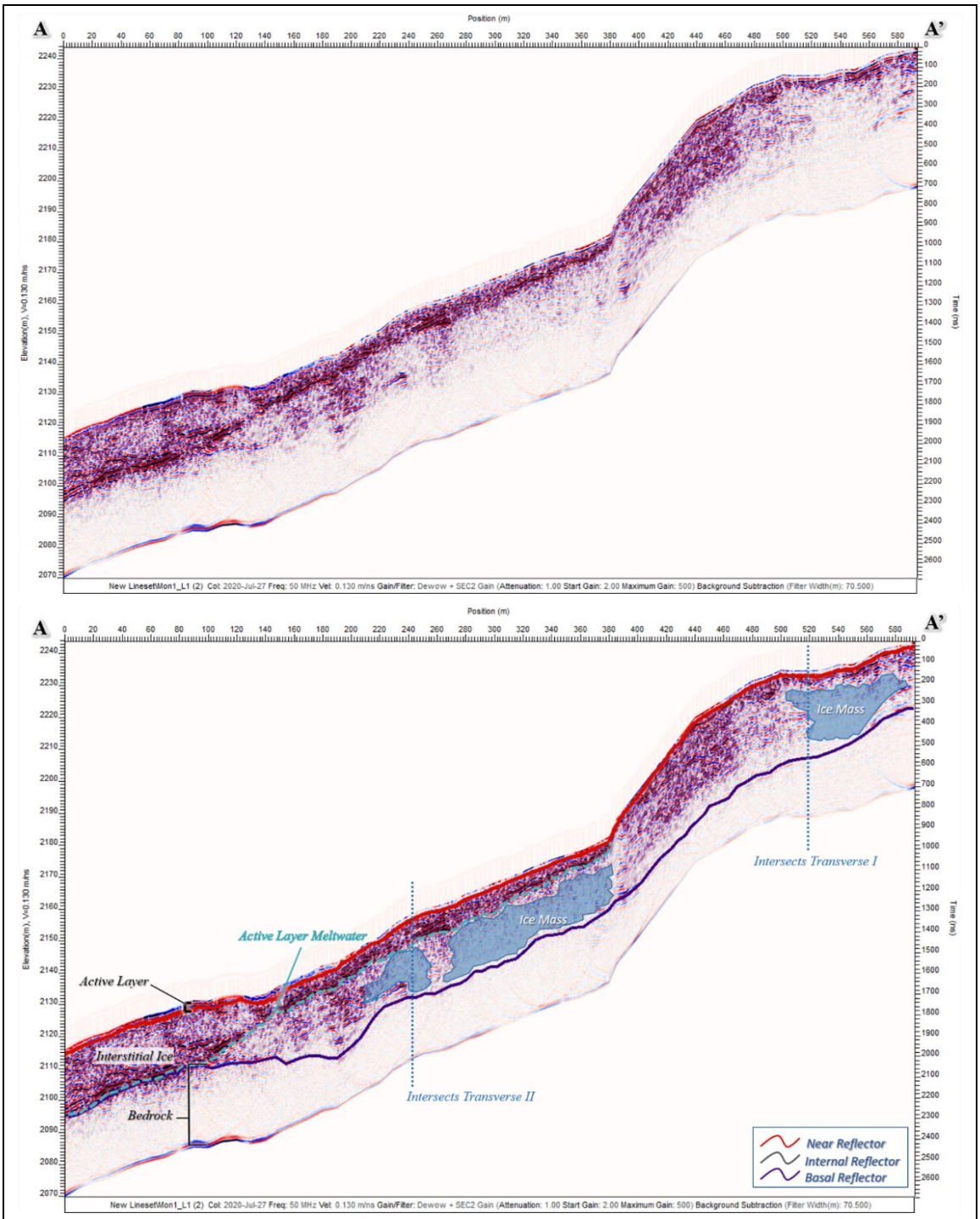

Figure 5.21. Migrated and topographically corrected longitudinal I GPR profile of Monument Creek 1 without interpretations (upper diagram) and with interpretations (lower diagram).

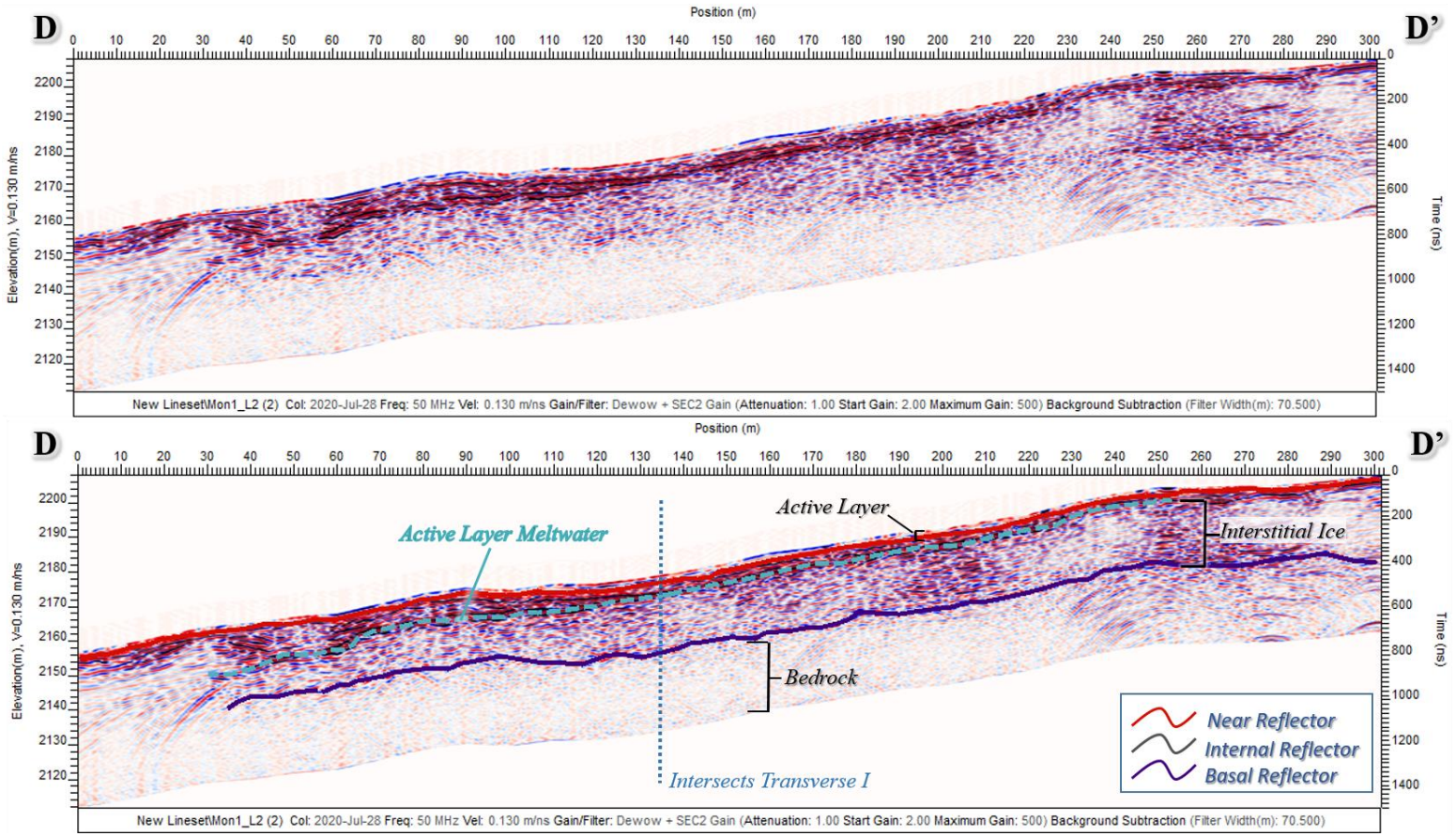

Figure 5.22. Migrated and topographically corrected longitudinal II GPR profile of Monument Creek 1 without interpretations (upper diagram) and with interpretations (lower diagram). The purple line ends where the bedrock contact was no longer detectable due to signal attenuation.

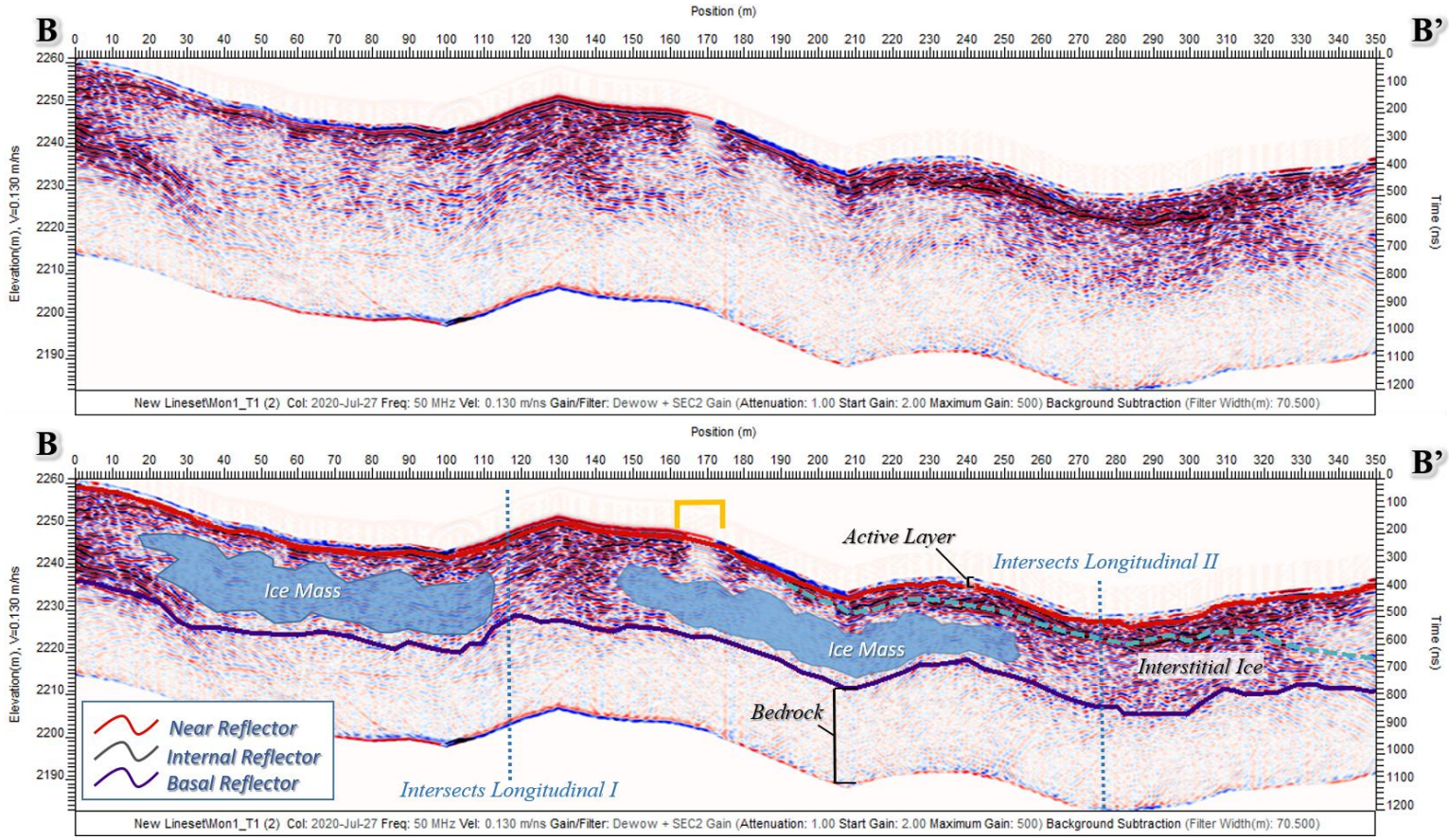

Figure 5.23. Migrated and topographically corrected transverse I GPR profile of Monument Creek 1 without interpretations (upper diagram) and with interpretations (lower diagram). The yellow bracket between 165-175 m marks a series of failed traces.

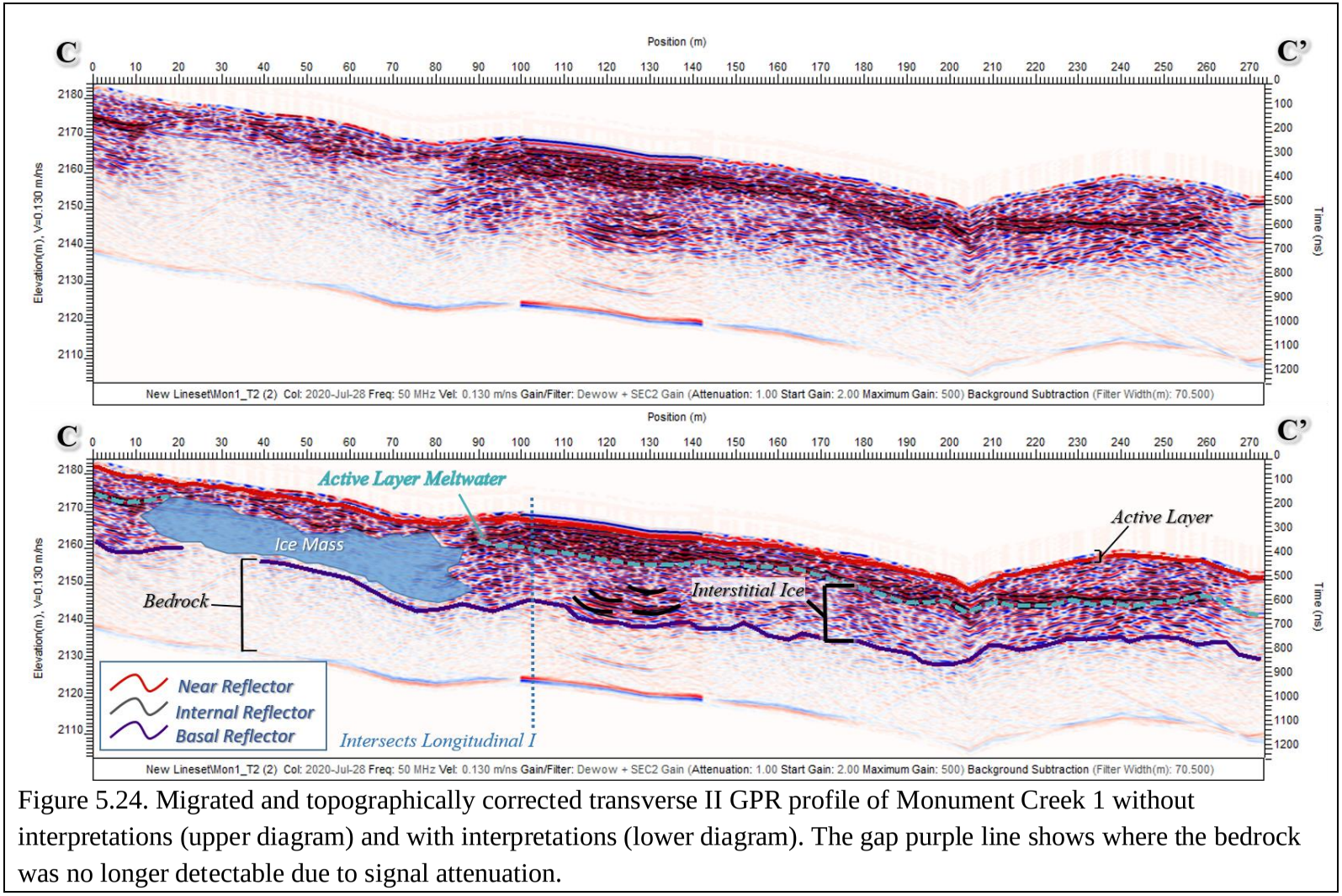

Figure 5.24. Migrated and topographically corrected transverse II GPR profile of Monument Creek 1 without interpretations (upper diagram) and with interpretations (lower diagram). The gap purple line shows where the bedrock was no longer detectable due to signal attenuation.

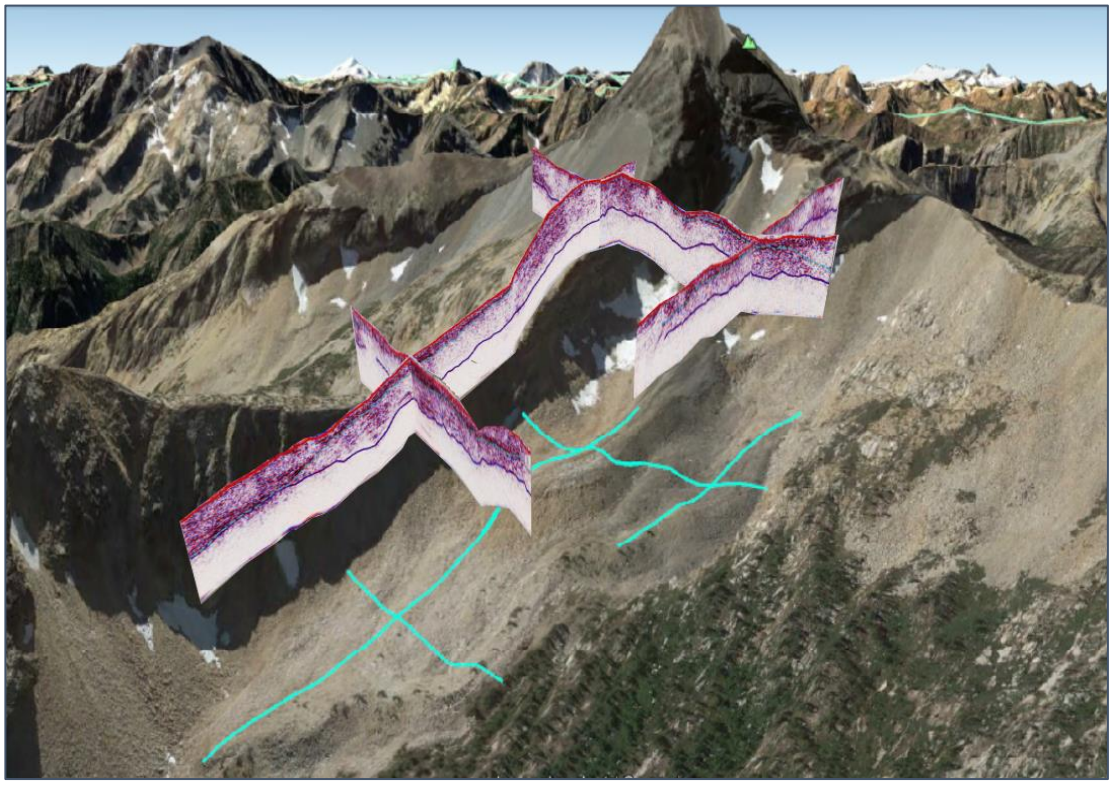

Figure 5.25. Fence diagram of the Monument Creek 1 rock glacier for comparison between the structure and composition of the interior and the surface morphology. Google Earth imagery from 8/19/2016.

Monument Creek 2 Rock Glacier

Monument Creek 2 (MC2) is an inactive, talus-derived rock glacier that shares an east-west trending sidewall with MC1 and has a RILA of 2,066 m (i.e., 287 m lower than MC1). MC2 is composed of angular granite, and its tongue-shaped morphology extends north at an 18° aspect (Lillquist and Weidenaar, 2021) (*Figure 5.26*). This feature has a length of 457 m and width of 288 m. Vegetation development and low angle, pressure ridges were documented near the gently sloped snout, indicative of its inactive state. No snow cover was observed at the surface of this rock glacier. Several outlet streams exited

the snout and contributed to Monument Creek, which has headwaters near MC1 and eventually flows into the Lost River, a tributary of the Methow River.

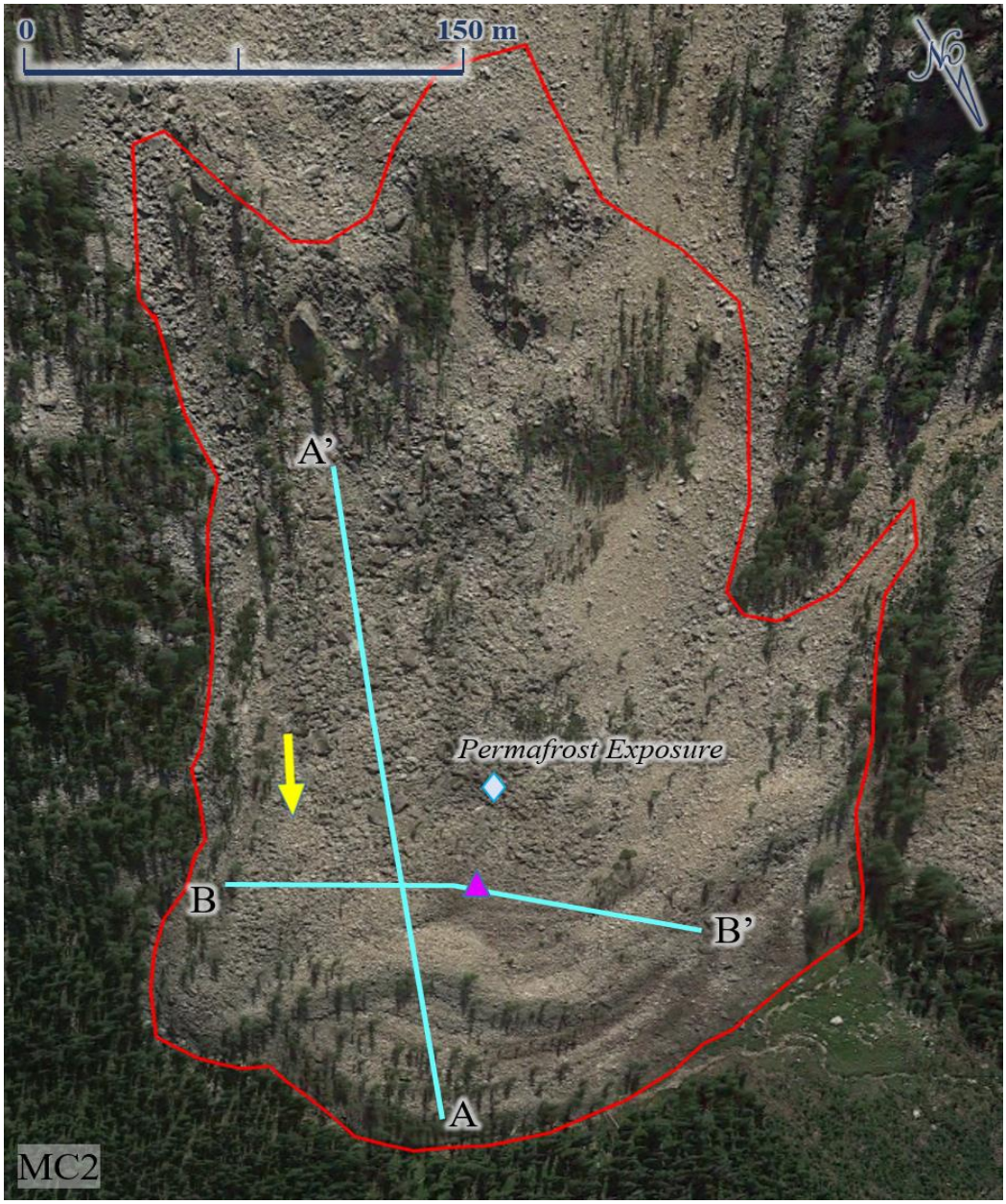

Figure 5.26. Planimetric view of the survey plan for the Monument Creek 2 rock glacier. The purple marker indicates the approximate location of the CMP. The blue marker shows the location where exposed permafrost was observed. Google Earth imagery from 8/19/2016.

During the GPR survey, permafrost was found 3 m beneath the surface (*Figures 5.26, 5.27*). This documented permafrost depth verifies the average active layer depth of 2.9 m, indicated by the near reflector in the GPR data. A clear basal reflector with an average depth of 17.1 m was interpreted as the bedrock contact (*Figures 5.27, 5.28*). This feature was composed largely of ice-cemented debris, as indicated by the relatively high concentration of diffracting signals, and propagation velocities ranging from 0.11-0.16 m/ns^{-1}, which Monnier and Kinnard (2013) and Kunz and Kneisel (2020) interpreted as permafrost. The sharp-bounded area of few diffracting signals (i.e., relatively homogenous material), between 0-90 m in *Figure 5.27*, with a deformation pattern that mirrors the pressure ridges at the surface, is likely an ice-rich zone (Kunz and Kneisel, 2020). Additionally, a surface depression can be observed under the CMP marker in *Figure 5.26* that was also captured in the topography of the transverse transect (110 -160 m in *Figure 5.28*) This depression corresponds with a subsurface zone of few diffracting signals, which may indicate an actively degrading ice lens related to the observed subsidence. Comparing surface observations with the GPR data validates the inactive, talus-derived classification of this rock glacier by Lillquist and Weidenaar (2021) and demonstrates the profound change in rock glacier activity from a 287 m decrease in RILA from MC1 to MC2.

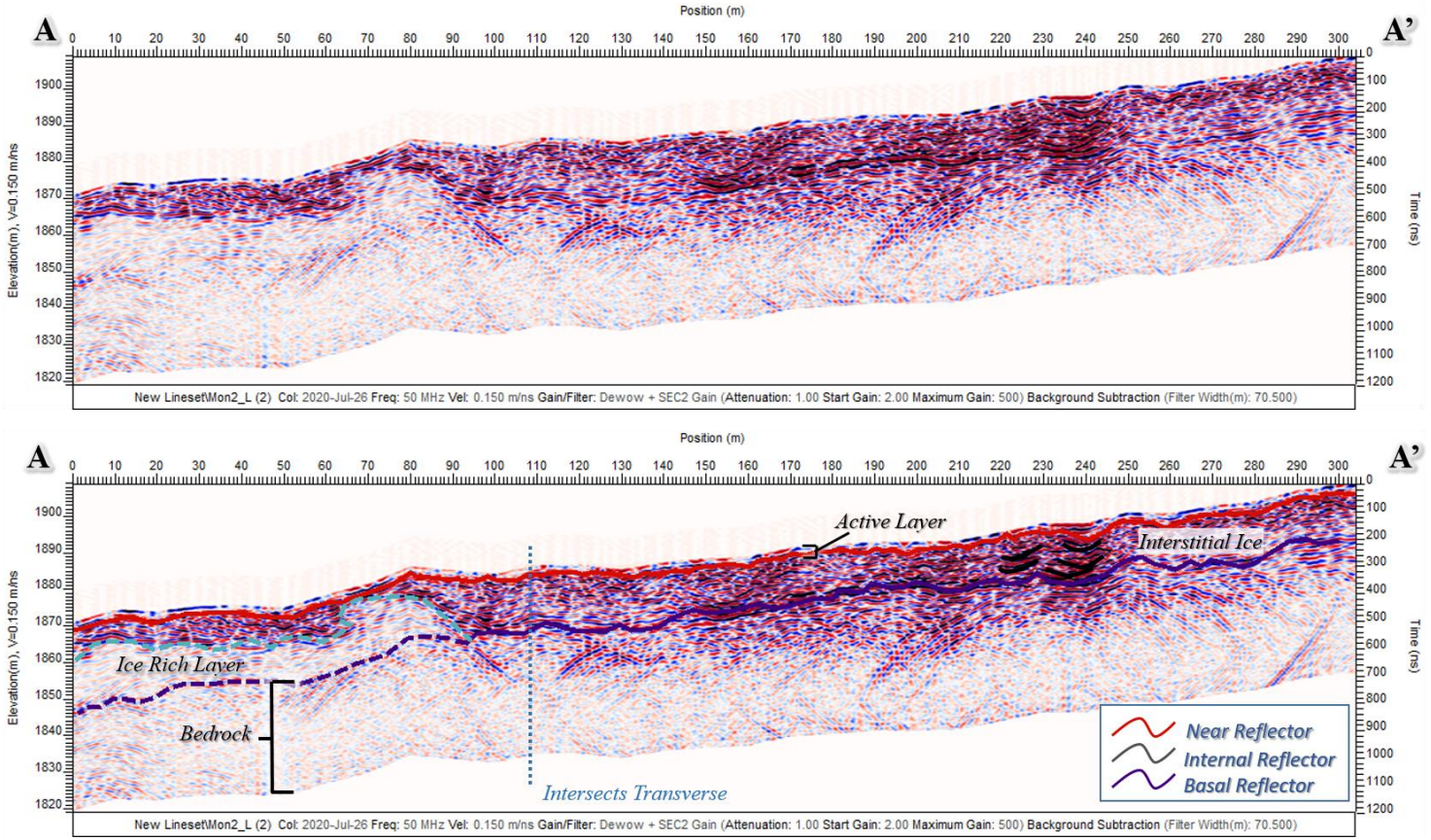

Figure 5.27. Migrated and topographically corrected longitudinal GPR profile of Monument Creek 2 without interpretations (upper diagram) and with interpretations (lower diagram). The purple dashed line represents the inferred bedrock depth.

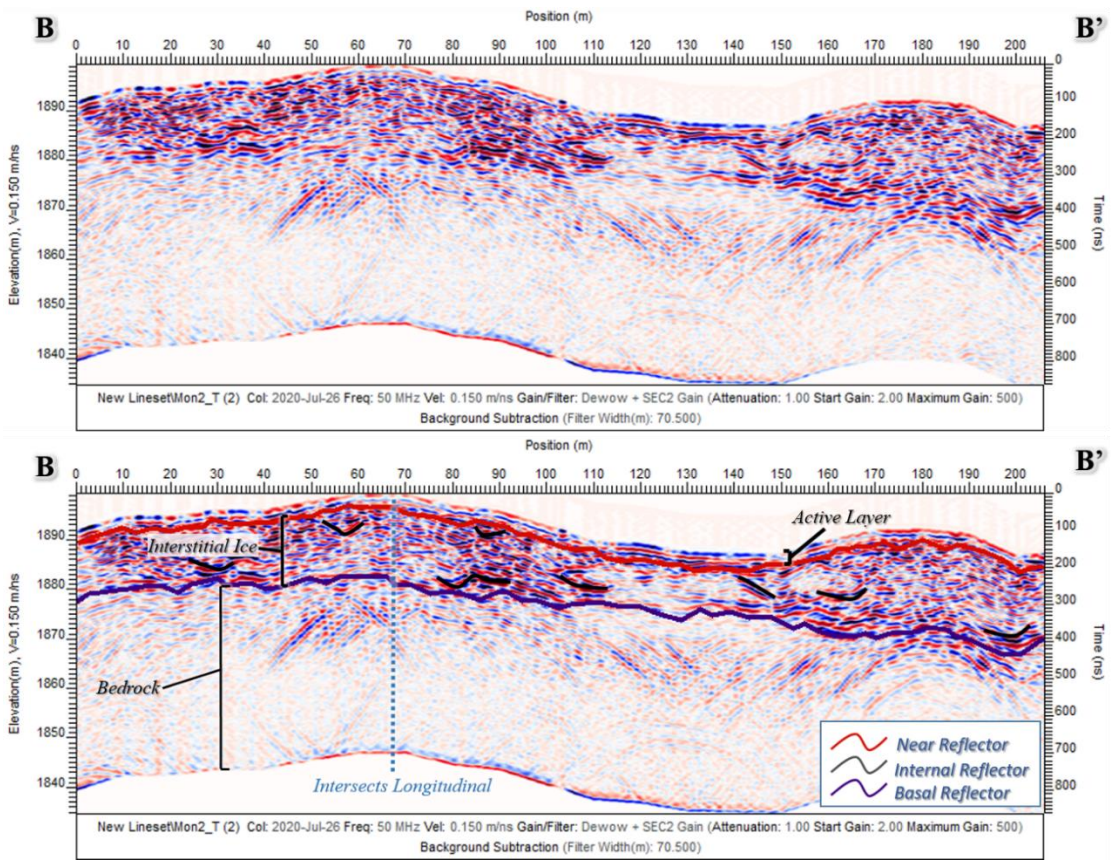

Figure 5.28. Migrated and topographically corrected transverse GPR profile of Monument Creek 2 without interpretations (upper diagram) and with interpretations (lower diagram).

Figure 5.29. Permafrost found 3 m below the surface of Monument Creek 2. Photo by Spencer Stinnett, 7/26/2020.

Eureka Creek 1 Rock Glacier

Eureka Creek 1 (EC1) is an inactive, talus-derived rock glacier that extends northeast at a 47° aspect from its headwall on Mount Rolo (*Figure 5.30*), with a RILA of 2,004 m (Lillquist and Weidenaar, 2021). This lobate feature was 112 m long and 264 m wide and composed of shale, sandstone, and conglomerate that fractured into large, blocky talus. The surface of EC1 was highly weathered, indicating relatively stable conditions. Longitudinal furrows were observed indicating extensional stress near the rooting zone, while transverse pressure ridges revealed compressional stress near the snout. Subalpine larch mantled the crest of each pressure ridge, and the outermost

pressure ridge had shrubs and soil development, indicating a relict lobe of the inactive feature. No snow or ice was present on the surface of EC1, but there were several streams leaving the snout and flowing into a subalpine meadow. Water from EC1 contributes to the Lost River and ultimately the Methow River.

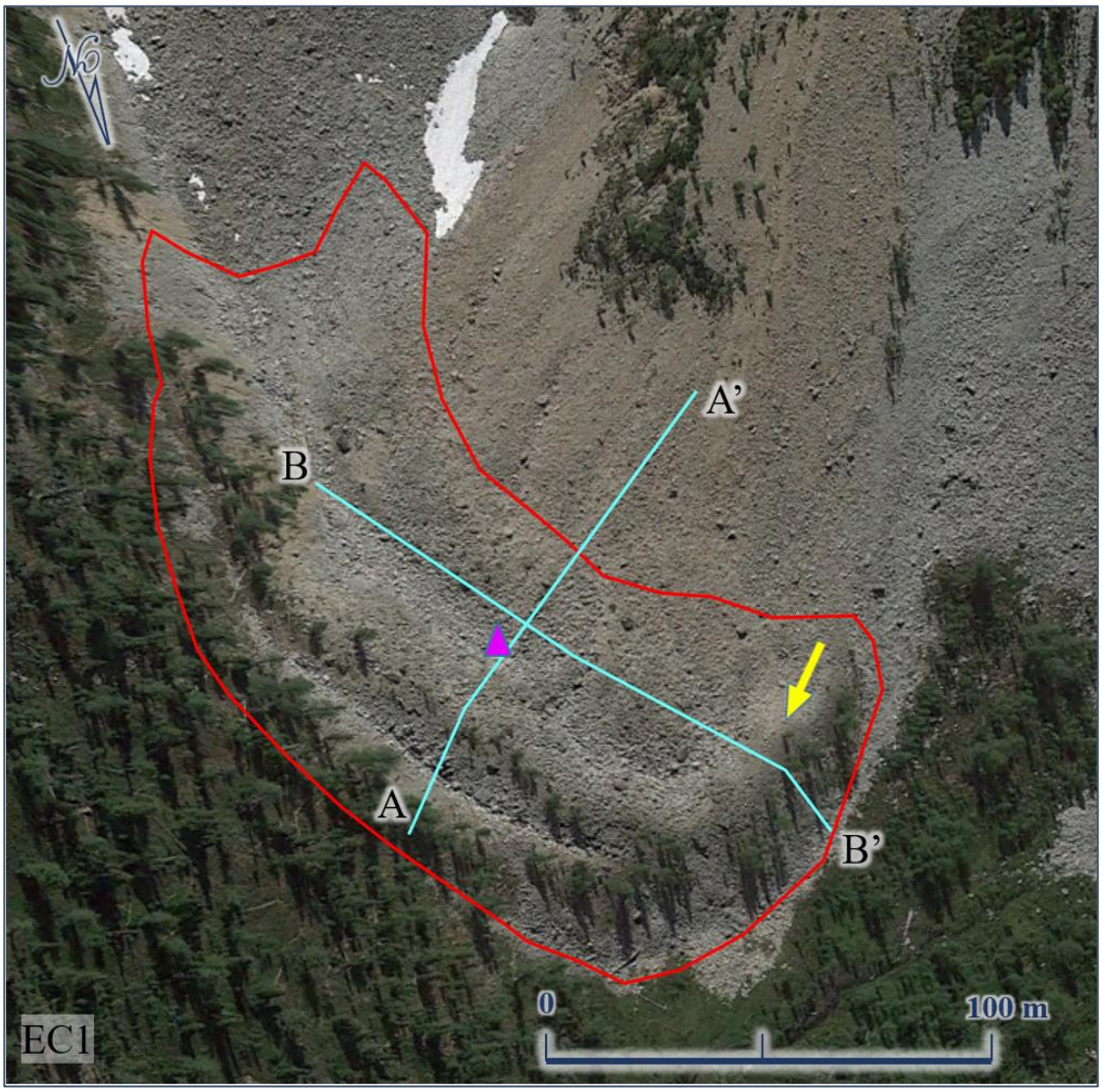

Figure 5.30. Planimetric view of the survey plan for the Eureka Creek 1 rock glacier. The purple marker indicates the approximate location of the CMP. The yellow arrow indicates flow direction. Google Earth imagery from 8/19/2016.

The survey of this rock glacier was particularly valuable because it provided subsurface information on the transition from an inactive (ice-filled) to a relict (ice-absent) state (*Figure 5.31*). This survey substantiates evidence for an ice-filled interior in these rock glaciers, because of the observed difference in properties (e.g., structure, EM velocities, and diffraction signal concentration) when such periglacial features no longer contain permafrost. Therefore, the GPR profile allowed for a comparison between relict and inactive GPR data to validate the ice content of other surveys.

The relict pressure ridge lacked linear reflectors that would suggest stratigraphic layers or stress planes. The GPR profile showed a high concentration of diffracting signals which indicates a heterogeneous mixture that is likely unconsolidated debris and soil. Propagation velocities recorded in the relict section were between 0.04-0.08 m/ns^{-1}, which suggest saturated or dry material and are significantly lower than the EM velocities for permafrost (i.e., 0.11-0.16 m/ns^{-1}) (Monnier and Kinnard, 2013; Kunz and Kneisel, 2020). The rest of the GPR profile is characteristically different from the relict lobe. The inactive feature shows variation in diffracting signal concentrations, indicating the well-documented heterogeneity in rock glacier composition (i.e., ice-rich and debris-rich zones), as proven from borehole studies (Haeberli, 1998; Arenson et al., 2002; Monnier and Kinnard, 2013); such variation was not observed in the relict lobe data. Furthermore, in the data for the inactive section of EC1, upglacier dipping internal reflectors correspond with the surface topography and indicate a shear plane (*Figure 5.31)*; such structures were not detected in the relict lobe.

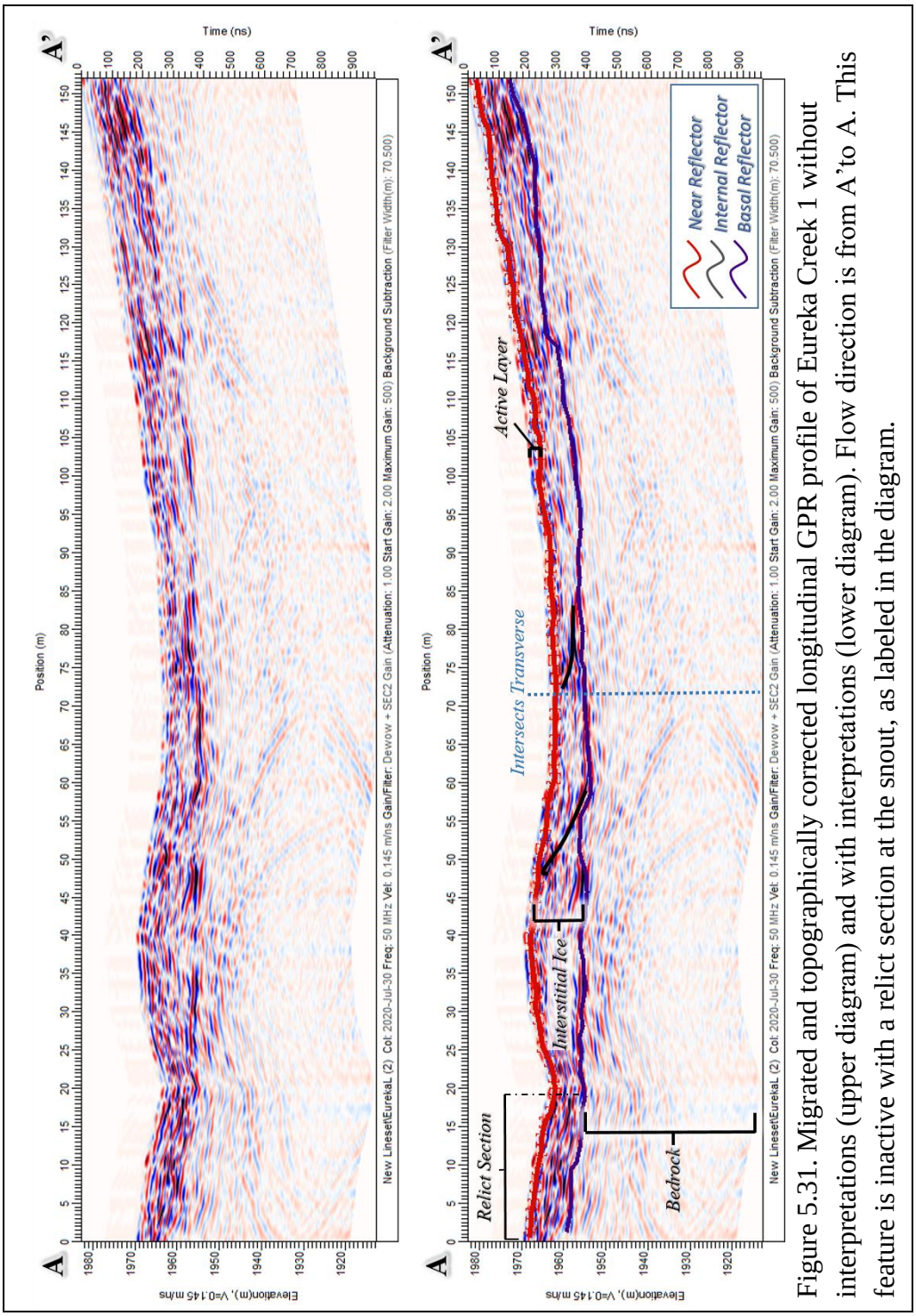

Figure 5.31. Migrated and topographically corrected longitudinal GPR profile of Eureka Creek 1 without interpretations (upper diagram) and with interpretations (lower diagram). Flow direction is from A'to A. This feature is inactive with a relict section at the snout, as labeled in the diagram.

In the GPR profile of EC1, a continuous near reflector with an average depth of 2 m indicated the base of the active layer. A distinct basal reflector with an average depth

of 10.6 m was interpreted as the bedrock contact. The average EM velocity recorded for the EC1 was 0.14 m/ns^{-1}, which likely reflects the greater influence of air voids in the active layer on the average velocity of such a thin feature. The propagation velocities, shear plane, and heterogeneity of material, indicated by variation in signal density, suggest a rock glacier that consists of ice-cemented debris, interspersed with debris-rich layers, thereby supporting the inactive, talus-derived classification by Lillquist and Weidenaar (2021).

A possible correlation exists between major surface depressions and subsurface ice in intact rock glaciers. For the first 90 m of *Figure 5.32*, or until the transverse transect intersects the longitudinal transect (*Figure 5.30*), a surface depression corresponds with a relatively high concentration of subsurface ice, for this feature. This was also observed in the major depression in the upper level of MC1, where there is a high confidence level of ice presence based on the diffraction signals and EM velocities of two intersecting transects (see 500 – 560 m in *Figure 5.21*; 20 - 120 m in *Figure 5.23*; and *Figure 5.25*). Similar observations were made on MC2 (see 110 – 160 m *Figure 5.28*), which had a major depression directly above a particularly ice-rich zone. If these observations prove to be a consistent pattern, the following are two possible explanations: 1) either there is a sink effect where snow accumulates preferentially in a depression and, under melting conditions, percolates into the underlying talus matrix and refreezes, resulting in a relatively high concentration of ice in the rock glacier beneath surface depressions; or 2) the depression is located in a localized area of subsidence due to subsurface permafrost decay, and the ice evident in the GPR imaging is ice that has not

yet degraded. It is possible that both scenarios are valid and applicable at different sites. For example, the sink effect theory is favorable at MC1 because the major surface depression was likely preexisting and inherited from a moraine. Moreover, Google Earth Imagery shows runnels in the snowpack that accumulated in this depression that indicate meltwater pathways percolating into the underlying talus. Furthermore, this rock glacier is active, so permafrost decay is unlikely. By comparison, permafrost degradation and subsequent subsidence are more likely the processes involved at MC2 and EC2, as both are inactive rock glaciers.

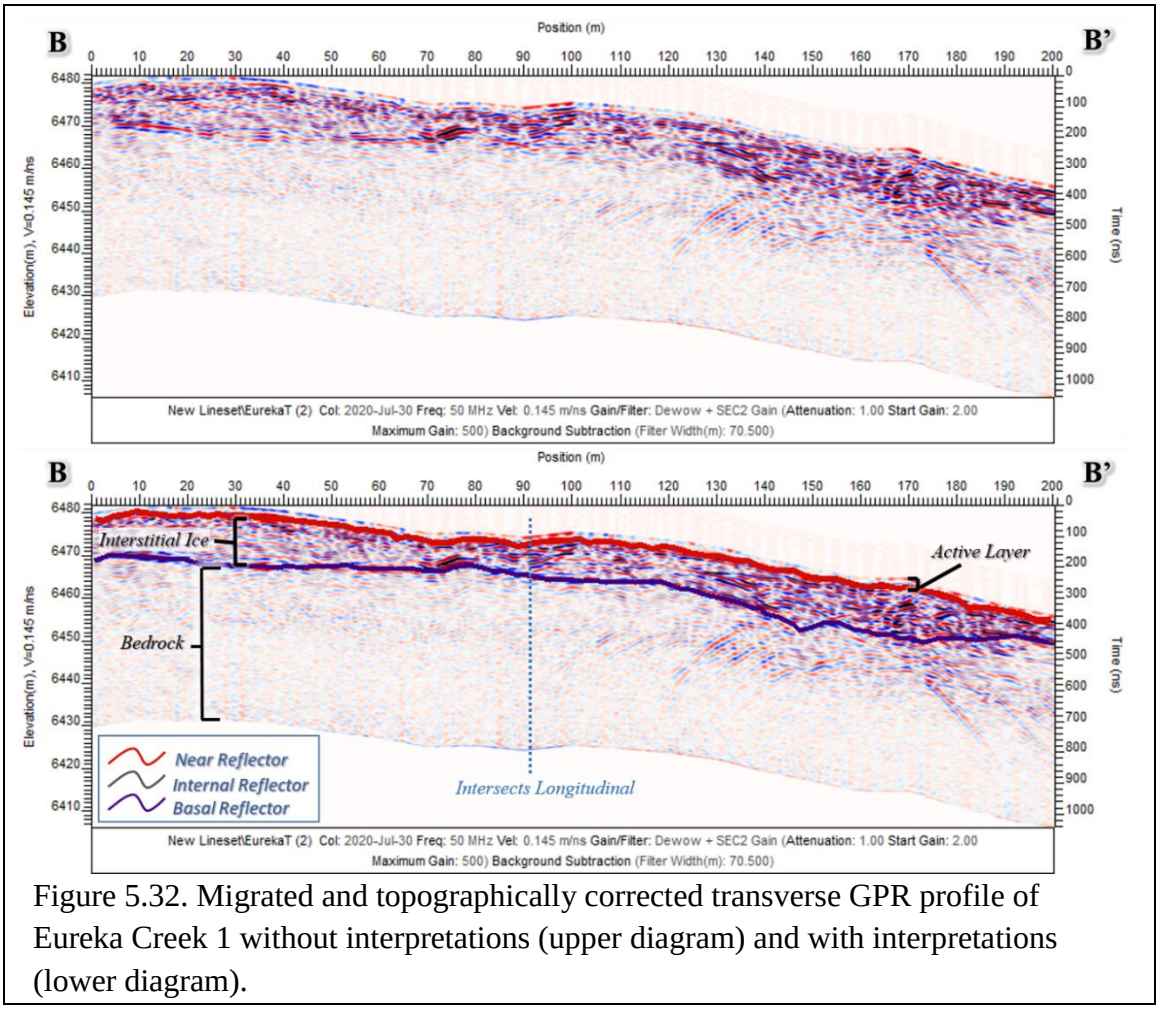

Figure 5.32. Migrated and topographically corrected transverse GPR profile of Eureka Creek 1 without interpretations (upper diagram) and with interpretations (lower diagram).

Canyon Creek Study Site

Barron Creek 1 Rock Glacier

Barron Creek 1 (BC1) flows northeast at a 64° aspect from the sidewall of a north-facing cirque on the west side of the Cascade Crest (*Figure 5.33*). BC1 is an inactive, talus-derived rock glacier that has the lowest RILA (1670 m) of all surveyed features. The pressure ridges were subtle and many subalpine larch trees grew on the snout and flanks. BC1 is tongue-shaped with a length of 180 m and a width of 177 m. The parent material of this site is shale, conglomerate, and sandstone that fractured into large, blocky talus. No ice or snow was observed on the surface of BC1, but several small outlet streams were exiting the low angle snout. Discharge from this feature feeds into Barron Creek which flows into Canyon Creek and contributes to the Skagit River.

In the GPR profile, a clear reflector running parallel to the rock glacier surface, with an average depth of 2.4 m, was interpreted as the base of the active layer. A distinct basal reflector was also detected with an average depth of 13.5 m, indicating the bedrock contact (*Figures 5.34, 5.35*). Additionally, this feature had an average EM velocity of 0.14 m/ns^{-1}. At 20-170 m upslope from the starting position (*Figure 5.34*), numerous up-glacier dipping internal reflectors suggest shear stress and a potential shear horizon where the majority of horizontal displacement occurs (Haeberli et al., 1998; Arenson et al., 2002; Ladanyi, 2003). Internal reflectors between 0 – 20 m (*Figure 5.34)* reveal extensional stress in response to steepened bedrock topography. The abundance of prominent shear and extensional stress indicators illustrate permafrost creep, which is likely augmented by the steep bedrock topography at this site. Furthermore, signal

density decreases with depth, and given that EM velocities range from 0.09-0.12 m/ns^{-1}, these data are evidence of a gradient from saturated debris to interstitial ice deeper in the feature. These findings are consistent with the inactive, talus-derived classification by Lillquist and Weidenaar (2021).

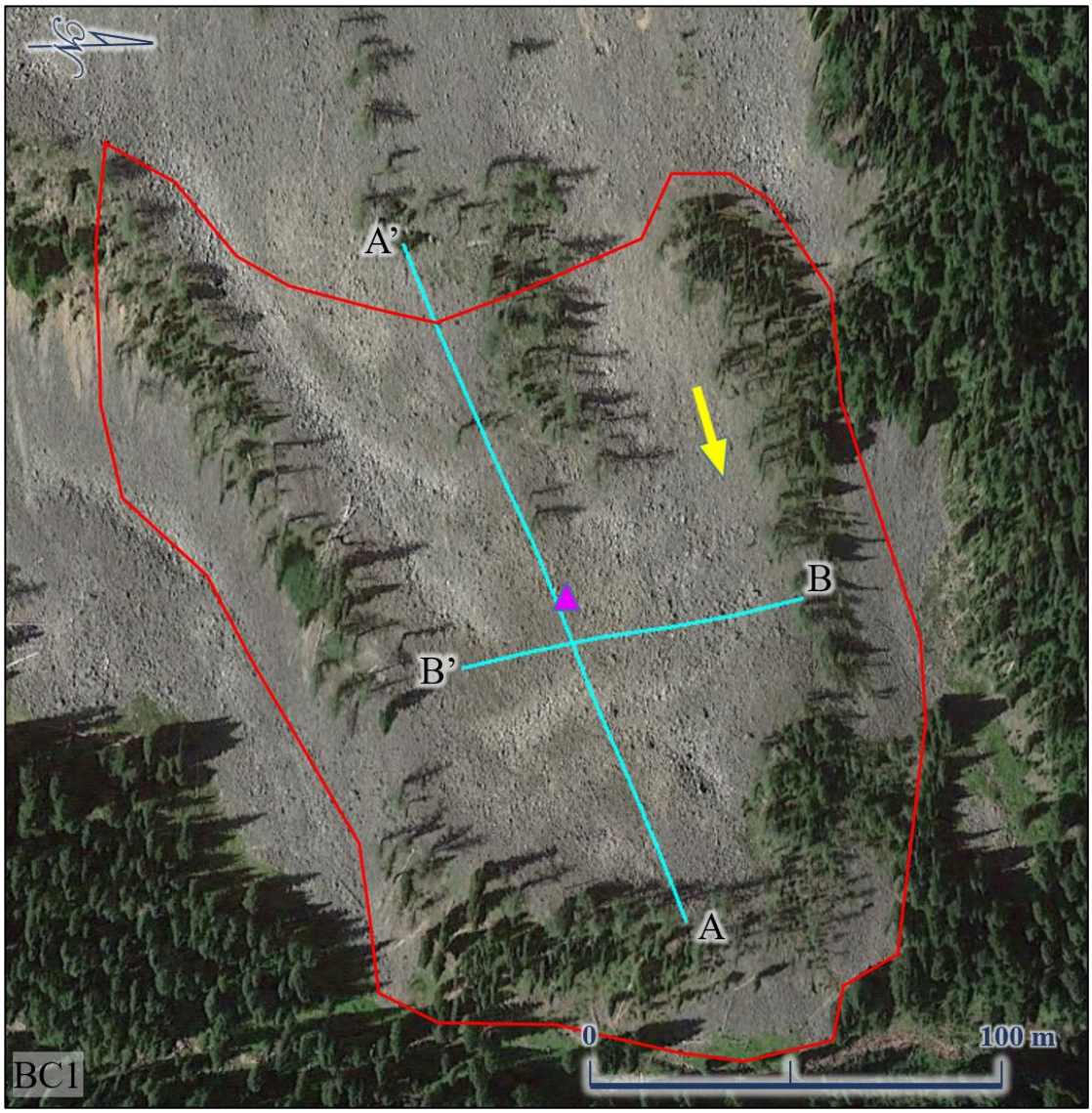

Figure 5.33. Planimetric view of the survey plan for the Barron Creek 1 rock glacier. The purple marker indicates the approximate location of the CMP. The yellow arrow indicates flow direction. Google Earth imagery from 8/19/2016.

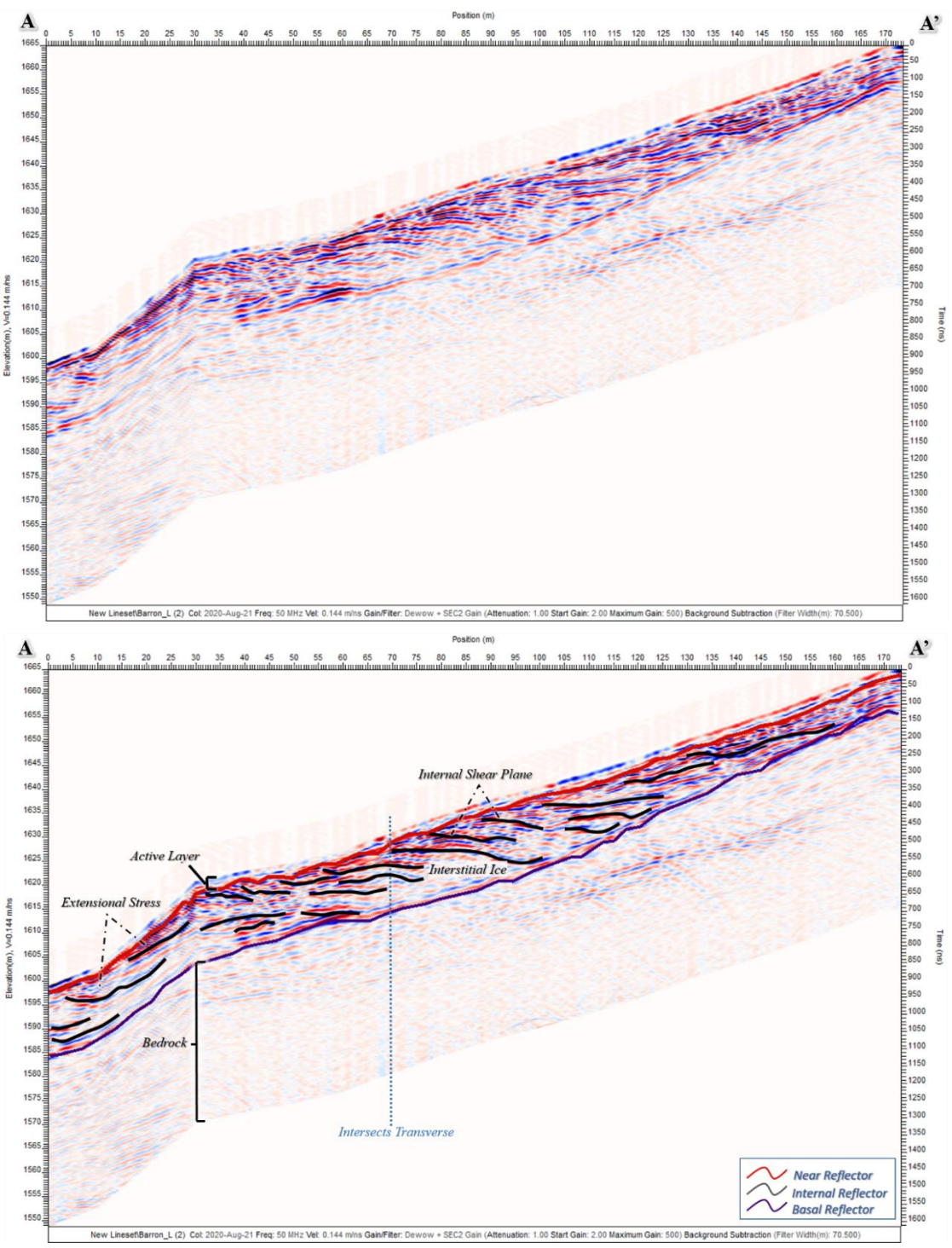

Figure 5.34. Migrated and topographically corrected longitudinal GPR profile of Barron Creek 1 without interpretations (upper diagram) and with interpretations (lower diagram).

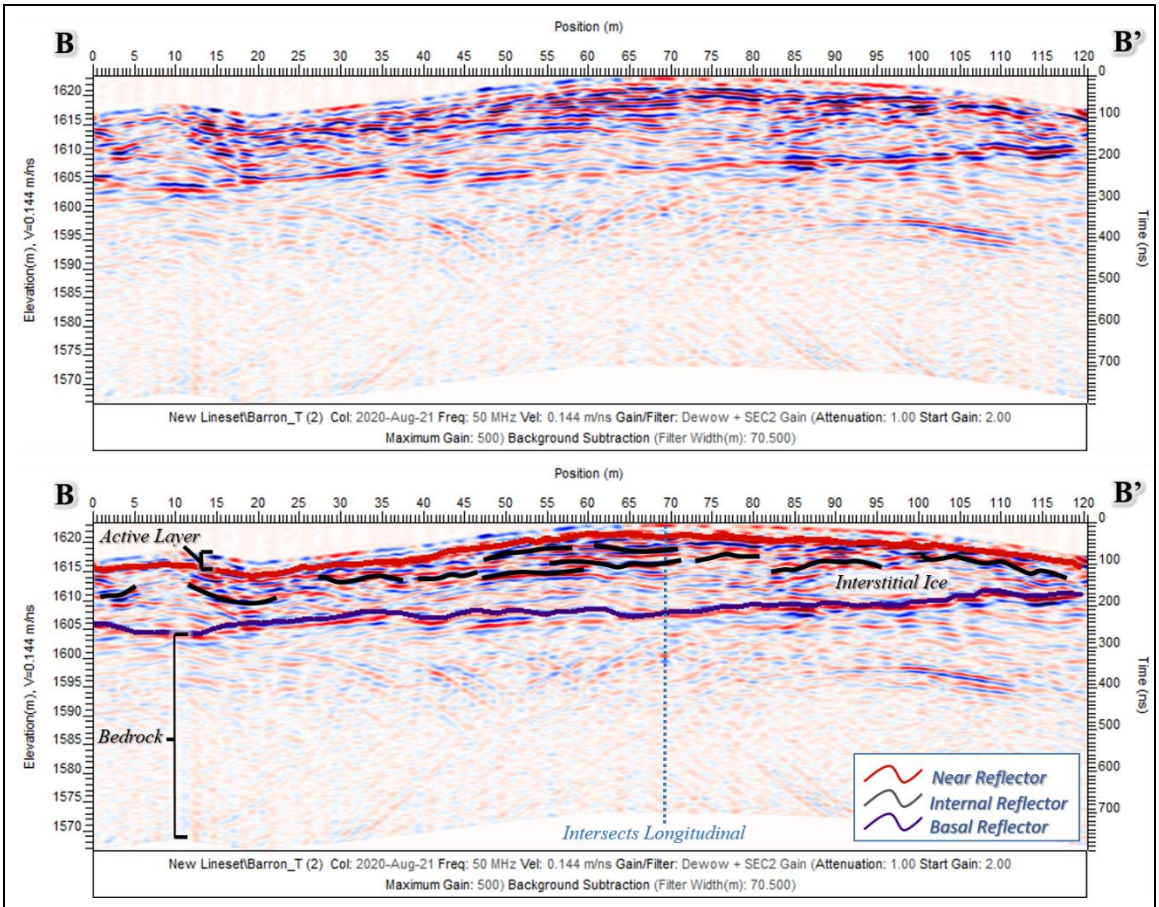

Figure 5.35. Migrated and topographically corrected transverse GPR profile of Barron Creek 1 without interpretations (upper diagram) and with interpretations (lower diagram).

Water Content

Ten of the 53 rock glaciers in the North Cascades transect were surveyed in this study. Combined, the surveyed sites account for 32% of the total rock glacier surface area in the transect. The WVEQ for the surveyed rock glaciers ranged from 27,287 m^3 (0.00003 km^3) to 2,708,499 m^3 (0.00271 km^3) (Table 6). The total WVEQ for GPR surveyed rock glaciers totalled 6,551,482 m^3 (0.00655 km^3). This value was extrapolated and scaled to the surface area of rock glaciers in the same elevation bracket

which yielded a North Cascades rock glacier WVEQ estimate of 19,748,801 m^3 (0.01975 km^3).

Table 6. WVEQ of surveyed rock glaciers and the extrapolated WVEQ of rock glaciers of similar elevation. The table includes the MAAT that permafrost in the study area will be exposed to throughout the 21st Century according to the ClimateNA Simulation.

Elevation Bracket	Name	RILA	WVEQ (m^3)	Total WVEQ (m^3) of surveyed rock glaciers in each elevation bracket	Extrapolated WVEQ (m^3) for all rock glaciers in each elevation bracket	% permafrost of total study area	2019 MAAT of each elevation bracket	2100 MAAT of each elevation bracket: RCP 2.6	2100 MAAT of each elevation bracket: RCP 8.5
East Side									
2180-2353 m	Monument 1	2353 m	2,708,499						
	Eightmile 1	2191 m	1,643,486	4,351,985	10,517,565	58%	1.3°C	3.6°C	8.9°C
2091-2172 m	Eightmile 2	2102 m	844,706						
	Copper Glance 10	2091 m	73,907	918,614	3,416,447	19%	1.6°C	3.9°C	9.2°C
1974-2067 m	Monument 2	2066 m	618,168						
	Copper Glance 2	2051 m	61,460						
	Eureka 1	2004 m	103,626						
	Copper Glance 3	1981 m	27,287	810,541	2,284,087	12%	1.8°C	4.1°C	9.4°C
1779-1962 m	Copper Glance 6	1779 m	345,360	345,360	2,033,245	11%	2.3°C	4.5°C	9.8°C
West Side									
1670-1981 m	Barron 1	1670 m	124,981	124,981	1,497,458		2.8°C	4.9°C	10.3°C
Totals:				6,551,482	19,748,801				

Geoecology

The WVEQ results were used to investigate the change in water content related to increased altitude and continentality (i.e., geoecological change). *Figure 5.36* compares the rock glacier quantity, surface area, and permafrost volume to show how these variables change across altitude in the North Cascades. In this study area, only six rock glaciers exist west of the Cascade Crest which is not a sufficiently large population to subdivide in a way that would produce meaningful data. Therefore, these results only include rock glaciers east of the Cascade Crest in this study area. These findings show an enhanced rock glacier water capacity at higher altitudes, with the highest elevation bracket comprising approximately one-third of the rock glaciers yet containing nearly two-thirds of the stored water.

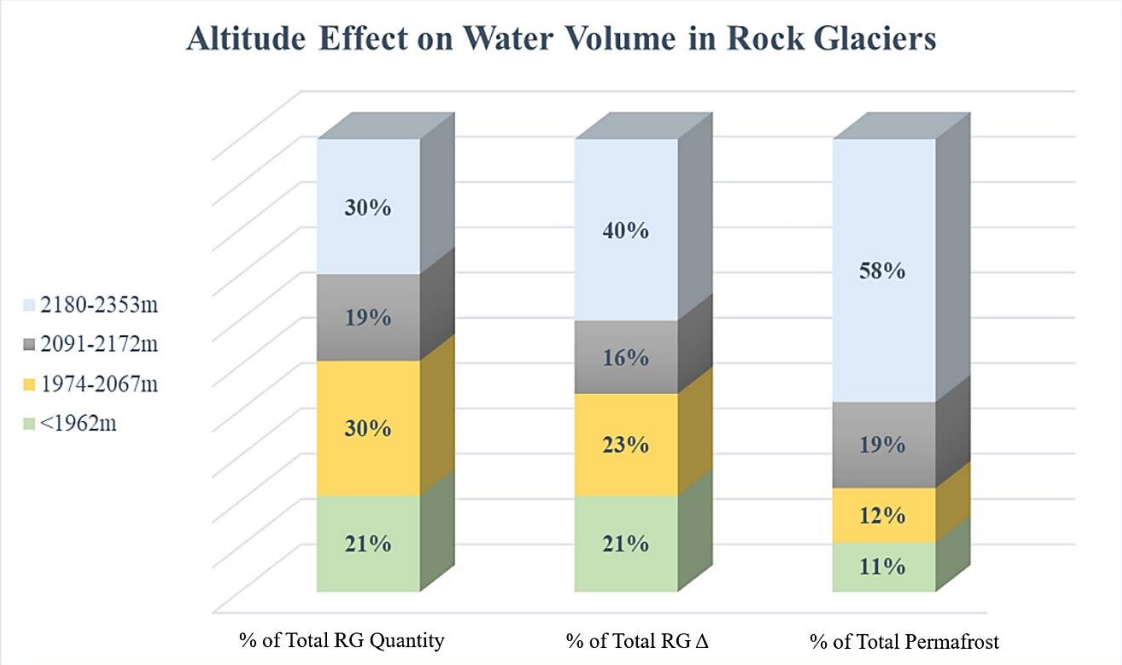

Figure 5.36. Water capacity of North Cascades rock glaciers in relationship to elevation. For example, although only 30% of the rock glaciers exist in the highest elevation bracket, they compose 58% of the total permafrost. The opposite effect is observed in the composition of lower elevation rock glaciers.

When comparing rock glacier WVEQ with continentality, the water volume of surveyed rock glaciers was normalized by surface area to show how the percentage of water volume in rock glaciers changed between the maritime Western Cascades to the semi-arid Eastern Cascades (*Figure 5.37*). Although the data show an overall increasing trend of water capacity with increased continentality, the observable difference is minor (i.e., the surveyed dataset is small, and the apparent trend is slight). To verify a relationship between rock glacier water capacity and continentality more surveys are necessary over a larger region.

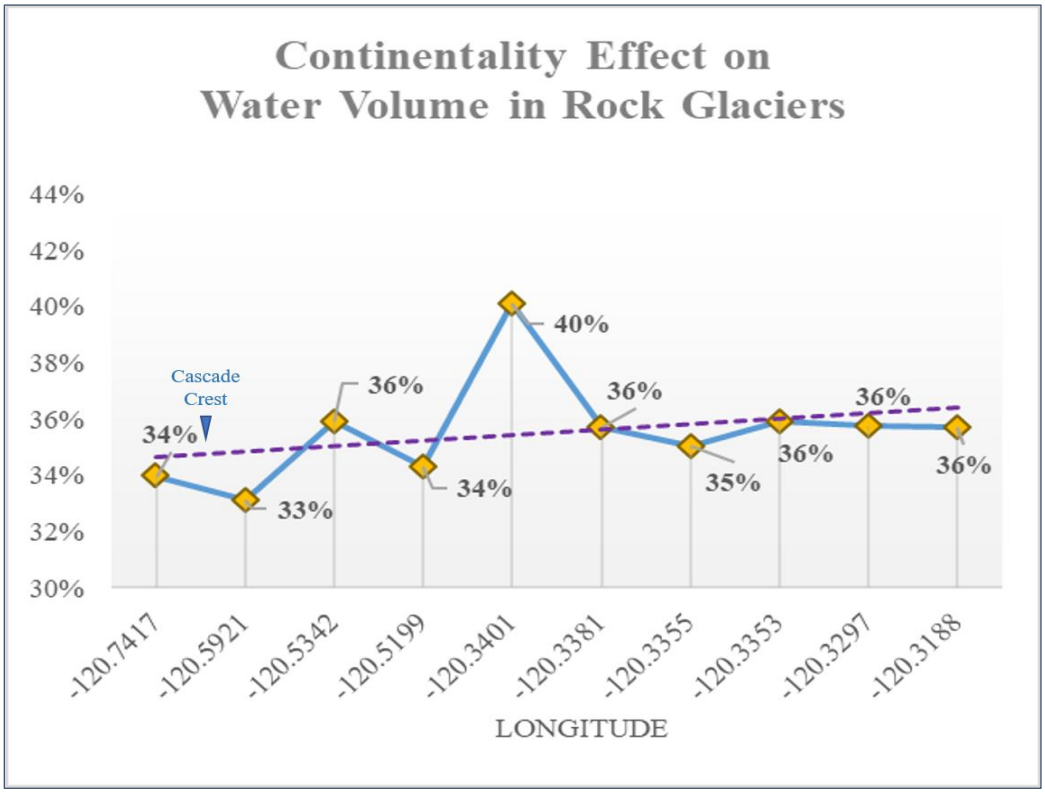

Figure 5.37. Maritime versus continental effect on water content of rock glaciers in the periglacial zone of the North Cascades.

Permafrost Distribution

A regional permafrost distribution map was modeled for the North Cascades based on regional mapping of RILA on intact rock glaciers and verified with field-based geophysical measurements indicating ice content (*Figure 5.38*). This map shows areas where discontinuous and continuous permafrost is likely, revealing the full extent of permafrost vulnerable to the simulated temperatures. This map does not account for glaciers and snowpack that exist at similar elevations. All of these are critical water resources for mountain biodiversity, ecosystem health, and community wellbeing.

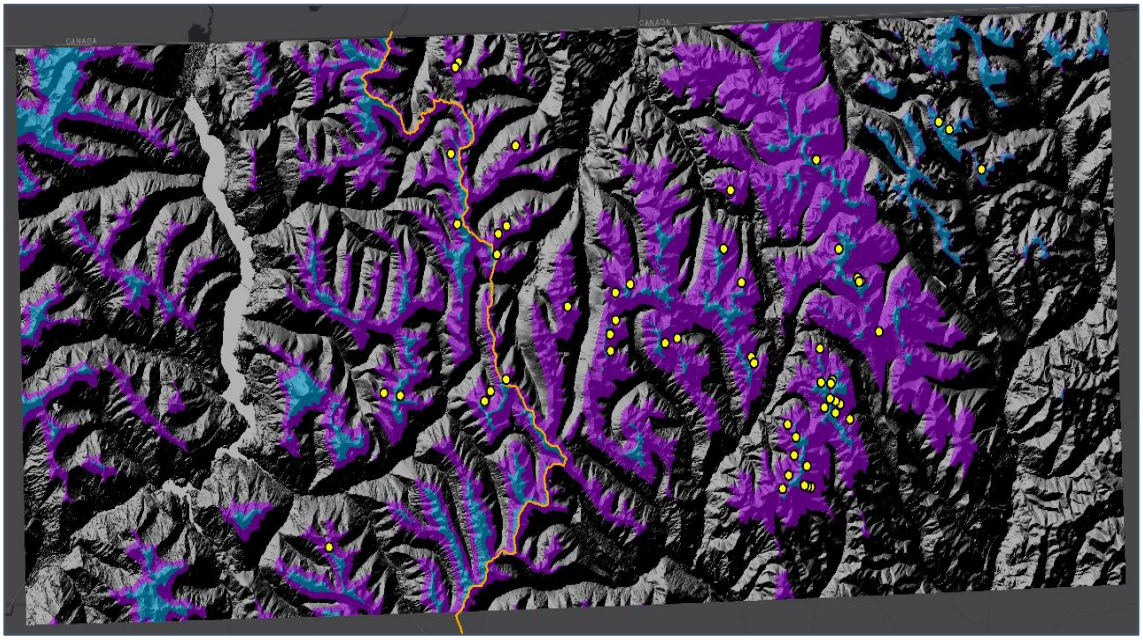

Figure 5.38. The North Cascades permafrost distribution derived from RILA. The yellow markers show rock glacier locations. The purple area shows elevations within the upper and lower bounds of the modern RILA of intact rock glaciers and indicates the area where discontinuous permafrost is likely. The blue area shows elevations above the upper limit of RILA where discontinuous permafrost is very likely and there is potential for continuous permafrost.

Climate Sensitivity

The ClimateNA simulation (Wang et al. 2016) was implemented to determine how much rock glacier permafrost will be subject to melting temperatures over the 21st century. This study compares the temperatures at each site in 2019 with RCP 2.6 and RCP 8.5 scenarios for 2100 (*Figure 5.39*). These data show a modeled MAAT range of 0-3°C in 2019 with only two rock glaciers (Monument Creek 1 and Lease Creek 2, location shown in *Figure 3.5*) having a MAAT of 0°C in this year. The MAAT of all other rock glaciers in the study area exceeds the necessary temperature threshold of 0°C for permafrost development and maintenance. Additionally, there is an observable pattern of amplified MAAT on rock glaciers west of the Cascade Crest in every scenario.

The EM1 rock glacier has a modeled 2019 MAAT of 1.7°C, which is consistent with data logger measurements from June, 2009 – Aug, 2010 that recorded a MAAT of -0.1 +/- 1.6°C at this site (Goshorn-Maroney, 2012). Additionally, MC1 and MC2 provide a good example of the observed effects from just a 1°C change in MAAT. MC1 (0°C MAAT) is active with an inflated appearance, steep snout, and fresh surface debris (*Figure 4.6*). In contrast, MC2 (1°C MAAT) is inactive with subsidence from partial ice loss, a less-pronounced snout, and weathered surface debris (*Figure 4.13*).

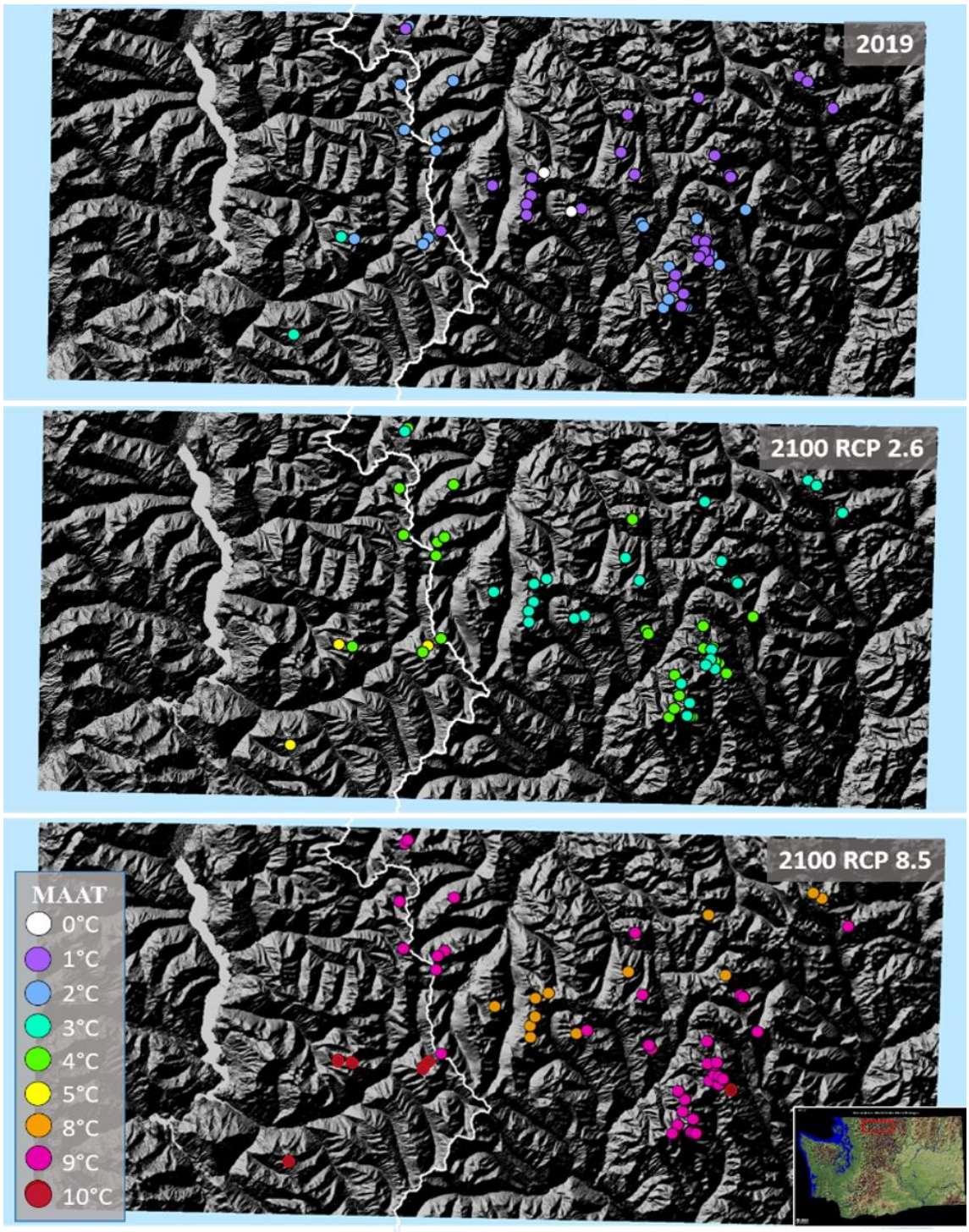

Figure 5.39. Modeled MAAT at North Cascades rock glacier sites in 2019 and the range of temperatures these sites will be exposed to in the 21st Century under different radiative forcing scenarios.

In the 2100 RCP 2.6 scenario, which is only achievable with strict climate mitigation policies and GHG reduction, the MAAT ranges from 3-5°C at the rock glacier sites. In the 2100 RCP 8.5 scenario, which is the current climate trajectory, rock glacier MAAT ranges from 8-10°C. Therefore, all rock glaciers in all elevation brackets of this study area will be subject to MAAT between 3-10°C by 2100. *Figure 5.40* shows the relationship between simulated temperature and elevation, with the lowest MAAT at the highest elevations in every scenario.

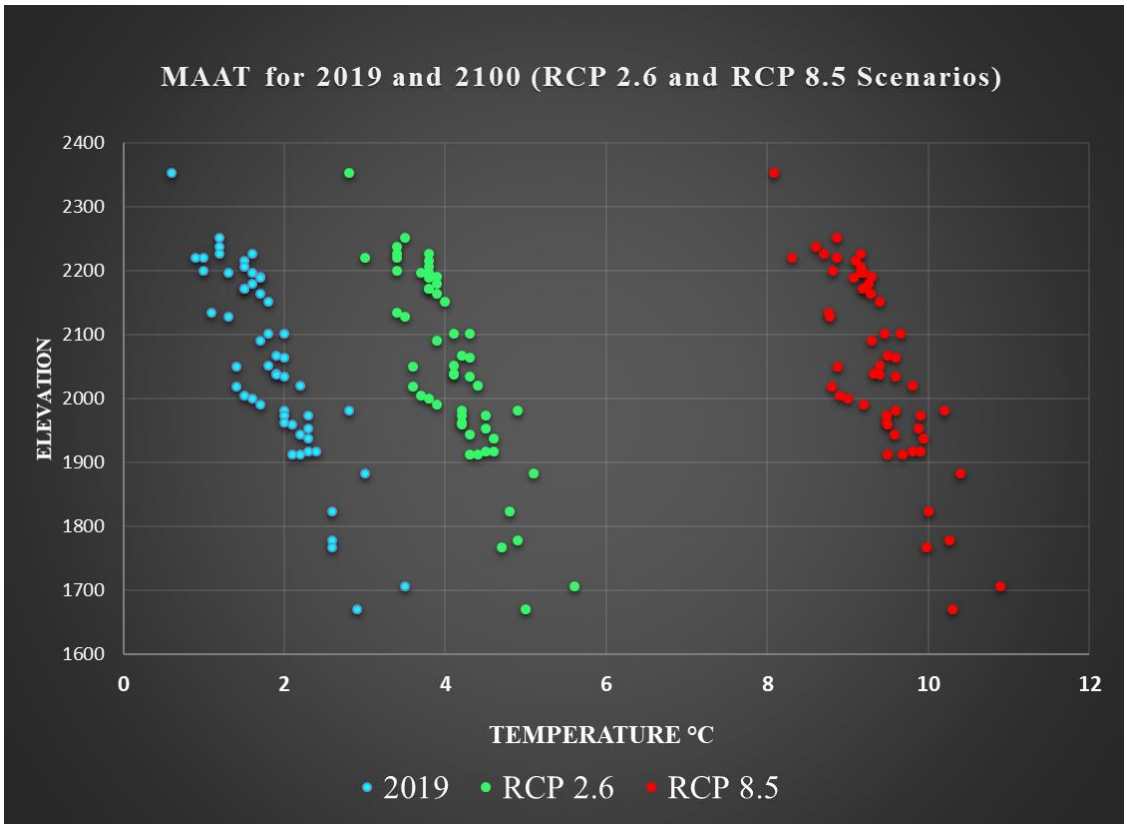

Figure 5.40 Modeled MAAT for each North Cascades rock glacier site in 2019 and for two climate scenarios in 2100 (RCP 2.6 and 8.5) compared to elevation.

In *Figure 5.41*, the simulated MAAT results reveal higher rates of temperature increase at higher elevations, a finding that is consistent with the growing evidence for

Elevation-Dependent Warming (EDW) in the literature (Bradley et al., 2004; Pepin and Lunquist, 2008; Salathé et al., 2010; Rangwala et al., 2013; Pepin et al., 2015; Karmalkar and Bradley, 2017; Palazzi et al., 2017, 2018; Minder et al., 2018).

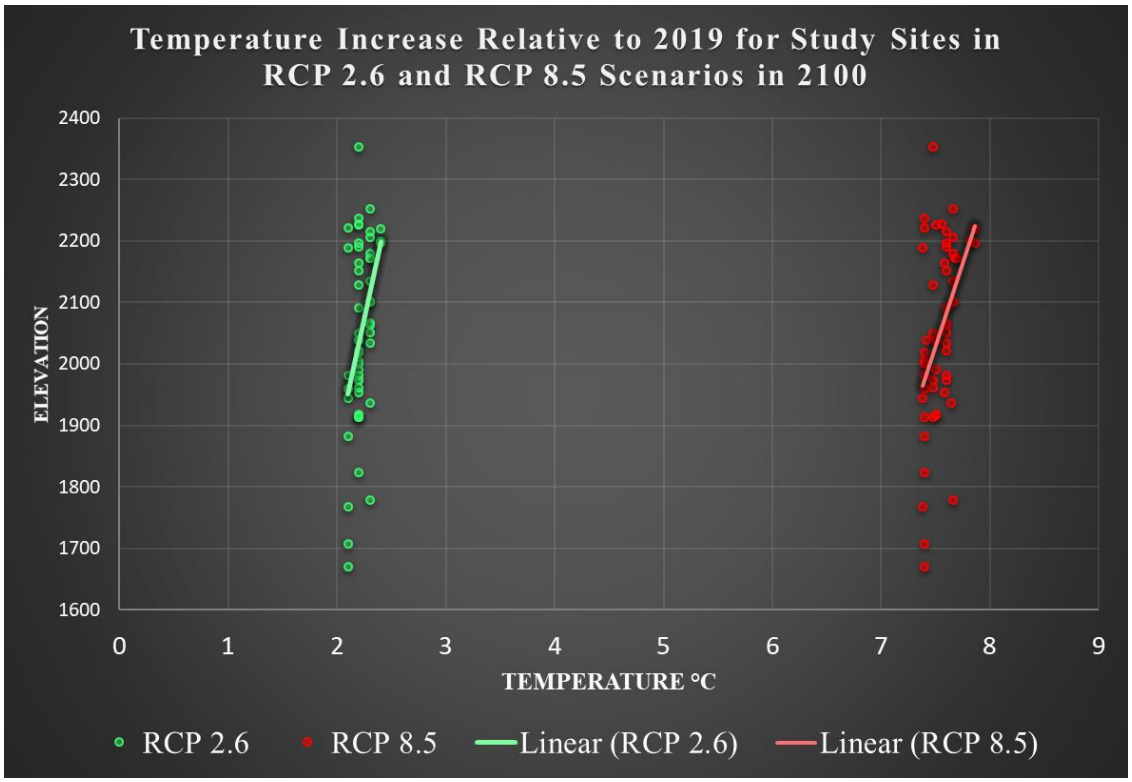

Figure 5.41. Modeled temperature increase of each North Cascades rock glacier site relative to 2019 temperature conditions. Notice that EDW is more prominent in the 8.5 scenario.

Elevation-Dependent Warming Synthesis

Elevation-Dependent Warming (EDW) has been documented around the world. The modeled maximum temperature increase (RCP 8.5) reaches 7°C by 2100 in the Andes (Urrutia and Vuille, 2009) and in the Rocky Mountains (Rhoades et al., 2017). In a global scale climate simulation, Nogués-Bravo et al., (2006) found that mid-high latitude mountains would experience increases of 5.4-6.7°C by 2085 in an RCP 8.5 scenario. Additionally, a simulation conducted in a transect along the axis of the American

Cordillera showed 2.5-3℃ MAAT increase above 3000 m, if global CO_2 concentrations were doubled (RCP 8.5 is a scenario with triple the global CO_2 concentrations) (Bradley et al., 2006). Furthermore, other studies have made EDW simulation reports more concrete with physical records from observation stations such as in the Tibetan Plateau where five stations documented 0.6-0.8℃/per decade increase between 1991-2012 at 3500 m elevation (i.e., 12.6 – 16.8℃ increase over 21 years) (Yan and Lui, 2014). Similarly, a study using 268 observation stations in the tropical Andes found a 0.11°C/per decade increase between 1939-1998 (the global average is 0.06°C/per decade) (Vuille et al., 2003).

The results in *Figure 5.40* not only exemplify EDW, but also suggest enhanced EDW with higher radiative forcing (i.e., the RCP 8.5 scenario has a steeper curve than that shown in the RCP 2.6 trend). The RCP 2.6 scenario shows a modeled MAAT increase ranging from 2.1-2.4°C and the RCP 8.5 MAAT increase is 7.4-7.9°C. These results are supported by similar EDW findings in mountain ranges across the globe (Urrutia and Vuille, 2009; Salathé et al., 2010; Karmalkar and Bradley, 2017). Moreover, due to the ablation effect associated with increased humidity, it is more likely that coastal mountains will experience enhanced sensitivity to EDW compared to continental environments (Rhoades et al., 2017), which explains the amplified warming of rock glaciers west of the Cascade Crest (*Figure 5.38*).

Water Content Synthesis

The rock glacier Water Volume Equivalence (WVEQ) results in this study have important implications for water resources in the Washington Cascades. The WVEQ for

the 53 rock glaciers in this study (i.e., 0.020 km^3) is nearly the volume previously estimated for the 130 intact rock glaciers in the entire Eastern Cascades Rock Glacier Inventory (i.e., 0.023 km^3) (Riffle, 2018). If the methods in this study are applied to the entire Eastern Cascades Rock Glacier Inventory (now including 140 intact rock glaciers), the total WVEQ estimate is 0.054 km^3 (Table 7).

Table 7. WVEQ estimates of the current work for comparison with Riffle (2018).

Water Content Synthesis				
	Quantity of Intact Rock Glaciers	Combined Surface Area (m^2)	WVEQ (m^3)	WVEQ (km^3)
North Cascades Rock Glaciers (current work)	53	2,278,118	19,748,801	0.019749
Eastern Cascade Rock Glacier Inventory (Riffle, 2018)	130	5,570,000	22,999,468	0.029994
Updated Eastern Cascade Rock Glacier Inventory (this study)	140	6,327,196	54,194,814	0.054195

A comparison of the regional water content of rock glaciers to glaciers is useful to understand their role in local hydrology, as seen throughout the literature (Brenning, 2005; Azócar and Brenning, 2010; Perruca and Angillieri, 2011; Rangecroft et al., 2015; Jones et al., 2018). Findings are typically communicated in a ratio of rock glacier to glacier water volume and range from 1:2.7 in Chile (Azócar and Brenning, 2010) to 1:83 in the Alps (Brenning, 2005). Riffle (2018) calculated the WVEQ of the 218 Eastern

Cascades glaciers using the area-volume scaling method by Chen and Ohmura (1990), which has a <5 percent uncertainty. My updated Eastern Cascades rock glacier inventory WVEQ of 54,194,814 m^3 compared to the Eastern Cascades glacier WVEQ of 1,074,000,000 m^3 (Riffle, 2018), equates to a ratio of 1:20 (Table 8). For reference, perennial snowfields in Washington state have an estimated WVEQ of 158,726,923 m^3 (Fountain et al., 2017). This 1:20 ratio is expected to change as glaciers retreat and new, glacier-derived rock glaciers are formed with climate change. This transition implies that rock glaciers could play a key role in local hydrology in the future, such as documented in the Great Basin (Millar and Westfall, 2019) and the Bolivian Andes (Rangecroft, 2015).

Table 8. Eastern rock glacier and glacier water resource value compilation.

Eastern Cascade Rock Glacier to Glacier Water Content			
	Quantity	Total Surface Area (km^2)	WVEQ (m^3)
Intact Rock Glaciers	140	6.33	54,194,814
Glaciers	218	46.51	1,074,000,000
Ratios	1:1.55	1:7.35	1:20

Management Implications

The findings of this research are significant for water managers of the Skagit and Methow drainages. The estimated North Cascades rock glacier water volume equivalence (WVEQ) that is available for discharge is 1,497,458 m^3 (1,214 AF) in the Skagit River

Watershed and 18,251,343 m^3 (14,797 AF) in the Methow River Watershed. The total WVEQ estimate of North Cascades rock glaciers in this study area is 19,748,801 m^3 (16,011 AF). Furthermore, the estimated total WVEQ available for discharge in the Eastern Cascades rock glacier inventory is 54,194,814 m^3 (43,937 AF). For reference, the Bumping Reservoir in the Yakima River Basin is 41,901,316 m^3 (33,970 AF) at full capacity.

With climate change in the 21st century, significant reductions will occur in glaciers and snowpack, which will have catastrophic effects on communities and ecosystems that depend on the alpine cryosphere as a water source. Although rock glaciers are comparatively climate resilient, sustained temperatures above 0°C will drive degradation of these water sources as well. However, rock glaciers can partially mitigate the water scarcity that some regions will experience with rapid depletion glaciers and snowpack. Furthermore, with deglaciation in mountain environments, corresponding formation of active, glacier-derived rock glaciers will occur as a resiliency mechanism of the alpine cryosphere (Anderson et al., 2018; Jones et al., 2019b). Therefore, there will be more rock glaciers to help provide water security for downstream communities and ecosystems as river base flow decreases from glacier and snowpack loss (Haeberli and Weingartner, 2020). This quickly changing environment will cause profound shifts in mountain geoecological belts, thus driving redistribution of plant and animal species, some of which will have increasingly limited habitat (Lutz et al., 2013; Pecl et al., 2017). Rock glaciers offer refugia for many of these species by providing talus shelter and cool, fresh water sources in a warming world (Millar and Westfall, 2019).

CHAPTER VI

CONCLUSIONS AND FUTURE RESEARCH

Conclusions

This research reveals that the mountain geoecological belts (the nival, periglacial and forest belts) in the North Cascades are identifiable using glaciers, rock glaciers, and timberline. Geoecological mapping showed the elevation range of each belt and how these elevation ranges change from a maritime to a more continental environment across the Cascade Crest (i.e., all geoecological belts rising in elevation with increased continentality). The periglacial belt was subdivided by natural breaks in the elevation of discrete rock glaciers, which did not reveal an elevation range wherein rock glaciers developed preferentially. This may reflect the variable of snow cover at higher elevations that is hiding rock glaciers from detection in aerial imagery and therefore are excluded from this dataset, such as the prospective rock glacier above CG6 (48.735568°, -120.321954°) in the Eightmile Creek study site.

Surveying the composition and structure of 10 rock glaciers with GPR showed that the average active layer thickness for these sites ranged from 1.6 – 4.6 m and the average permafrost thickness ranged from 8.5 – 27.2 m. The average EM velocity for these rock glaciers ranged from 0.13 – 0.153 m/ns^{-1}, which is consistent with the literature on the detection of permafrost (Monnier and Kinnard, 2013; Kunz and Kneisel, 2020). Shear stress was the most common expression of stress observed from the GPR data, which was clearly visible in four of the surveys. Likely, shear stress was the most prominent because it is caused by differential deformation velocities which develop from the heterogeneous composition of the rock glacier (Haeberli et al., 1988; Arenson et al.,

2002). Two GPR profiles displayed compressional stress in response to a decrease in bedrock slope. Only the BC1 survey displayed clear signals of extensional stress, although there are several other sites where extensional stress is expected in response to significant steepening of the bedrock such as in MC1, EM1, and EM2.

The ten rock glacier geophysical surveys enabled the study of rock glacier water capacity in relation to altitude and continentality. No appreciable difference was detected in rock glacier water capacity across a marine to continental climate gradient, and more research is necessary to better understand this concept across larger spatial scales. Furthermore, no elevation bracket of preferential rock glacier development was found; however, the 2180-2353 m elevation bracket contained the majority (58%) of the WEVQ of the four elevation brackets in this study. This is arguably an even more important finding because it means that water content may be distributed differently than can be observed by only recording rock glacier distribution. This should be considered in rock glacier analyses as water resources in other mountain areas.

The ClimateNA simulation revealed that all rock glaciers in the North Cascades will be exposed to melting temperatures in the 21st Century. The 2180-2353 m elevation bracket is a climate-sensitive altitude threshold because it contains nearly 2/3 of the total water content of North Cascades rock glaciers and will experience the most significant MAAT increase with EDW. The rock glaciers with the highest modeled MAAT for the 21st Century exist at the lowest elevations or on the marine, west side of the Cascade Crest (likely associated with the increased downward longwave radiation related to higher humidity in a marine environment).

Policy Implications

Several nations are working to protect their glacial and periglacial environment for its water resource value. Environmental stewardship of these areas will be critical as mountain water storage becomes increasingly limited with climate change. Fortunately, the rock glaciers in this study are in the Pasayten Wilderness so they are already a protected water resource. For the semi-arid Eastern Cascades, there are 140 intact rock glaciers that contain a total water volume exceeding that of Bumping Reservoir. These rock glaciers seasonally melt and help support river base flow. Water rights are often over-allocated and water scarcity is expected to increase as snowpack and glaciers diminish with climate change. Rock glaciers will outlast glacier and snowpack water reserves and will likely contribute more meltwater to river base flow as their active layers thicken and more glacier-derived rock glaciers are formed, thereby providing partial relief to ecosystems and communities.

Future Research

Including the current work, only three scientific investigations (Goshorn-Maroney, 2012; Riffle, 2018) have used geophysical techniques on rock glaciers in the Washington Cascades. It is critical to verify these findings with other geophysical instruments. In particular, electrical-resistivity would be quite useful in confirming the ice content and genesis indicated by ground penetrating radar surveys, such as illustrated by Kunz and Kneisel (2020). Additionally, I was only able to record geophysical data on one Western Cascades rock glacier, and time is limited to capture information on these intact features, as they experience the highest MAAT of all the rock glaciers in this study

area. Therefore, more research should be conducted in the Western Cascades to better understand the relationship between rock glacier water capacity and continentality. Furthermore, future surveys on rock glaciers should always record the slope angle of the snout while in the field to support evidence of permafrost creep and therefore rock glacier activity level. Moreover, other periglacial features exist in the Cascades that potentially contain permafrost and contribute to mountain hydrology such as protalus lobes and protalus ramparts. Surveying these features and quantifying their total water content would be useful supplementary data to the rock glacier inventory for water resource managers.

In addition to geophysical exploration of the internal environment of rock glaciers, it is also important to understand how much water these features are contributing annually to river base flow. Discharge monitoring stations could offer valuable information on the role of rock glaciers in the hydrologic system by recording the volume and timing of water exiting these features. Finally, studies such as Jones et al., (2019b) have used photogrammetry to understand the glacier-rock glacier continuum and assess the likelihood of a glacier transitioning into a rock glacier, rather than completely melting. This study found that access to a large catchment area greatly increased likelihood of a glacier-rock glacier transition, whereas large lateral moraines decreased the connectivity and therefore the opportunity of rock glacier formation. This type of study is crucial for mountain environments, such as the Cascades, in order to most effectively manage our water resources in a warming world.

REFERENCES

Abatzoglou, J. T., D. E. Rupp, and P. W. Mote. 2014. "Seasonal Climate Variability and Change in the Pacific Northwest of the United States." *Journal of Climate* 27 (5): 2125–42.

Allen, S., I. Owens, C. Huggel. 2008. "A First Estimate of Mountain Permafrost Distribution in the Mount Cook Region of New Zealand's Southern Alps: A First Estimate of Mountain Permafrost Distribution in the Mount Cook Region of New Zealand's Southern Alps." *Ninth International Conference on Permafrost*, Fairbanks, Alaska. July: 37–42.

Anderson, R. S., L. S. Anderson, W. H. Armstrong, M. W. Rossi, and S. E. Crump. 2018. "Glaciation of Alpine Valleys: The Glacier – Debris-Covered Glacier – Rock Glacier Continuum." *Geomorphology* 311: 127–42.

Annan, A. P. 2003. *Ground Penetrating Radar Principles, Procedures & Applications*. Mississauga, Ontario, Canada: Sensors & Software Inc.

Arenson, L. U., M. Hoelzle, and S. Springman. 2002. "Borehole Deformation Measurements and Internal Structure of Some Rock Glaciers in Switzerland." *Permafrost and Periglacial Processes* 13 (2): 117–35.

Arenson, L. U., and M. Jakob. 2010. "The Significance of Rock Glaciers in the Dry Andes - A Discussion of Azócar and Brenning (2010) and Brenning and Azócar (2010)." *Permafrost and Periglacial Processes* 21 (3): 282–85.

Arno, S. F. 1966. "Interpreting the Timberline: An Aid to Help Park Naturalists to Acquaint Visitors with the Subalpine-Alpine Ecotone of Western North America." Master's Thesis, University of Montana.

———. 1984. *Timberline: Mountain and Arctic Forest Frontiers*. Seattle: The Mountaineers.

Azócar, G. F., and A. Brenning. 2010. "Hydrological and Geomorphological Significance of Rock Glaciers in the Dry Andes, Chile (27°-33°s)." *Permafrost and Periglacial Processes* 21 (1): 42–53.

Ballentyne, C. 2002. "The Conachair Protalus Rampart, St Kilda." *Scottish Geographical Journal* 118(4), 434-350

Barsch, D. 1996. *Rock-glaciers: Indicators for the Present and Former Geoecology in High Mountain Environments*. Berlin: Springer.

Berthier, E., Y. Arnaud, R. Kumar, S. Ahmad, P. Wagnon, and P. Chevallier. 2006. "Remote Sensing Estimates of Glacier Mass Balances in the Himachal Pradesh (Western Himalaya, India)." *Remote Sensing of Environment* 108 (3): 327–38.

Berthling, I. 2011. "Beyond Confusion: Rock Glaciers as Cryo-Conditioned Landforms." *Geomorphology* 131 (3–4): 98–106.

Bradley, R. S., F. T. Keimig, and H. F. Diaz. 2004. "Projected Temperature Changes along the American Cordillera and the Planned GCOS Network." *Geophysical Research Letters* 31 (16): 2–5.

Bradley, R. S., M. Vuille, H. F. Diaz, and W. Vergara. 2006. "Threats to Water Supplies in the Tropical Andes." *Science* 312 (5781): 1755–56.

Brenning, A. 2005 "Geomorphological, Hydrological and Climatic Significance of Rock Glaciers in the Andes of Central Chile (33-35°S)." *Permafrost and Periglacial Processes* 16, no. 3 (2005): 231–40.

Brenning, A., and D. Trombotto. 2006. "Logistic Regression Modeling of Rock Glacier and Glacier Distribution: Topographic and Climatic Controls in the Semi-Arid Andes." *Geomorphology* 81 (1–2): 141–54.

Brighenti, S., M. Tolotti, M. C. Bruno, M. Engel, G. Wharton, L. Cerasino, V. Mair, and W. Bertoldi. 2019. "After the Peak Water: The Increasing Influence of Rock Glaciers on Alpine River Systems." *Hydrological Processes* 33 (21): 2804–23.

Büdel, J. 1982. *Climatic Geomorphology.* Translated book by Lenore Fischer and Detlef Busche. Princeton: Princeton University Press.

Capps, S. R. 1910. "Rock Glaciers in Alaska." *The Journal of Geology* 18, no. 4: 359–75.

Cederholm, C. J., D. H. Johnson, R. E. Bilby, L.G. Dominguez, A. M. Garrett, W. H. Graeber, E. L. Greda, M. D. Kunze, B.G., Marcot, J. F. Palmisano, R. W. Plotnikoff, W. G. Pearcy, C. A. Simenstad, and P. C. Trotter. 2000. *Pacific Salmon and Wildlife - Ecological Contexts, Relationships, and Implications for Management*. Special Edition Technical Report, Prepared for D. H. Johnson and T. A. O'Neil (Managing directors), Wildlife-Habitat Relationships in Oregon and Washington. Washington Department of Fish and Wildlife, Olympia, Washington.

Charbonneau, A. A., and D. J. Smith. 2018. "An Inventory of Rock Glaciers in the Central British Columbia Coast Mountains, Canada, from High Resolution Google Earth Imagery." *Arctic, Antarctic, and Alpine Research* 50 (1).

Cheng, Y., H. Liu, H. Wang, Q. Hao, Y. Han, K. Duan, and Z. Dong. 2020. “Climate-Driven Holocene Migration of Forest-Steppe Ecotone in the Tien Mountains.” *Forests* 11 (11): 1–16.

Christel, L., and D. Torunczyk. 2017. “Sovereignties in Conflict: Socio-Environmental Mobilization and the Glaciers Law in Argentina” *Centrum Voor Studie En Documentatie van Latijns Amerika (CEDLA).* 47-68

Chylek, P., J. Li, M. K. Dubey, M. Wang, and G. Lesins. 2011. “Observed and Model Simulated 20th Century Arctic Temperature Variability: Canadian Earth System Model CanESM2.” *Atmospheric Chemistry and Physics Discussions* 11 (8): 22893–907.

Climate Impacts Group, 2021. Pacific Northwest Climate Projections. https://cig.uw.edu/resources/analysis-tools/projections/ (Accessed 27 July 2021).

Cogley, J. G., and M. S. McIntyre. 2003. “Hess Altitudes and Other Morphological Estimators of Glacier Equilibrium Lines.” *Arctic, Antarctic, and Alpine Research* 35 (4): 482–88.

Cohen, J. S., H. B. Zeff, and J. D. Herman. 2020. “Adaptation of Multiobjective Reservoir Operations to Snowpack Decline in the Western United States.” *Journal of Water Resources Planning and Management* 146 (12): 04020091.

Corte, A. E. 1987. “Rock Glaciers Taxonomy” in *Rock Glaciers,* ed. J. R. Giardino, J. F. Shroder, jr. and J. D. Vitek. Boston: Allen and Unwin, 27-40.

Crandell, D. R., and R. D. Miller. 1974 “Quaternary Stratigraphy and Extent of Glaciation in the Mount Rainier Region, Washington.” *U. S. Geological Survey Professional Paper*, 59.

Cryosphere Glossary, National Snow and Ice Data Center (NSIDC). 2021. https://nsidc.org/cryosphere/glossary/term/permafrost. (Accessed 21 June 2021)

Dąbski, Maciej. 2019. “Should Glaciers Be Considered Permafrost?” *Geosciences (Switzerland)* 9 (12): 2–5.

Degenhardt, J. J. 2009. “Development of Tongue-Shaped and Multilobate Rock Glaciers in Alpine Environments - Interpretations from Ground Penetrating Radar Surveys.” *Geomorphology* 109 (3–4): 94–107.

Dipietro, J. A. 2018. *Geology and Landscape Evolution: General Principles Applied to the United States 2nd ed.* Elsevier.

Dobiński, W. 2018. “Permafrost: Definition and Extent.” *International Encyclopedia of Geography*, 1–10.

Elsner, M. M., L. Cuo, N. Voisin, J. S. Deems, A. F. Hamlet, J. A. Vano, K. E. B. Mickelson, S. Y. Lee, and D. P. Lettenmaier. 2010. “Implications of 21st Century Climate Change for the Hydrology of Washington State.” *Climatic Change* 102 (1–2): 225–60.

ESRI. 2011. ArcGIS Desktop: Release 10. Redlands, CA: Environmental Systems Research Institute.

Fagre, D. B., D. L. Peterson, and A. E. Hessl. 2003. “Taking the Pulse of Mountains: Ecosystem Responses to Climatic Variability.” *Climatic Change* 59 (1–2): 263–82.

Fountain, A. G., B. Glenn, and H. J. Basagic. 2017. “The Geography of Glaciers and Perennial Snowfields in the American West.” *Arctic, Antarctic, and Alpine Research* 49 (3): 391–410.

Fukui, K., T. Sone, J. A. Strelin, C. A. Torielli, J. Mori, and Y. Fujii. 2008. “Dynamics and GPR Stratigraphy of a Polar Rock Glacier on James Ross Island, Antarctic Peninsula.” *Journal of Glaciology* 54 (186): 445–51.

García, M. G., E. S. Cañadas, J. J. S. Blasco, and J. J. G. Trueba. 2017. “Surface Dynamic of a Protalus Lobe in the Temperate High Mountain. Western Maladeta, Pyrenees.” *Catena* 149: 689–700.

Giardino, J. R., J. F. Shroder, Jr., and J. D. Vitek. 1987. *Rock Glaciers*. Winchester, MA: Allen & Unwin.

Giardino, J. R., and S. G. Vick. 1987. “Geologic Engineering Aspects of Rock Glaciers” In *Rock Glaciers*, edited by Giardino, J. R., J. F. Shroder, Jr., and J. D. Vitek, 265-287. Winchester, MA: Allen & Unwin, Inc.

Google Earth Pro. Version 7.3. http://www.earth.google.com (Accessed 3 March 2021).

Goshorn-Maroney, J. 2012. “Thermal Conditions and Movement of Rock Glaciers in the North Cascades, Washington.” Master’s thesis, Western Washington University.

Granshaw, F. D, and A. G. Fountain. 2006. “Glacier Change (1958 – 1998) in the North Cascades National Park Complex, Washington, USA” *Journal of Glaciology* 52 (177): 251–56.

Gray, C. 2019. “Regional Modeling of the Glaciers of the North Cascades Mountains , Washington , USA” Master’s Thesis, Portland State University

Gross, G., H. Kerschner, and G. Patzelt. 1977: Methodische Untersuchungen tiber die Schneegrenze in Alpinen Gletscher gebieten. *Zeitschrift fur Gletscherkunde und Glazialgeologie,* 12: 223-251.

Guodong, C., and F. Dramis. 1992. "Distribution of Mountain Permafrost and Climate." *Permafrost and Periglacial Processes* 3 (2): 83–91.

Haeberli, W. 1975. "Mitteilung der Versdramuchsanstalt für Wasserbau, Hydrologie und Glaziologie" PhD Thesis, Zürich Herausgegeben.

———. 2000. "Modern Research Perspectives Relating to Permafrost Creep and Rock Glaciers: A Discussion." *Permafrost and Periglacial Processes* 11 (4): 290–93.

Haeberli, W., J. Huder, H. R. Keusen, J. Pika, and H. Rathlisberger. 1988. "Core Drilling through Rock Glacier Permafrost" *Versuchsanstalt fur Wasserbau, Hydrologie und Glaziologie,* ETH Zurich, Switzerland.

Haeberli, W., B. Hallet, L. Arenson, R. Elconin, O. Humlum, A. Kääb, V. Kaufmann, et al., 2006. "Permafrost Creep and Rock Glacier Dynamics." *Permafrost and Periglacial Processes* 17, no. 3: 189–214.

Haeberli, W., and R. Weingartner. 2020. "In Full Transition: Key Impacts of Vanishing Mountain Ice on Water-Security at Local to Global Scales." *Water Security* 11 (April): 100074.

Harris, C., and J. B. Murton. 2005. "Interactions between Glaciers and Permafrost: An Introduction." *Geological Society Special Publication* 242: 1–9.

Haugerud, R. A., and R.W. Tabor. 2009. "Geologic Map of the North Cascade Range, Washington." USGS Report.

Hess, H. 1904. *Die Gletscher*. Braunschweig, Vieweg & Sohn.

Höllermann, P. 1985. "The Periglacial Belt of Mid-Latitude Mountains from a Geoecological Point of View" *Erdkunde* Band, 39.

Hooke, R., and P. Hudleston. 1978. "Origin of Foliation in Glaciers," *Journal of Glaciology* 20(83): 285-299.

Humlum, O. 1982. "Rock Glacier Types on Disko, Central West Greenland" *Geografisk Tidsskrift* 82: 59-66.

———. 1988. “Rock Glacier Appearance Level and Rock Glacier Initiation Line Altitude: A Methodological Approach to the Study of Rock Glaciers.” *Arctic & Alpine Research* 20 (2): 160–78.

IPCC, 2014: Climate Change 2014: Synthesis Report. Contribution of Working Groups I, II and III to the Fifth Assessment Report of the Intergovernmental Panel on Climate Change [Core Writing Team, R.K. Pachauri and L.A. Meyer (eds.)]. IPCC, Geneva, Switzerland, 151 pp.

Iribarren, P. A., J. Kinney, M. Schaefer, S. Harrison, R. Wilson, A. Segovia, M. Bruno, F. Guerra, D. Farías, J. M. Reynolds, N. Glasser. 2018. “Glacier protection laws: potential conflicts in managing glacial hazards and adapting to climate change.” *Ambio: A Journal of the Human Environment*. 47, no. 8: 835–45.

Ives, J. D. 2012. “The Origins of Mountain Geoecology.” *Pirineos* 167 (167): 15–27.

Janke, J. R. 2007. “Colorado Front Range Rock Glaciers: Distribution and Topographic Characteristics.” *Arctic, Antarctic, and Alpine Research* 39 (1): 74–83.

Johnson, B. G., G. Thackray, and R. Van Kirk. 2007. “The Effect of Topography, Latitude, and Lithology on Rock Glacier Distribution in the Lemhi Range, Central Idaho, USA.” *Geomorphology* 91 (1–2): 38–50.

Johnson, G., H. Chang, and A. Fountain. 2020. “Rock Glaciers of the Contiguous United States: GIS Inventory and Spatial Distribution Patterns.” *Earth System Science Data Discussions*, no. September: 1–26.

Jones, D. B., S. Harrison, K. Anderson, and W. B. Whalley. 2019a. “Rock Glaciers and Mountain Hydrology: A Review.” *Earth-Science Reviews* 193: 66–90.

Jones, D. B., S. Harrison, S. and K. Anderson. 2019b. “Mountain Glacier-to-Rock Glacier Transition.” *Global and Planetary Change* 181: 102999.

Jones, D.B., S. Harrison, K. Anderson, R. A. Betts. 2018 “Mountain rock glaciers contain globally significant water stores.” *Scientific Reports* 8:2834

Jones, D. B., S. Harrison, K. Anderson, H.L. Selley, J. L. Wood, and R.A. Betts. 2017. “The Distribution and Hydrological Significance of Rock Glaciers in the Nepalese Himalaya” *Global and Planetary Change* 160: 123-142.

Karmalkar, A. V., and R. S. Bradley. 2017. “Consequences of Global Warming of 1.5 °c and 2 °c for Regional Temperature and Precipitation Changes in the Contiguous United States.” *PLoS ONE* 12 (1): 1–17.

Kaser, G. 2006. “Mountain Glaciers” in *Glacier Science and Environmental Change*. Ed P. G. Knight. Blackwell Publishing Ltd. 268-270

Kaspari, S. D., D. Pittenger, T. M. Jenk, U. Morgenstern, M. Schwikowski, N. Buenning, and L. Stott. 2020. “Twentieth Century Black Carbon and Dust Deposition on South Cascade Glacier, Washington State, USA, as Reconstructed From a 158-m-Long Ice Core.” *Journal of Geophysical Research: Atmospheres* 125 (11): 0–2.

Khadim, A. N. 2016. “Defending Glaciers in Argentina.” *Peace Review* 28 (1): 65–75.

Kunz, J., and C. Kneisel. 2020. “Glacier–Permafrost Interaction at a Thrust Moraine Complex in the Glacier Forefield Muragl, Swiss Alps.” *Geosciences (Switzerland)* 10 (6).

Kupfer, J. A., and D. M. Cairns. 1996. “The Suitability of Montane Ecotones as Indicators of Global Climatic Change.” *Progress in Physical Geography* 20 (3): 253–72.

Ladanyi, B. 2003. “Rheology of Ice/Rock Systems and Interfaces.” *Proc. of the 8th Int. Conf. on Permafrost*, 22–25.

Leonard, K. C., and A. G. Fountain. 2003. “Map-Based Methods for Estimating Glacier Equilibrium-Line Altitudes.” *Journal of Glaciology* 49 (166): 329–36.

Ley para la Preservación de los Glaciares y del Ambiente Periglacial de Argentina [Law for the Preservation of the Glaciers and the Periglacial Environment of Argentina], 2010. Ley: 26.639

Lilleøren, K. S., and B. Etzelmüller. 2011. “A Regional Inventory of Rock Glaciers and Ice-Cored Moraines in Norway.” *Geografiska Annaler, Series A: Physical Geography* 93 (3): 175–91.

Lillquist, K., and M. Weidenaar. Submitted text. “Rock Glaciers in the Eastern Cascades, Washington,” *Geomorphology*.

López-Martínez, J., E. Serrano, T. Schmid, S. Mink, and C. Linés. 2011. “Periglacial Processes and Landforms in the South Shetland Islands (Northern Antarctic Peninsula Region).” *Geomorphology* 155–156: 62–79.

Luckman, B. H., and K. J. Crockett. 1978. “Distribution and Characteristics of Rock Glaciers in the Southern Part of Jasper National Park, Alberta.” *Canadian Journal of Earth Sciences* 15 (4): 540–50.

Lutz, D. A., R. L. Powell, and M. R. Silman. 2013. “Four Decades of Andean Timberline Migration and Implications for Biodiversity Loss with Climate Change.” *PloS One* 8 (9): 1–9.

Mack, R. N., N. W. Rutter, and S. Valastro. 1979. “Holocene Vegetation History of the Okanogan Valley, Washington.” *Quaternary Research* 12 (2): 212–25.

Martin, E. H., and W. B. Whalley. 1987. “Rock Glaciers: Part 1: Rock Glacier Morphology: Classification and Distribution.” *Progress in Physical Geography* 11, no. 2: 260–82.

Maurer, H. and C. Hauck. 2007. “Instruments and Methods: Geophysical Imaging of Alpine Rock Glaciers.” *Journal of Glaciology* 53 (180): 110–20.

Millar, C., and R. Westfall. 2019. “Geographic, Hydrological, and Climatic Significance of Rock Glaciers in the Great Basin, USA.” *Arctic, Antarctic, and Alpine Research* 51 (1): 232–49.

Minder, J. R., P. W. Mote, J. D. Lundquist. 2010 “Surface temperature lapse rate over complex terrain: Lessons from the Cascade Mountains” *Journal of Geophysical Research*, Vol, 115, D14122.

Moir, W., and L. Huckaby. 1994. “Displacement Ecology of Trees near Upper Timberline” *International Conference on Bear Research and Management* 9: 35–42.

Monnier, S. and C. Kinnard. 2013. “Internal Structure and Composition of a Rock Glacier in the Andes (Upper Choapa Valley, Chile) Using Borehole Information and Ground-Penetrating Radar.” *Annals of Glaciology* 54 (64): 61–72.

———. 2015. “Internal Structure and Composition of a Rock Glacier in the Dry Andes, Inferred from Ground-Penetrating Radar Data and Its Artefacts.” *Permafrost and Periglacial Processes* 26 (4): 335–46.

Monnier, S., C. Camerllynck. and F, Rejiba. 2008. “Ground Penetrating Radar Survey and Stratigraphic Interpretation of the Plan Du Lac Rock Glaciers, Vanoise Massif, Northern French Alps.” *Permafrost and Periglacial Processes* 136: 107–36.

Monnier, S., C. Camerlynck, F. Rejiba, C. Kinnard, T. Feuillet, and A. Dhemaied. 2011. “Structure and Genesis of the Thabor Rock Glacier (Northern French Alps) Determined from Morphological and Ground-Penetrating Radar Surveys.” *Geomorphology* 134 (3–4): 269–79.

Moore, R. D., B. Pelto, B. Menounos, and D. Hutchinson. 2020. “Detecting the Effects of Sustained Glacier Wastage on Streamflow in Variably Glacierized Catchments.” *Frontiers in Earth Science* 8.

Morris, S. 1987. “Regional and Topoclimatic Implications of Rock Glacier Stratigraphy: Blanca Massif, Colorado” in *Rock Glaciers,* ed. J. R. Giardino, J. F. Shroder, jr. and J. D. Vitek. Boston: Allen and Unwin, 107-126.

Mote, P., A. Hamlet, and E. Salathé. 2007. “Has Spring Snowpack Declined in the Washington Cascades?” *Hydrology and Earth System Sciences* 12 (1): 193–206.

Mote, P. 2003. “Trends in Temperature and Precipitation in the Pacific Northwest during the Twentieth Century.” *Northwest Science* 77 (4): 271–82.

Mote, P., S. Li, D. Lettenmaier, M. Xiao, and R. Engel. 2018. “Dramatic Declines in Snowpack in the Western US.” *Npj Climate and Atmospheric Science* 1 (1).

NCGCP (North Cascade Glacier Climate Project) 2020. North Cascades Glaciers, Washington. https://glaciers.nichols.edu/ (Accessed 08 March 2020).

NHD (National Hydrology Dataset) 2020. Washington State Hydrology. https://geo.wa.gov/datasets/waecy::wa-hydrography-nhd-flowline/about (Accessed 09 March 2020).

Noetzle, J., S. Gruber, T. Kohl, N. Salzmann, and W. Haeberli. 2007. “Three-Dimensional Distribution and Evolution of Permafrost Temperatures in Idealized High-Mountain Topography.” *Journal of Geophysical Research: Earth Surface* 112 (2).

Nogués-Bravo, D., M. B. Araújo, M. P. Errea, and J. P. Martínez-Rica. 2006. “Exposure of Global Mountain Systems to Climate Warming during the 21st Century.” *Global Environmental Change* 17 (3–4): 420–28.

Nolin, A. W. 2012. “Perspectives on Climate Change, Mountain Hydrology, and Water Resources in the Oregon Cascades, USA.” *Mountain Research and Development* 32 (SUPPL. 1).

NRCS (Natural Resources Conservation Service). 2021. MF Nooksack, Washington. https://wcc.sc.egov.usda.gov/nwcc/site?sitenum=1011 (Accessed 07 May 2021).

———. 2021. Harts Pass, Washington. https://wcc.sc.egov.usda.gov/nwcc/site?sitenum=1011 (Accessed 07 May 2021).

———. 2021. Salmon Meadows, Washington. https://wcc.sc.egov.usda.gov/nwcc/site?sitenum=1011 (Accessed 07 May 2021).

O'Donnell, C., J. Recharte and A. Taber. 2016 "Climate Change, Mountain People and Water Resources-the Experiences of the Mountain Institute, Peru" *Unasylva* 67(246), 75-80.

Olyphant, G. 1977. "Topoclimate and the Depth of Cirque Erosion." *Geografiska Annaler: Series A, Physical Geography* 59, no. 3–4: 209–13.

Onaca, A., F. Ardelean, P. Urdea, and B. Magori. 2017. "Southern Carpathian Rock Glaciers: Inventory, Distribution and Environmental Controlling Factors." *Geomorphology* 293: 391–404.

O'Neal, M. A., B. Hanson, S. Carisio, and A. Satinsky. 2015. "Detecting Recent Changes in the Areal Extent of North Cascades Glaciers, USA." *Quaternary Research (United States)* 84 (2): 151–58.

Opdam, P., S. Luque, and K. B. Jones. 2009. "Changing Landscapes to Accommodate for Climate Change Impacts: A Call for Landscape Ecology." *Landscape Ecology* 24 (6): 715–21.

Osborn, G. D. 1975. "Advancing Rock Glaciers in the Lake Louise Area, Banff National Park, Alberta." *Canadian Journal of Earth Sciences* 12, no. 6: 1060–62.

Palazzi, E., L. Filippi, and J. V. Hardenberg. 2017. "Insights into Elevation-Dependent Warming in the Tibetan Plateau-Himalayas from CMIP5 Model Simulations." *Climate Dynamics* 48 (11–12): 3991–4008.

Palazzi, E. L., L. Mortarini, S. Terzago, and J. V. Hardenberg. 2018. "Elevation-Dependent Warming in Global Climate Model Simulations at High Spatial Resolution." *Climate Dynamics* 52 (5–6): 2685–2702.

Paterson, W. S. B. 1994. *The Physics of Glaciers*, 3rd ed. Oxford: Pergamon.

Pecl, G. T., Araújo, M. B., Bell, J. D., Blanchard, J., Bonebrake, T. C., Chen, I. C., Clark, T. D., et al. 2017. "Biodiversity Redistribution under Climate Change: Impacts on Ecosystems and Human Well-Being." *Science* 355 (6332).

Peili, S., W. Ning, and G. S. Rawat. 2020. "The Distribution Patterns of Timberline and Its Response to Climate Change in the Himalayas." *Journal of Resources and Ecology* 11 (4): 342.

Pelto, M. S. 2006. “The Current Disequilibrium of North Cascade Glaciers” *Hydrological Processes* 20, 769-779 (2006)

———. 2008. “Impact of Climate Change on North Cascade Alpine Glaciers, and Alpine Runoff.” Northwest Science 82 (1): 65–75.

Pepin, N., R. S. Bradley, H. F. Diaz, M. Baraer, E. B. Caceres, N. Forsythe, H. Fowler, et al. 2015. “Elevation-Dependent Warming in Mountain Regions of the World.” *Nature Climate Change* 5 (5): 424–30.

Perucca, L., and M. Angillieri. 2011. “Glaciers and Rock Glaciers’ Distribution at 28° SL, Dry Andes of Argentina, and Some Considerations about Their Hydrological Significance.” *Environmental Earth Sciences* 64, no. 8: 2079–89.

Porter, S. C. 1977. “Present and Past Glaciation Threshold in the Cascade Range, Washington, U.S.A.: Topographic and Climatic Controls, and Paleoclimatic Implications.” *Journal of Glaciology* 18 (78): 101–16.

PRISM Climate Group, 2020. PRISM Data Extractor. Oregon State University.

Rabatel, A., A. Letréguilly, J. Dedieu, and N. Eckert. 2013. “Changes in Glacier Equilibrium-Line Altitude in the Western Alps from 1984 to 2010: Evaluation by Remote Sensing and Modeling of the Morpho-Topographic and Climate Controls.” *Cryosphere* 7 (5): 1455–71.

Rangecroft, S. 2015. “Rock Glaciers and Climate Change in the Bolivian Andes, Mapping New Water Resources.” *University of Exeter*, no.: 1–20.

Rangwala, I., and J. R. Miller. 2012. “Climate Change in Mountains: A Review of Elevation-Dependent Warming and Its Possible Causes.” *Climatic Change* 114 (3–4): 527–47.

Rangwala, I., E. Sinsky, and J. R. Miller. 2013. “Amplified Warming Projections for High Altitude Regions of the Northern Hemisphere Mid-Latitudes from CMIP5 Models.” *Environmental Research Letters* 8 (2).

Rhoades, A. M., P. A. Ullrich, C. M. Zarzycki, H. Johansen, S. A. Margulis, H. Morrison, Z. Xu, and W. D. Collins. 2018. “Sensitivity of Mountain Hydroclimate Simulations in Variable-Resolution CESM to Microphysics and Horizontal Resolution.” *Journal of Advances in Modeling Earth Systems* 10 (6): 1357–80.

Riedel. J., R. A. Haugerud, and J. J. Clague. 2007. “Geomorphology of a Cordilleran Ice Sheet Drainage Network Through Breached Divides in the North Cascades Mountains of Washington and British Columbia” *Geomorphology* 91: 1-18

Riedel, J.L. 2017. “Deglaciation of the North Cascade Range, Washington and British Columbia, from the Last Glacial Maximum to the Holocene.” *Cuadernos de Investigación Geográfica* 43 (2): 467.

Riffle, A. 2018. “Internal Composition, Structure, and Hydrological Significance of Rock Glaciers in the Eastern Cascades, Washington,” Master’s Thesis, Central Washington University

Risser P. G., J. R. Karr, and R.T. Forman. 1984. “Landscape Ecology: directions and approaches.” *Illinois Natural History Survey Special Publ. 2*, University of Illinois, Urbana

Sakio, H., and T. Masuzawa. 2020. “Advancing Timberline on Mt. Fuji between 1978 and 2018.” *Plants* 9 (11): 1–15.

Salathé, E. P., L. R. Leung, Y. Qian, and Y. Zhang. 2010. “Regional Climate Model Projections for the State of Washington.” *Climatic Change* 102 (1–2): 51–75.

Schaffer, N., S. MacDonell, M. Réveillet, E. Yáñez, and R. Valois. 2019. “Rock Glaciers as a Water Resource in a Changing Climate in the Semiarid Chilean Andes.” *Regional Environmental Change* 19 (5): 1263–79.

Serrano, E., M. Oliva, M. González-García, J. I. López-Moreno, J. González-Trueba, R. Martín-Moreno, M. Gómez-Lende, J. Martín-Díaz, J. Nofre, and P. Palma. 2018. “Post-Little Ice Age Paraglacial Processes and Landforms in the High Iberian Mountains: A Review.” *Land Degradation and Development* 29 (11): 4186–4208.

Slaymaker, O. 2011. “Criteria to Distinguish between Periglacial, Proglacial and Paraglacial Environments.” *Quaestiones Geographicae* 30 (1): 85–94.

Stoffel, K. L., and McGroder. 1990. Geologic Map of the Robinson Mtn. 1:100,000 Quadrangle, Washington: Washington Division of Geology and Earth Resources, Open File Report 90-5. Scale 1:100,000.

Troll, C. 1971. “Landscape Ecology (Geoecology) and Biogeocenology – A Terminological Study” *Geoforum.* Vol 2(4), p. 43-46

Urrutia, R., and M. Vuille. 2009. “Climate Change Projections for the Tropical Andes Using a Regional Climate Model: Temperature and Precipitation Simulations for the End of the 21st Century.” *Journal of Geophysical Research Atmospheres* 114 (2): 1–15.

Vitek, J. D., and J.R. Giardino. 1987. “Rock Glaciers: A Review of the Knowledge Base” in *Rock Glaciers,* ed. J. R. Giardino, J. F. Shroder, jr. and J. D. Vitek. Boston: Allen and Unwin, 1-26.

Vuille, M., R. S. Bradley, M. Werner, and F. Keimig. 2003. “20th Century Climate Change in the Tropical Andes: Observations and Model Results,” 75–99.

Wahrhaftig, C. 1987. “The Foreword” in *Rock Glaciers,* ed. J. R. Giardino, J. F. Shroder, jr. and J. D. Vitek. Boston: Allen and Unwin vii-xiv.

Wahrhaftig, C. and A. Cox. 1959. “Rock Glaciers in the Alaska Range” *Bulletin of the Geological Society of America.* Vol. 70: 383–436.

Wang T, A. Hamann, D. Spittlehouse, C. Carroll. 2016. “Locally Downscaled and Spatially Customizable Climate Data for Historical and Future Periods for North America.” *PLoS ONE* 11(6)

Wardle, P. 1971. “An explanation of alpine timberline, New Zealand” *Journal of Botany*, 9:3, 371-402

Washburn, A. L.1980. *Geocryology.* John Wiley &Sons, New York.

Weidenaar, M. 2013. “Rock Glaciers in the Eastern Cascade Range, Washington, USA.” Undergraduate Thesis, Central Washington University.

WGMS (World Glacier Monitoring Service) 2020. North Cascades Glaciers, Washington. https://wgms.ch/data_exploration/ (Accessed 03 March 2020).

Whalley, W. B. 1997. “Protalus Ramparts, Rock Glaciers and Protalus Lobes in the Lake District,” no. January 1997.

White, S. E. 1976. “Rock Glaciers and Block Fields, Review and New Data.” *Quaternary Research* 6, no. 1: 77–97.

Willis, M., A. Melkonian, M. Pritchard, and J. Ramage. 2011. “Ice Loss Rates at the Northern Patagonian Icefield Derived Using a Decade of Satellite Remote Sensing.” *Remote Sensing of Environment* 117: 184–98.

WRCC (Western Regional Climate Center) 2020. Glacier Ranger Station, Washington. https://wrcc.dri.edu/cgi-bin/cliMAIN.pl?wa3160 (accessed 03 March 2020).

———. 2020. Mazama, Washington. https://wrcc.dri.edu/cgi-bin/cliMAIN.pl?wa5133 (accessed 03 March 2020).

———. 2020. Ross Dam, Washington. https://wrcc.dri.edu/cgi-bin/cliMAIN.pl?wa7185 (accessed 03 March 2020).

Wu, J., and R. Hobbs. 2007. “Landscape Ecology: The State-of-the-Science.” *Key Topics in Landscape Ecology,* no. September: 271–87.

Wulf, A. 2015. *The Invention of Nature: Alexander von Humboldt's New World*. New York: Alfred A. Knopf. 2015.

Yan, L., and X. Liu. “Has Climatic Warming Over the Tibetan Plateau Paused or Continued in Recent Years?” J. Earth Ocean Atmos. Sci. 1, 13–28 (2014).

Young, K., and J. Lipton. 2006. “Adaptive Governance and Climate Change in the Tropical Highlands of Western South America.” *Climatic Change* 78 (1): 63–102.

Young, K., A. Ponette-González, M. H. Polk, and J. K. Lipton. 2017. “Snowlines and Treelines in the Tropical Andes.” *Annals of the American Association of Geographers* 107 (2): 429–40.

Zemp, M., W. Haeberli, M. Hoelzle. and F. Paul. 2006. “Alpine Glaciers to Disappear Within Decades?” *Geophysical Research Letters*, Vol. 33. L13504